Model Based and Intelligent Monitoring and Control of Lithium-ion Batteries

by

Mohammad Foad Samadi

M.Sc., Petroleum University of Technology, 2008
B.Sc., Ferdowsi University of Mashhad, 2005

Dissertation Submitted in Partial Fulfillment of the
Requirements for the Degree of
Doctor of Philosophy

in the
School of Engineering Science
Faculty of Applied Science

SIMON FRASER UNIVERSITY
Spring 2016

Approval

Name:	**Mohammad Foad Samadi**
Degree:	**Doctor of Philosophy (Electrical Engineering)**
Title:	***Model Based and Intelligent Monitoring and Control of Lithium-ion Batteries***
Examining Committee:	**Chair:** Dr. John Jones Associate Professor

Dr. Mehrdad Saif
Senior Supervisor
Professor _____

Dr. Mehrdad Moallem
Supervisor
Professor _____

Dr. Ahmad Rad
Internal Examiner
Professor _____

Dr. Voiko Loukanov
External Examiner
CEO
D&V Electronics LTD. _____

Date Defended: 19 Feb 2016

Abstract

Increased concerns over the limited sources of energy and environmental impact of the petroleum-based transportation infrastructure have led to increasing interest in an electric transportation infrastructure. Battery technology and battery management is a key component in this regard and has indeed remained as a central challenge in vehicle electrification. This thesis deals with monitoring and control of Lithium ion batteries. The objective is to provide novel solutions to some of the challenging issues from a control theoretic perspective. The research stream in this thesis is headed towards three general directions, i.e. monitoring, diagnostics, and control.

The proposed monitoring approaches are introduced as model-based and data-based approaches. The main objective in model-based approaches is to employ the high-fidelity physics-based models of the battery for monitoring. In this thesis, two particle-filtering methods are proposed for state, and joint state and parameter estimation of such models. The data based approaches try to come up with new ideas to monitor the battery accurately but with minimum computational load. In this regard, two different approaches are considered. A Takagi-Sugeno fuzzy model is developed for Li-ion battery where by the virtue of multiple-model structure of T-S model, the non-linearities of battery dynamics and corresponding parameters can appropriately be accounted for, while keeping the local models linear and easy-to-implement control/estimation algorithms. In another work, the "Dynamic Resistance" concept is introduced which can bring a new dimension to battery monitoring. This parameter considers changes in overall interface resistances that may develop during cell aging and is modeled versus the state of charge and total power throughput of the battery using a heuristic neural network to monitor the state of charge and state of health of the battery.

In another study, fault diagnosis problem of Li-ion batteries is rather comprehensively reviewed, and some of the proposed models for failure mechanism are presented and some fault-detection algorithms for some common failure mechanism are developed. Finally, the battery equalization which is essentially a safety measure in battery operation is studied. A nonlinear model predictive control (NMPC) solution for control of a cell-balancing circuit composed of Cuk converters is developed.

Keywords: Li-ion Battery; Battery Management System; State of Charge; State of Health; Cell Balancing; Dynamic Resistance

Dedication

To my great parents,
who have blessed me with their endless love.
And to my beloved wife,
who has been a constant source of support, encouragement and inspiration.

Acknowledgements

Praise and thanks be to the beneficent God who with his boundless mercies has bestowed his favors upon me in each moment of my life. This thesis appears in its current form due to the assistance and guidance of several people. I would therefore like to offer my sincere thanks to all of them.

I wish to express my deepest sense of gratitude to Dr. Mehrdad Saif, for having dedicated to me his constant guidance, profound knowledge and experience throughout my Ph.D. studies. I surely recognize that without his help and kind consideration, this work would never have come into existence. I cannot express my appreciation for his enthusiasm throughout my academic career at Simon Fraser University. I would also like to express my gratitude to the members of my supervisory and examination committee, Dr. Mehrdad Moallem, Dr. Ahmad Rad, and Dr. Voiko Loukanov for agreeing to serve in the committee and sharing their comments to improve this work.

My sincere thanks also goes to Dr. Nazri for his continuous support during my research, for his motivation and open arms to share his immense knowledge. His guidance helped me during this research. It was particularly kind of him to allow me to have access to his laboratory and experimental results. I would like to thank Dr. Mahdi Alavi, who as a good friend and colleague, was always willing to help and give his best.

I would like to thank all my teachers and friends at Simon Fraser University for their invaluable sincerity and support during my graduate and undergraduate courses of study.

I am deeply thankful to my wonderful parents, and brothers, Danyal and Amir, for all their love and encouragement. They have always been there to support me even though they were thousands of miles away. I saved the last spot for the person who deserved this degree as much as I did. I don't know how I could manage this without her. Bita, I can not thank you enough for everything.

Mohammad Foad Samadi
May 2015

Table of Contents

List of Tables

List of Figures

Chapter 1

Introduction

1.1 Thesis Motivation

Energy and environmental based issues have become the major areas of concern for policy makers. In this regard, an ever-increasing trend towards alternative clean sources of energy such as solar, wind, and geothermal can be observed during the last 20 years. Parallel to policy shift from fossil fuels to other sources of energy, transportation industries have also changed their policies and have been constantly searching for alternatives to internal combustion (IC) engines. Currently, energy storage devices mainly include chemical batteries, flywheels, ultracapacitors and fuel cells. Figure (1.1) shows the energy density and power density of most widely used energy storage devices.

On average, accumulators such as lead-acid, nickel-metal hydride and lithium-ion (Li-ion) batteries have a service life of between three and ten years. They function on electrochemical principles. Energy storage devices such as double layer capacitors, in contrast, store energy electrostatically. They last almost indefinitely and exhibit high power densities. However, their energy densities are low. Therefore, their primary use is to cover peak loads such as engine starts or acceleration in hybrid applications. As Figure (1.1) shows, Lithium ion batteries exhibits the most optimal characteristics in terms of energy density vs. power density.

Li-ion battery have thus been established as a leading candidate for the next generation of automotive and aerospace applications. Compared to alternative battery technologies, they provide one of the best energy-to-weight ratios, exhibit no memory effect, possess higher life-span, and have low self-discharge when not in use [16, 2].

Despite the consensus about their benefits, their development and recent progress has been slow due to issues related to improving energy density, power capability, monitoring and safety aspects of the lithium batteries. Therefore, Li-ion batteries define a broad range of areas of challenges for research and development. That has been the subject of active research in the last decade. This study is motivated by the premise that the Li-ion (and like

chemistry such as Li-polymer, Li-air, etc) batteries represent a promising alternative source of energy for transportation systems. Particularly, automotive industries have been actively working on electric vehicles (i.e. EV, HEV and PHEV) in both research and production phases during the last decade.

Control theory has the capacity to provide solutions to a number of challenges in regards to Li-ion batteries. Monitoring, safety and optimality of usage are some areas of concern that can be addressed from a control perspective. Therefore, developing a control theoretic approach towards these issues can open a new window to some existing challenges of Li-ion batteries.

In all Li-ion battery applications, prediction of state of charge of the battery has the highest priority for the user. In particular, for vehicle applications, drivers need to know how much further they can travel before their vehicle batteries require a recharge. The state of charge (SoC) of a battery or pack of batteries is analogous to a fuel gauge in an internal combustion vehicle. Accuracy of the prediction is also very important in optimal utilization of the battery's capability. Therefore, as HEVs/EVs grow in popularity and complexity, new monitoring methods are needed to better track performance.

Furthermore, the design process and the real-time control of the electric vehicles drivetrain, including the energy storage, rely on accurate estimations of battery wear as a function of operating conditions and usage. This is addressed via state-of-health (SOH) estimation. This parameter is also very crucial in optimal utilization of the battery.

The power and energy capabilities of a battery pack greatly depend on operating conditions, like charge/discharge current rate, state of charge, load characteristics, and temperature. Furthermore, it is important to avoid or contain the circumstances that could damage the battery or could lead to safety issues for the surrounding environment. Especially, for a battery chemistry like the lithium-based ones, and especially in a high-power context, events like overcharge, overdischarge and excessive heating can lead to irreversible and possibly destructive processes. Hence, fault monitoring and preventive measures such as cell-balancing plays an important role in safe utilization of the battery.

All the hardware and software associated with battery monitoring, control and protection are gathered in what is called the "battery management system (BMS)". This is a system that keeps the battery ready to deliver full power when necessary and a system that can extend the life of the battery. The BMS should include systems that control the charging regime and those that manage thermal issues as well.

Although great improvements have been made in BMS technology, they still fall short in many areas. Monitoring, fault detection, control, and protection are all areas that need further development to cope with the users' demand. Thus, the general objective of this study is to deepen the insight in the shortcomings and existing challenges and develop advanced methods for BMS from a control point of view.

1.2 Thesis Objective

The research objectives in this thesis are broad, however, all of them are geared toward advancement of BMS. They are meant to enhance the current estimation and control capabilities of BMS. The main focus in this regard are model-based estimation and monitoring schemes. The objectives are summarized as follows.

Estimation and Monitoring

In this thesis, as implied earlier, we focus on advanced online battery monitoring methods. The developed methods aim at estimation of the main parameters of concern for BMS (i.e. SoC, SoH) using high-fidelity models. The prevailing approach in practice is to use equivalent circuit models in model-based approaches to battery monitoring. In this thesis, we strive to explore new methodologies to employ the high fidelity physics-based model of the system for battery monitoring. Moreover, the main goal is to develop state and parameter estimation techniques for monitoring of the battery. Considering the parameter estimation alongside the state estimation is in fact the first step towards embedding the aging of the battery and its impact on parameters in monitoring scheme.

Modeling

The goal is to develop models that can capture the nonlinearity of battery dynamics, however need lower computational load to be simulated with respect to physics-based model. Moreover, a big challenge with physics-based models is that they are composed of partial differential equations where most of the control and estimation methods are developed for ordinary differential equations. Therefore, we aim at developing models that are more appropriate for application of the control approaches to for battery monitoring.

Health Monitoring

Health monitoring of the battery is a rather complicated interdisciplinary problem. In this regard, a complete study on degradation processes, their interaction, associated impact on model parameters and their model is conducted. From a monitoring point of view, development of parameter estimation scheme mentioned earlier would be the first step towards taking the aging processes of battery into account. A fault detection approach for one of the major failures of the battery system is also developed.

Moreover, a new concept named *"Dynamic resistance"* is introduced which can contribute to health monitoring of the battery. The main idea is to monitor the spontaneous response of the battery to a pulse current. This resistance is related to electronic resistance of the battery and is a function of the charge/discharge cycle number of the battery. Mod-

eling of dynamic resistance helps to propose a new framework for health monitoring of the battery.

Cell Balancing

Cell balancing is in fact a preventive measure for protection of the cells. It is also conducive to optimal utilization of the battery by reducing the conservative safety margins that are usually considered to prevent overcharge/overdischarge of the battery. The goal is to tackle the problem of a cell-balancing circuit composed of Cuk-converter using a model-predictive control approach. To the best of our knowledge, this is the first effort of its kind to apply a model-based control algorithm to cell-balancing problem. The appealing feature of this approach is that it can incorporate the dynamic constraints of battery equalization problem within the control framework and also the optimization objectives can directly be defined in terms of a minimization problem.

1.3 Thesis Organization

The remainder of this thesis is organized as follows. Chapter 2 reviews the principles of the Li-ion battery and presents the physics-based model of the battery. The principles and main tasks of BMS are also reviewed in this chapter. Monitoring approaches to Li-ion battery are explored in Chapter 3. Two novel model-based methodologies for state and state and parameter estimation based on a Bayesian approach are developed in this chapter.

Chapter 4 introduces two new data-based approaches to battery modeling and monitoring. The first study is a fuzzy modeling approach to Li-ion battery to address the existing challenges with physics-based model. The second approach is a novel methodology developed for SoC and SoH of the battery based on measurement of introduced parameter called “Dynamic Resistance”. The features and potentials of this new methodology are explored and illustrated through experiment. The diagnostics of the battery and the existing challenges are reviewed comprehensively in Chapter 5. This study is accompanied with developing of a fault detection approaches for plating mechanism and positive electrode dissolution which are common and important failures in battery systems. Chapter 6 considers the cell-balancing problem. The basics of the problem is reviewed and a novel control framework based on model-based predictive control methodology is developed for this problem. Finally, Chapter 7 draws the conclusion of the work and it glances over open problems and possible developments.

Due to the abundance of the mathematical equations and models used in this Thesis, using the same letters for different variables was inevitable. However, the explanation under each subject clarifies the meaning of the variables completely and removes any ambiguity. Moreover, nomenclature tables specific to each subject are given in Appendix A to make the following of the formulas and equations easier for the reader.

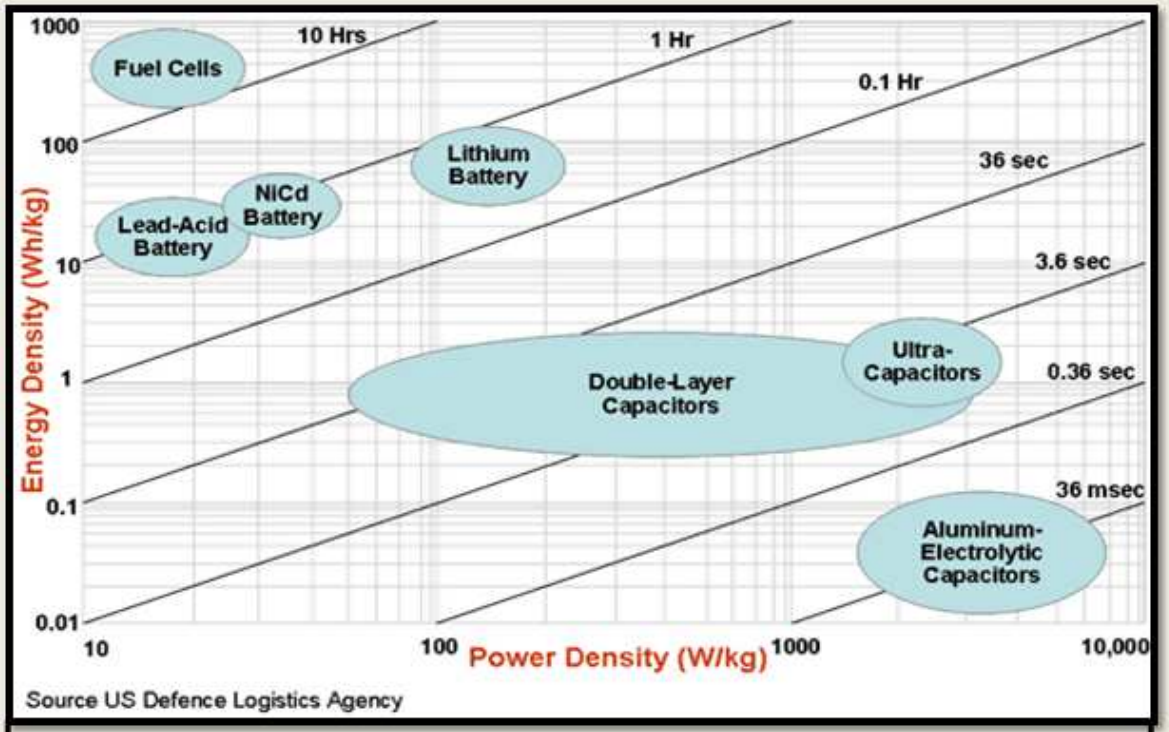

Battery type	Energy density Wh/Kg	Power density W/Kg	Service life in cycles/years
Lead-acid battery	30-50	150-300	300-1000/3-5
Nickel-metal hydride battery	90-150	200-300	>1000/>5
Lithium-ion battery	90-150	500->2000	>2000/5-10
Supercaps (double layer capac.)	3-5	2000-10000	1000000/unlimited

Figure 1.1: Energy density vs power density of different energy-storage devices. The charge time of them is also shown in the diagonal lines [127].

Chapter 2

Li-ion Battery Principles and Battery Management System

2.1 Li-ion Battery

A Li-ion battery generally consists of four main components: porous positive and negative electrodes, electrolyte and separator. During operation of Li-ion battery, Li ions (Li^+) are the charge carrier inside the battery, and shuttle back and forth between the positive and the negative electrodes through an electrolyte medium. In charge (discharge) process, the Li ions are extracted from (inserted into) the positive electrode and are inserted into (extracted from) the negative electrode. Electrolyte serves as a medium for Li ions transport between the two electrodes. The positive and negative electrodes are separated electrically with a separator containing the electrolyte which is in fact an electrical insulator and prevents electron transfer between positive and negative electrodes. The electrons are instead collected by positive and negative current collectors at the two terminals through an outside circuit where current flows. Figure (2.1) shows a schematic of the Li-ion battery.
In the following some relevant terms that are used throughout this thesis are explained.

- **Lattice**: In a typical Li-ion cell, both electrodes have lattice sites that can store Lithium ion [23]. Lattice sites are related to crystal structure of the negative and positive electrodes. They are modified during lithium insertion and extraction, and electrodes may go under a rich lattice modifications (e.g. phase changes, lattice gliding, symmetry changes, bi-phasic transformation) during charge and discharge [30, 31].

- **Active Material**: The lattice in negative electrode is typically a graphite lattice in most of the commercial lithium ion batteries, whereas in the positive electrode is a metal oxide (or a blend of multiple metal oxides) lattice (e.g. $LiCoO_2$, $LiMn_2O_4$, etc). Other types of negative and positive electrode materials are also being used in

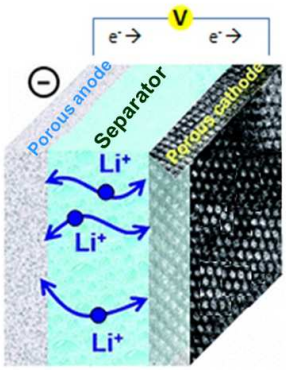

Figure 2.1: Schematic of a Li-ion cell. Positive and negative electrodes are composed of porous materials and separator is filled with electrolyte that facilitates the ion conduction between the negative and positive electrodes.

some commercial cells, i.e. polyanion positive electrode, $LiFePO_4$, Li_2MnSiO_4 and alloy anode materials such as $Li-Si$, $Li-Sn$, etc are under intense development.

- **Lithium insertion/extraction**: The moving of lithium ions into the lattice site is called insertion (intercalation) whereas moving of the lithium ions out of lattice site is called extraction (deintercalation). In the charging (discharging) process, Lithium insertion in (extraction of) the negative electrode and Lithium extraction of (insertion in) positive electrode occurs.

- **Binder**: It refers to an elastomeric polymer added to electrode particles in order to bond the active electrode material powder together and to the current collector. In fact, it acts as glue for particles to bond them together and to the current collector. Carboxymethyl cellulose (CMC) and poly vinylidene difluoride (PVdF) are the commonly used binders.

- **Composite Electrode**: It refers to the mixture of active material, binder and other additives (e.g. conductive carbon for improving the conductivity). For example, the composite positive electrode is typically a mixture as: $x.LiCoO_2+(1-x).LiMn_2O_4+y.C+z.binder$ where x ranges between $0-0.5$, and y and z range between $0.03-0.1$. Recently, battery manufacturers are engineering composite electrode made of materials with high power capability and materials of high energy to achieve desired Power/Energy characteristic.

- **Current Collector**: They are metallic foils at the two ends of the battery that collect/extract and take in/out the electricity during charge-discharge process. Aluminum (Al) foils and Copper (Cu) foils are usually used at the positive and negative current collectors, respectively. The anode and cathode slurries are coated on to re-

spective foil types, dried and pressed to adjust desired adhesion thickness and electrode porosity.

- **Solvent**: The electrolyte of the Li-ion battery, acting as a Lithium-ion carrier between the positive and the negative electrodes is usually composed of an organic solvent and a Lithium salt. The commonly used organic solvents are combinations of cyclic and linear organic carbonates, such as ethylene carbonate and dimethyl carbonate where the lithium salt is usually $LiPF_6$. Other lithium salts are also used in lithium battery, i.e. $LiBF_4$ or $LiCIO_4$. In the following, solvent always refers to the solvent part of the electrolyte. Solvent free electrolytes such as polymeric and ceramic electrolytes are also being considered.

- **Transport properties**: This refers to the properties representing the Li ion transport in the electrolyte or electrode lattice such as diffusion, conductivity, transference number, ion exchange processes, etc.

- **Oxidation**: It refers to the loss of electrons or an increase in oxidation state by a molecule, atom, or ion. For instance, $LiCo^{III}O_2 \rightarrow Co^{IV}O_2 + Li^+ + e^-$, where cobalt ion is oxidized from oxidation state III to IV by loss of electrons, or $Anion^- \rightarrow Oxidation\ Products + e^-$.

- **Reduction**: It refers to the gain of electrons or a decrease in oxidation state by a molecule, atom, or ion. For instance, $Cation^+ + e^- \rightarrow Reduction\ Products$, this is a reverse oxidation process.

- **Decomposition**: It refers to the separation of a chemical compound to simpler compounds or elements. This process is usually involves breaking chemical bonds.

- **Porosity**: It is a fraction of the volume of voids over the total volume in a material.

2.2 Li-ion Battery Modeling

The battery model plays a key role in the design of the monitoring and control schemes in a BMS. The mathematical modeling approaches to Li-ion battery can generally be classified under three main categories, namely Equivalent Circuit Models, Empirical Models and Electrochemical Models. In the following, the basic principles of each modeling approach is briefly reviewed.

2.2.1 Equivalent circuit models (ECM)

Conventionally, batteries are modeled as some electrical circuit. Different configurations, ranging from simple to complex circuits, are proposed for battery simulation. The model parameters do not necessarily represent any physical significance but the output of the

circuit (i.e. voltage, in most of cases) shows a rather good correlation with the output of the battery system. The advantage of the equivalent circuit models is that they are easy to use, however, not sufficiently accurate. Moreover, the model parameters are usually accurate for a limited range of SoC and charge/discharge rates. The performance of the model is also very dependent on the applied driving cycle or charge/discharge schemes, such as constant voltage-constant current, pulse, etc. In fact, the dynamical behavior of a Li-ion battery depends on many factors [99] such as temperature, state-of-charge, history of operation, operating frequency, etc, among which only a few of them are grasped and considered within the best of the developed models. The passive and interactive equivalent circuit models have been reviewed in the past [49, 50].

2.2.2 Empirical Models (EPM)

Empirical models consider the battery as a black-box and try to model the battery mathematically. The main idea is to derive a model which can be represented in state-space format and is easily adoptable for control and monitoring purposes. The parameters of the model do not necessarily bear any physical significance but the objective is to find a model that can describe the battery under a wide range of operations. They have shown to possess superior accuracy over the equivalent circuit models, particularly when a wider range of battery operation in terms of charge/discharge rate is desired. However, if the health of the battery is concerned, appropriate transformations between the model parameters and the actual battery parameters are required. To the best of our knowledge, there are no proposals that can relate the empirical models to actual battery parameters. Plett [87], has proposed the most prominent empirical models.

2.2.3 Electrochemical models (EM)

Electrochemical models rely on the actual physical laws that govern the motion of lithium ions in a battery which include mass and charge balances during the charge and discharge of the battery. They overcome the drawbacks of the aforementioned models, i.e. limited range validity and physical significance of the model parameters. However, the main problem with these models is their complicated mathematical nature. Doyle, Fuller and Newman originally developed the electrochemical models for Li-ion battery model [35, 41]. There have been many efforts to simplify or reduce the model equations and alleviate the problem of computational load [121, 120].

Due to the promising features of EM such as accuracy and physical significance of the model parameters, they are mainly employed for development of monitoring and estimation approaches in this thesis. This type of model is further discussed in the next section.

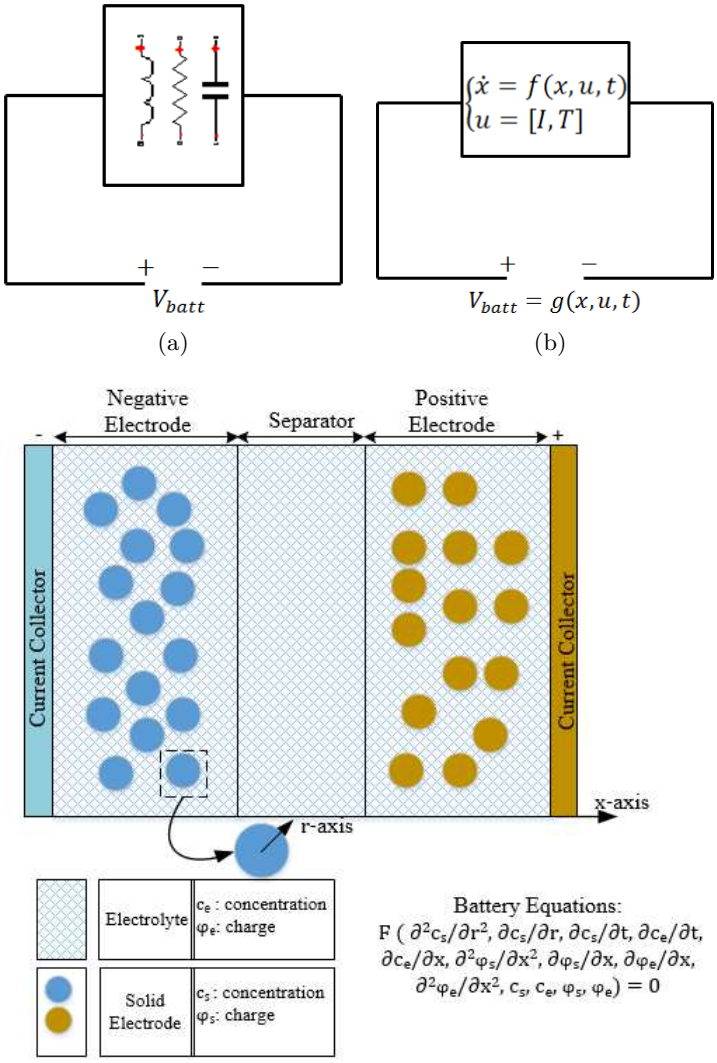

Figure 2.2: Schematic of different battery model structures: (a) Equivalent circuit model, (b) Empirical model where x represents the states of the model and u denotes the input which is generally composed of current and temperature, and (c) Electrochemical model which is composed of a set of algebraic partial differential equations describing the dynamics of the battery at each domain.

2.3 Electrochemical Model of Li-Ion Cell

In this part, we shall briefly explain the physics-based model of the battery expressed in terms of electrochemical equations. Fundamentally, the electrochemical governing equations of a Li-ion battery can be described by considering four basic equations, namely conservation of mass, which translates into concentration of Lithium in solid electrode phases and in liquid electrolyte phase, and conservation of charge in solid electrodes and liquid electrolyte phases.

The electrochemical equations are mainly expressed in terms of four field quantities, i.e. solid and electrolyte concentration ($c_s(r,x,t)$,$c_e(x,t)$) and solid and electrolyte potentials ($\phi_s(x,t)$,$\phi_e(x,t)$). These quantities obey Fick's law for diffusion, Ohm's law and Kirchhoff's law for charge transport, respectively, and are coupled through a well-known Butler-Volmer electrochemical kinetic equation expressing the rate of electrochemical reaction ($J_{Li,j}$).

To model the diffusion of Li-ions in solid and electrolyte phases, the active material of each electrode is approximated with continuum of sphere particles residing in a conducting porous matrix. The battery model presented here is considered in a pseudo-2 dimensional plane. The transport of lithium ions is modeled both along the main dimension, i.e. x-axis, and also within the particles which is modeled by adding a pseudo dimension, i.e. r-axis, in order to model the radial direction in the active material particles. Figure (2.3) shows the pseudo-2D dimension considered for the battery modeling. The battery equations are written for the three different parts of the battery, the negative electrode ($j = n$), the separator ($j = s$), and the positive electrode ($j = p$).

The conservation of lithium equation considers the flow of Li-ions in solid particles and electrolyte due to concentration-gradient-induced diffusion as follows:

$$\frac{\partial}{\partial t}c_{s,j}(x,r,t) = \frac{1}{r^2}\frac{\partial}{\partial r}\left(D_{s,j}r^2\frac{\partial c_{s,j}}{\partial r}\right), \quad j = n,p \tag{2.1}$$

$$\frac{\partial}{\partial t}\left(\epsilon_{e,j}c_e(x,t)\right) = \frac{\partial}{\partial x}\left(D_{eff,j}\frac{\partial c_e}{\partial x}\right) + (1-t_+^0)a_jFJ_{Li,j}(x,t), \quad j = n,s,p \tag{2.2}$$

The boundary conditions corresponding to Lithium ion conservation equations are given by:

$$\begin{aligned}
&\frac{\partial c_{s,j}}{\partial r}|_{r=0} = 0, \quad \frac{\partial c_{s,j}}{\partial r}|_{r=R_{s,j}} = -J_{Li,j}\\
&\frac{\partial c_e}{\partial x}|_{x=0^-} = 0, \quad \frac{\partial c_e}{\partial x}|_{x=L^+} = 0\\
&D_{eff,n}\frac{\partial c_e}{\partial x}|_{x=L^-} = D_{eff,s}\frac{\partial c_e}{\partial x}|_{x=0^{sep}}\\
&D_{eff,s}\frac{\partial c_e}{\partial x}|_{x=L^{sep}} = D_{eff,p}\frac{\partial c_e}{\partial x}|_{x=0^+}
\end{aligned} \tag{2.3}$$

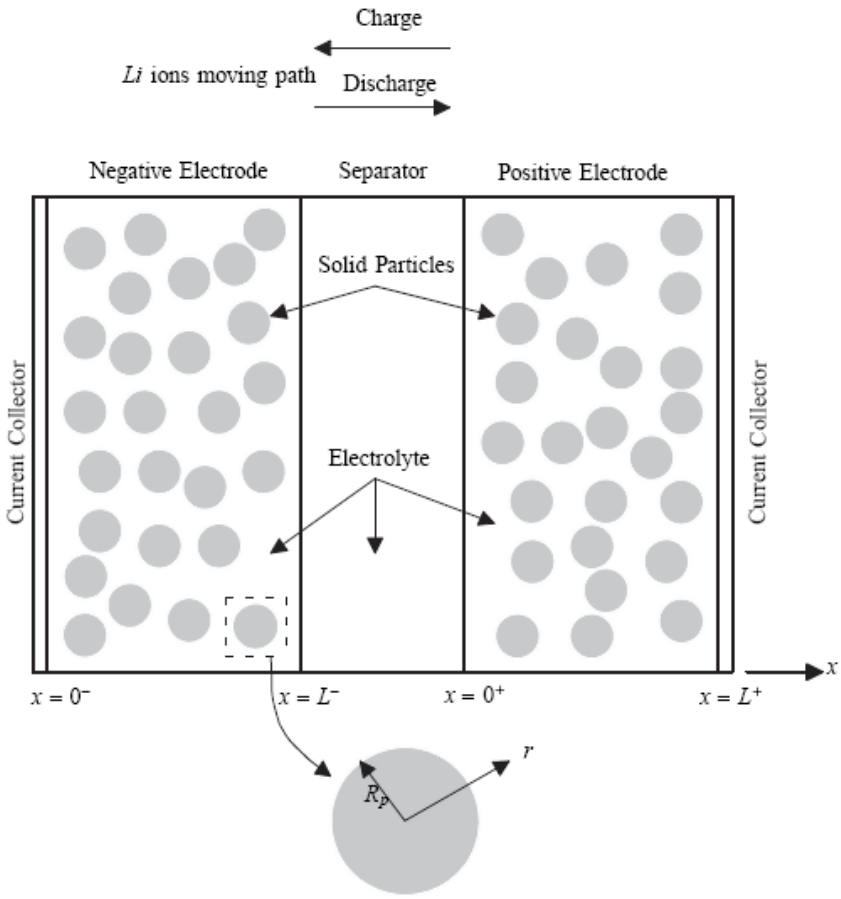

Figure 2.3: Schematic of a Lithium-ion battery where the active materials at electrodes are modeled with particle spheres embedded in a conducting porous matrix [33].

where c_s and c_e represent the concentration of lithium at solid state and electrolyte state, respectively. The parameter D_s expresses the diffusion coefficient of Li-ions at solid state, ϵ_e is the volume fraction of electrolyte phase, D_{eff} presents the effective diffusion coefficient at electrolyte phase that can be calculated as $D_{eff} = D_e \epsilon_e^p$, where D_e is diffusion coefficient and p is called Bruggeman coefficient. The conservation of charge in solid and electrolyte phases is expressed as follows:

$$\frac{\partial}{\partial x}\left(\sigma_{eff,j}\frac{\partial \phi_{s,j}(x,t)}{\partial x}\right) = a_j F J_{Li,j}(x,t), \quad j = n,p \tag{2.4}$$

$$-\frac{\partial}{\partial x}\left(\kappa_{eff,j}\frac{\partial \phi_e(x,t)}{\partial x}\right) + \beta\frac{\partial}{\partial x}\left(\kappa_{eff,j}\frac{\partial \ln c_e}{\partial x}\right) = a_j F J_{Li,j}(x,t), \quad j = n,s,p \tag{2.5}$$

The boundary conditions corresponding to charge equations are given by:

$$\begin{cases} -\sigma_{eff,n}\dfrac{\partial\phi_{s,n}}{\partial x}|_{x=0^-} &= -I \\ -\sigma_{eff,p}\dfrac{\partial\phi_{s,p}}{\partial x}|_{x=L^+} &= -I \\ \dfrac{\partial\phi_{s,n}}{\partial x}|_{x=L^-} &= 0 \\ \dfrac{\partial\phi_{s,p}}{\partial x}|_{x=0^+} &= 0 \end{cases} \tag{2.6}$$

$$\begin{cases} \dfrac{\partial\phi_e}{\partial x}|_{x=0^-} &= 0 \\ \dfrac{\partial\phi_e}{\partial x}|_{x=L^+} &= 0 \\ -\kappa_{eff,n}\dfrac{\partial\phi_e}{\partial x}|_{x=L^-} &= -\kappa_{eff,s}\dfrac{\partial\phi_e}{\partial x}|_{x=0^{sep}} \\ -\kappa_{eff,s}\dfrac{\partial\phi_e}{\partial x}|_{x=L^{sep}} &= -\kappa_{eff,p}\dfrac{\partial\phi_e}{\partial x}|_{x=0^+} \end{cases} \tag{2.7}$$

where ϕ_s and ϕ_e represent the electric potential at solid and electrolyte phases, respectively, σ_{eff} and κ_{eff} represent the effective conductivity and ionic conductivity at solid electrode and electrolyte, respectively. These effective values can be calculated as $\sigma_{eff} = \sigma\epsilon_s$ and $\kappa_{eff} = \kappa\epsilon_e^p$ where σ is solid phase conductivity, κ is electrolyte phase ionic conductivity and ϵ_s indicates the active material volume fraction. The parameter a_j stands for specific interfacial area and β is a coefficient representing the diffusion conductivity.

The above set of partial differential equations (PDE) (2.1-2.7) is coupled with the following algebraic Butler-Volmer equation presenting the molar flux $J_{Li,j}$ of lithium ions at the surface of spherical particle. The value of $J_{Li,j}$ which is related to the rate of reaction at electrode surface is exponentially related to the positive and negative electrode overpotentials. The overall cell overpotential at various state of charge contains components of kinetic, ohmic and concentration overpotentials.

$$J_{Li,j}(x,t) = i_{0,j}(x,t) \times \left[exp\left(\frac{\alpha_a F}{RT}\eta_j(x,t)\right) - exp\left(-\frac{\alpha_c F}{RT}\eta_j(x,t)\right)\right] \quad j = n,p \tag{2.8}$$

where $i_{0,j}$ denotes the exchange current density and η_j the over-potential. They are given as follows:

$$i_{0,j}(x,t) = k_j\left(c_e(x,t)\right)^{\alpha_a}\left(c_{s,max,j} - c_{s,surf,j}(x,t)\right)^{\alpha_a} \cdot \left(c_{s,surf,j}(x,t)\right)^{\alpha_c} \tag{2.9}$$

$$\eta_j(x,t) = \phi_{s,j}(x,t) - \phi_e(x,t) - U_j\left(c_{s,surf,j}(x,t)\right) \tag{2.10}$$

where $c_{s,surf,j}$ denotes the concentration at the surface of solid particle and U_j the open circuit voltage. The open circuit voltage is dependent only on the surface concentration. The overall set of equations (2.4-2.8) constitute a set of partial-differential-algebraic-equations (PDAE) that can describe the dynamics of a typical Li-ion battery. The nomenclature of

the battery model and corresponding boundary conditions to this model are given in the Appendix A. The voltage of the battery is defined as the difference between the potentials at the two terminals as follows:

$$V(t) = \phi_{s,p}(x = L^+, t) - \phi_{s,n}(x = 0^-, t) \tag{2.11}$$

2.3.1 Discretization

Equations (2.1-2.5) are discretized and solved together to find the field quantities of interest at each (x, r, t) [51]. All domains, i.e. negative electrode, separator and positive electrode, are discretized along the x-axis into N_n, N_s, and N_p control volumes, respectively. The r-dimension regarding to the diffusion of Lithium ions in solid particles is also discretized into N_r control volumes. A typical volume for the pseudo 2-dimensional system is shown in Figure (2.4).

Thus, at every x-coordinate, we have $N_r + 3$ unknowns for electrode domains which are corresponding to $c_{s,j}(1 : N_r)$, c_e, ϕ_s, and ϕ_e and 2 unknowns for separator domain which are due to c_e, and ϕ_e. Discretization of the Equations (2.1-2.5) gives the following system:

$$\begin{aligned}
\frac{dc_{s_1}}{dt} &= \frac{D_s}{r_1^2}\frac{r_2^2(c_{s_2} - c_{s_1})}{\Delta_r^2} \\
\frac{dc_{s_q}}{dt} &= D_s\left[\frac{1}{\Delta_r^2}(c_{s_{q+1}} + c_{s_{q-1}}) - \frac{2}{\Delta_r^2}c_{s_q}\right. \\
&\quad \left. + \frac{1}{\Delta_r}\frac{1}{r_q}(c_{s_{q+1}} - c_{s_{q-1}})\right], \quad q = 2, \ldots, N_r - 1 \\
\frac{dc_{s_q}}{dt} &= -\frac{r_{q+1}^2}{r_q^2\Delta_r}\frac{J_{Li_i}}{D_s} - \frac{D_s}{r_q^2}\frac{r_{q-1}^2(c_{s_q} - c_{s_{q-1}})}{\Delta_r^2}, \quad q = N_r \\
\epsilon\frac{dc_e}{dt} &= D_{eff}\frac{c_{e_{i+1}} - 2c_{e_i} + c_{e_{i-1}}}{\Delta_x^2} + (1 - t_+^0)a_j F J_{Li_i} \\
a_j F J_{Li_i} &= \sigma_{eff}\frac{\phi_{s_i+1} - \phi_{s_i} - \phi_{s_{i-1}}}{\Delta_x^2} \\
a_j F J_{Li_i} &= -\frac{\kappa_{eff_{i^+}}(\phi_{e_{i+1}} - \phi_{e_i}) - \kappa_{eff_{i^-}}(\phi_{e_i} - \phi_{e_{i-1}})}{\Delta_x^2} \\
&\quad + \frac{\kappa^D_{eff_{i^+}}(c_{e_{i+1}} - c_{e_i}) - \kappa^D_{eff_{i^-}}(c_{e_i} - c_{e_{i-1}})}{\Delta_x^2}
\end{aligned} \tag{2.12}$$

where $\Delta_x = L_j/N_j$ for 3 domains of $j = n, s, p$, $\Delta_r = R_s/N_r$, $r_q = q\Delta_r$, $\kappa^D_{eff} = \kappa_{eff} \cdot \beta/c_e$, $\kappa_{eff_{i^\mp}} = \dfrac{2\kappa_{eff_{i\mp1}}\kappa_{eff_i}}{(\kappa_{eff_{i\mp1}} + \kappa_{eff_i})}$ and similarly for $\kappa^D_{eff_{i^\mp}}$. The above system is solved for $i = \{1 : N_n + N_s + N_p\}$ and the respective values of each domain is substituted for each parameter. The surface concentration is indicated as $c_{s,surf} = c_{s_{N_r}}$.

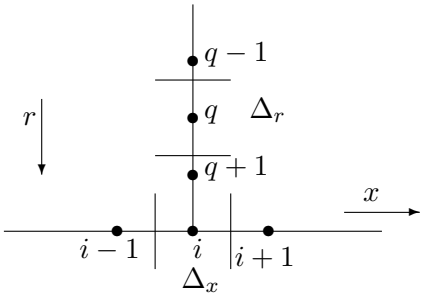

Figure 2.4: A typical control volume

2.3.2 Model Reduction

For automotive applications, a simplified battery model that delivers a good accuracy while ensuring the maximum computational cost reduction is required. Hence, due to the complicated nature and high computational load of associated PDAEs of the battery model, there has been many efforts to reduce the order of the model or approximate the model with a state space model.

As discretization of the full model Eq. (2.12) shows, most of the unknowns are extracted from the discretization of the diffusion equation (2.1) inside the particle with associated boundary conditions (2.3). Therefore, simplifying or reduction of diffusion equation has been the core of many of the reduction methods. This is generally called Macro-Micro scale coupled simulation or reformulation of diffusion in solid phase [51]. In this Thesis, we have adopted a Macro-Micro model proposed by Subramanian et. al. [121].

In this model, the electrolyte concentration $c_e(x,t)$ is assumed to be uniform and the radial distribution of the Li concentration in solid phase is approximated with a fourth order polynomial as follows:

$$c_j(x,r,t) = \gamma_{1,j}(t) + \gamma_{2,j}(t)\frac{r^2}{R_{s,j}^2} + \gamma_{3,j}(t)\frac{r^4}{R_{s,j}^4},\ j = n,p. \tag{2.13}$$

The mass transfer in the solid material is expressed in terms of volume averaged concentration ($\bar{c}_s(x,t)$), particle surface concentration ($c_{se}(x,t)$), and averaged concentration flux ($\bar{q}_s(x,t)$), where the volume is $V_R = 4/3\ \pi R_s^3$.

$$\bar{c}_s(x,t) = 1/V_R \int_{r=0}^{R_s} c_s(r,x,t)\cdot 4\pi r^2 dr \tag{2.14}$$

$$\bar{q}_s(x,t) = 1/V_R \int_{r=0}^{R_s} \left(\frac{d}{dr}c_s(r,x,t)\right).4\pi r^2 dr \tag{2.15}$$

$$c_{se}(x,t) = c_s(r=R_s,x,t) \tag{2.16}$$

Substitution of Eq.(2.13) into Eqs.(2.1) and (2.3) and evaluating the values given in Eqs.(2.14)-(2.16) will result in the following equations for coefficients in Eq.(2.13):

$$\gamma_{1,j}(t) = \frac{39}{4}c_{se,j} - 3R_s\bar{q}_{s,j} - \frac{35}{4}\bar{c}_{s,j} \tag{2.17}$$

$$\gamma_{2,j}(t) = -35c_{se,j} + 10R_s\bar{q}_{s,j} + 35\bar{c}_{s,j} \tag{2.18}$$

$$\gamma_{3,j}(t) = \frac{105}{4}c_{se,j} - 7R_s\bar{q}_{s,j} - \frac{105}{4}\bar{c}_{s,j} \tag{2.19}$$

Hence, the concentration profile given by Eq.(2.13) is now derived in terms of the volume-averaged concentration ($\bar{c}_s(x,t)$), the volume-averaged concentration flux ($\bar{q}_s(x,t)$), and the surface concentration ($c_{se}(x,t)$). Now, we shall derive three equations to solve for the average concentration, the surface concentration, and the average flux. The equation for the volume-averaged concentration is obtained by volume averaging the entire governing Eq.(2.1) as follows:

$$\int_{r=0}^{R_s} 3\frac{r^2}{R_s^2}\left[\frac{\partial c_s}{\partial t} - D_s\frac{1}{r^2}\frac{\partial}{\partial r}\left(r^2\frac{\partial c_s}{\partial r}\right)\right] d\left(\frac{r}{R_s}\right) = 0 \tag{2.20}$$

The second equation for the volume-averaged flux is obtained by volume averaging the differential of the governing equation (2.1) as follows:

$$\int_{r=0}^{R_s} 3\frac{r^2}{R_s^2}\frac{\partial\left[\frac{\partial c_s}{\partial t} - D_s\frac{1}{r^2}\frac{\partial}{\partial r}\left(r^2\frac{\partial c_s}{\partial r}\right)\right]}{\partial r} d\left(\frac{r}{R_s}\right) = 0 \tag{2.21}$$

The third equation is also obtained by evaluating the boundary condition at $r = R_s$ and the total set of equations is given as:

$$\frac{\partial}{\partial t}\bar{c}_{s,j}(x,t) = -\frac{3}{R_{s,j}}J_{Li,j}(x,t) \tag{2.22}$$

$$\frac{\partial}{\partial t}\bar{q}_{s,j}(x,t) = -\frac{30D_{s,j}}{R_{s,j}^2}\bar{q}_{s,j}(x,t) - \frac{45}{2R_{s,j}^2}J_{Li,j}(x,t) \tag{2.23}$$

$$c_{se,j}(x,t) = \bar{c}_{s,j} + \frac{8R_{s,j}}{35}\bar{q}_{s,j} - \frac{R_{s,j}}{35D_{s,j}}J_{Li,j}(x,t) \tag{2.24}$$

Considering the assumption of the uniformity of the electrolyte concentration, c_e, will also simplify the Eqs.(2.2,2.4,2.5) for negative and positive electrode (i.e. $j = n, p$) as follows:

$$\frac{\partial}{\partial x}i_{e,j}(x,t) = \frac{3\epsilon_{s,j}}{R_{s,j}}FJ_{Li,j}(x,t) \tag{2.25}$$

$$\frac{\partial}{\partial x}\phi_{s,j}(x,t) = \frac{i_{e,j}(x,t) - I(t)}{\sigma_{eff,j}} \tag{2.26}$$

$$\frac{\partial}{\partial x}\phi_{e}(x,t) = -\frac{i_{e,j}(x,t)}{\kappa_{eff,j}} \tag{2.27}$$

The electrolyte dynamics in separator is also simply added by:

$$\frac{\partial}{\partial x}\phi_{e}(x,t) = -\frac{I}{\kappa_{eff,s}} \tag{2.28}$$

The molar flux follows the Eq.(2.8) where

$$i_{0,j}(x,t) = k_j \left(c_e(x,t)\right)^{\alpha_a} \left(c_{s,max,j} - c_{se,j}(x,t)\right)^{\alpha_a} \cdot \left(\bar{c}_{s,j}(x,t)\right)^{\alpha_c} \tag{2.29}$$

$$\eta_j(x,t) = \phi_{s,j}(x,t) - \phi_e(x,t) - U_j\left(c_{se,j}(x,t)\right) \tag{2.30}$$

The set of Equations (2.22-2.28) can be solved by considering the following set of initial and boundary equations using control volume discretization.

$$\begin{aligned}
&\bar{c}_{s,j}(x,t=0) = \bar{c}^0_{s,j},\ j = n,p \\
&\bar{q}_{s,j}(x,t=0) = \bar{q}^0_{s,j},\ j = n,p \\
&i_{e,n}(x=0^-,t) = 0, && i_{e,n}(x=L^-,t) = I(t) \\
&i_{e,p}(x=0^+,t) = I(t), && i_{e,p}(x=L^+,t) = 0 \\
&\phi_{s,n}(x=0^-,t) = 0.
\end{aligned} \tag{2.31}$$

The simulation studies shows some discrepancy between the macro-micro model and full model in high charge/discharge rates. However, in low/medium rates, the results of this model can track the full model results [51].

2.4 Battery Management System

BMS is considered as the brain of the battery, which consists of electrical circuits and embedded algorithms to operate battery system safely and efficiently according to the demands of other vehicle components. It is basically comprised of sensors, actuators and controllers which have various algorithms and signal wires [70]. There is still no consensus about the BMS tasks, however we adopt the broad view of an advanced BMS tasks. Its tasks can generally be classified under "Monitoring" and "Control" categories. Figure (2.5) shows the schematic of a typical BMS and some basic functions. In the following, some of the main features and function requirements of BMS are reviewed.

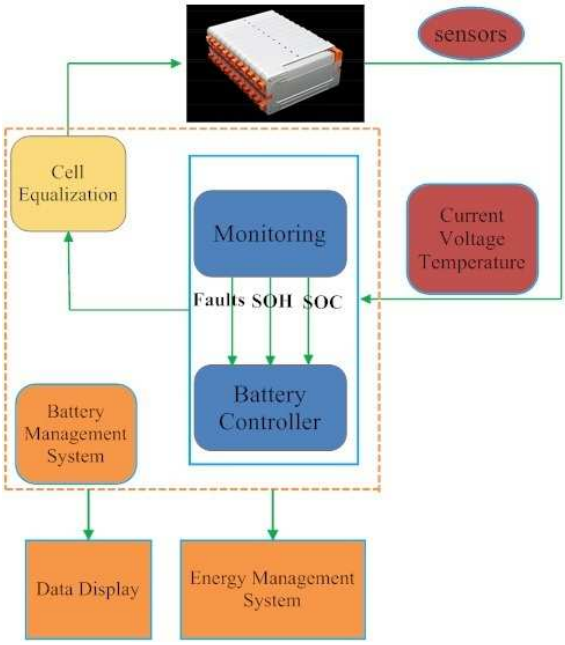

Figure 2.5: An overview of BMS functions.

2.4.1 Monitoring

Monitoring includes all the functions that measure or estimate the main parameters of concern and pass it either to the user or control functions. The main monitoring functions can be defined as:

1. **Measurement (Data Acquisition)**: It includes measurement of physical parameters such as current and voltage of the battery cells and the temperature distribution inside and outside of the battery pack. This information forms the basis for other tasks of BMS. Measurement of other parameters of the battery such as impedance, etc would also be highly desirable from control point of view, however, with the current technology normally is infeasible during the normal operation of the battery. As a result, certain parameters of the battery are usually need to be estimated.

2. **Estimation**: The condition of the battery is mainly described through three indicators which are state of charge (SoC), state of health (SoH), and state of life (SoL). These parameters are not directly measurable and thus need to be inferred based on the available measurement from the battery along with estimation of other quantities of interest. Depending on the adopted estimation method, certain other parameters of the battery might also be needed.

   Safety monitoring of the battery might also require certain parameters of the battery such as impedance, physical properties of battery components such as electrolyte or

solid material, etc. Those parameters would also need estimation schemes if they are not directly measured. This will be explored more in the Chapter 3.

3. **Fault Detection and Diagnosis (Safety Monitoring)**: There are a number of different sources for faults within the battery management system including sensor faults, actuator faults, power electronics circuits faults (i.e. charging circuit, safety circuits, cell balancing circuit, etc), network faults and battery faults. The BMS is responsible to monitor the system and detect all the faults and produce appropriate signals.

   Battery faults can generally be classified into two category of abrupt and gradual faults. Gradual faults can be attributed to the aging of the battery and thus need to be considered within the battery estimation module. The abrupt faults are those failures that might lead to immediate hazardous conditions and need immediate treatment by the BMS. They can generally be identified as overcharge, overdischarge, electrical leakage, high temperature, short-circuiting, case rupture, over-fast temperature rise, etc. These processes need immediate action and response by the BMS.

2.4.2 Control

The control tasks of BMS are generally concerned with the management of charge/discharge scheme and thermal management of the battery. The objective is to control these processes such that the demands of the system are met with maximum efficiency, the life-span of the battery is enhanced, and safety of the system is guaranteed.

1. **Safe and Optimal Utilization of the Battery:** The charge/discharge scheme of the battery should be controlled such that the battery is kept within the safe margins. Moreover, another control objective is to optimize the battery's life-time. Therefore, information collected by monitoring from the age of the battery is crucial to optimal utilization of the battery. This also has a close link with energy optimization in hybrid vehicles.

2. **Cell Balancing**: The aim of the cell balancing circuit is to balance the cells within a pack while they are charging or discharging to make sure that their state of charge remain the same or within a very narrow band, and hence, there is no danger of over-charge or over-discharge of the cells. Even an over-charge/discharge of one single cell within a pack can put the cell in danger of a thermal runaway that can eventually lead to an explosion in the whole pack. This topic is visited with more details in Chapter 6.

3. **Thermal Management**: Advanced BMS should be capable of collecting the temperature distribution over the battery pack. Based on the demands of the system and

the desired performance requirements, it can then decide to cool or heat the battery system.

4. **Energy Optimization**: Hybrid vehicles have multiple sources of energy, i.e. battery and gasoline-powered internal combustion engine or ultra capacitor, fuel cell, etc. Hence, a unit is required to optimally manage the contribution of each source to satisfy the overall energy demands of the vehicle. Different characteristics such as energy efficiency, emission, and battery life time, are considered to formulate the energy optimization algorithm.

2.5 Summary

This chapter provides an introduction to Li-ion battery principles. The main focus of this Thesis is on model-based approaches and therefore, the modeling approaches developed for battery are reviewed. The first principles physics-based model of the Li-ion battery is reviewed with some details. The monitoring approaches that are developed in the next chapter are centered around this model. Moreover, the objectives, components, tasks and challenging issues of a battery management system are also briefly reviewed.

Chapter 3

Battery Monitoring

3.1 Performance Metrics in a Battery

Monitoring of the battery is a field in which the current battery conditions are studied and future performance of the battery is predicted in terms of certain measurements. The most desirable performance metrics for a battery are basically a measure of how much energy is stored in the battery and how long the stored energy can be used given the load demand (i.e., current $I(t)$). For this purpose, the most commonly used parameters for characterizing a battery's performance are the state of charge (SoC) and state of health (SoH) of the battery.

3.1.1 State of Charge (SoC)

The ratio of concentration of lithium in the solid electrode to its maximum possible concentration is defined as the state of charge (SoC) of the battery [23]. This definition assumes 100% of useable lithium ion in negative electrode at full charge state (100% SoC), and 100% lithium ion extraction from the negative electrode in fully discharged cell (0% SoC), assuming no excess anode or cathode. The SoC term in fact characterizes the available energy in the battery. In other words, it is the fuel gauge of the battery, and hence, represents the most prominent parameter in BMS design. Bulk SoC is a measure of average utilization of the entire electrode and is defined as follows [23]:

$$SoC_j^b(t) \triangleq \frac{3}{L_j R_{s,j}^3} \int_{x=0_j}^{L_j} \int_{r=0}^{R_{s,j}} r^2 \frac{c_{s,j}(x,r,t)}{c_{s,max,j}} dr dx, \;\; j = n(-), p(+) \tag{3.1}$$

Surface SoC is also defined as the utilization at the surface of the solid particle. This measure is directly related to the instantaneous available power in the cell, and is generally defined as:

$$SoC_j^s(t) \triangleq \frac{1}{L_j} \int_{x=0_j}^{L_j} \frac{c_{s,surf,j}(x,t)}{c_{s,max,j}} dx \tag{3.2}$$

3.1.2 State of Health (SoH)

In contrast to SoC, there is not an established definition for state of health (SoH) of a battery. This parameter, though very important in battery management, has found different definitions in the literature. In a broad physical meaning, SoH has been defined as the *"ability of a cell to store energy, source and sink high currents and retain charge over extended periods relative to its initial or nominal capabilities"* [11, 57]. From this perspective, SoH covers a broad range of physical conditions of a battery such as loss of nominal capacity due to aging (external behavior), or corrosion (internal behavior) [62]. In some cases, particularly for HEV applications, initial SoH is defined in terms of the energy density of fresh cell, and life span of the battery is considered to the point that final SoH reaches the minimum of 80% of the initial energy density. However, this definition has not yet been considered as a common performance metric among the researches.

There is also another variable defined for battery health monitoring, identified as State of Life (SoL). It refers to the remaining life of the battery. SoL tries to predict how many more (charge/discharge) cycles the battery would be usable. However, SoL prediction is a very complicated problem that has a close relationship with monitoring the age of the battery and needs much more research scrutiny from an electrochemical point of view.

3.2 Literature Review

In this section, we will briefly review the proposed methods for SoC and SoH estimation available in the literature. The features of each method, and the remaining challenges are also explored in this section.

3.2.1 SoC Estimation

SoC estimation methods are generally divided into direct and indirect methods [22]. Direct methods measure the SoC based on the calculation of energy usage of the battery and are generally recognized as ampere-hour (coulomb) counting methods. The general formula for the method is given in Eq.(3.3), where Q denotes the nominal capacity of the battery and I is the current. The drawback is that initial SoC needs to be known and these methods suffer from accumulation of error due to the integration involved in the process. Conventionally, η is considered equal to 1, however, there have been some modifications using intelligent methods to improve the performance of the method by adjusting η adaptively [22, 45].

$$SoC = SoC_0 - 1/Q \int_{t_0}^{t} \eta I(\tau) d\tau \tag{3.3}$$

Indirect methods try to estimate the SoC using the measurement or calculation of some other parameter. They are generally divided into *data-based* and *model-based* methods.

Data-based methods employ the impedance [98, 19, 36] or open-circuit voltage of the battery [114, 91] to evaluate the SoC. The drawback of these methods is that they need some extra measurements that is generally not available in real-time. Another category of data-based methods are artificial intelligence-based methods where fuzzy logic [68, 110] or neural network [21] methodologies are adopted to develop a SoC estimation technique. The drawback of these methods is that their accuracy is highly dependent to the training data. Therefore, they are only accurate for a specific battery chemistry with the characteristics that are captured by training data set. Hence, model-based methods have attracted the most research efforts due to the feasibility of real-time application and promising results. The model-based methods consider a model for the battery, i.e. the models discussed in Chapter 2, and apply estimation approaches to evaluate the SoC. The main applied estimation techniques are as follows:

1. **Filter Design**: Suppose the discrete-time model for the battery is provided as follows:

$$\begin{aligned} x(k+1) &= F(x(k), u(k)) + G(x(k), u(k))w(k) \\ y(k) &= H(x(k), u(k)) + v(k) \end{aligned} \tag{3.4}$$

where x denotes the states of the system, y the output and u the input. v and w indicate the process (state) and observation (measurement) noise, respectively. Function F, G and H represent some nonlinear mapping. In the battery model, the states of the system include SoC and maybe some other quantities of the system, output is usually the voltage and the input could be current and temperature of the system. The aim is to estimate the states of the system, given the outputs. Filtering methods consider this problem in a stochastic setting where the goal is to determine conditional density of state given the outputs (i.e. measurements) as $p_{x|y}(x(T)|Y(T))$ where $Y(T) = \{y(0), y(1), \dots, y(T)\}$, and T denotes the current sample time. Kalman filter-based methods are the major filtering approaches that have been developed for this problem [109, 95].

Kalman Filter: Kalman filter (KF) is derived as the optimal solution to the above problem for unconstrained, linear systems (i.e. F and H are linear mappings) subject to normally distributed process and measurement noise (i.e. $G = I$, w and v are normal Gaussian noise). However, the battery model is usually a nonlinear system , so the KF is not directly applicable. For nonlinear system estimation, extended Kalman filter (EKF) and unscented Kalman filter (UKF) are developed based on the principles of KF. EKF linearizes the nonlinear system, then applies the Kalman filter to obtain the state estimates [115]. EKF has extensively employed for SoC estimation using different model structures [33, 101, 88, 64, 65].

In contrast, UKF do not linearize the model at a single point but represent the nonlinear response by several points, namely sigma points and their associate weights [52]. UKF is also applied for battery state estimation [102, 89]. The interested reader is referred to [109] for more details on principles of Kalman filter-based methods.

2. **Observer Design**: Another approach to the state estimation problem is to design a new system, namely an observer, that attempts to estimate the internal states of the original system. Consider the system (3.4), the idea of an observer is to design a system as:

$$\begin{aligned} x_o(k+1) &= F_o(x_o(k), u(k), y(k)) \\ y_o(k) &= H_o(x_o(k), u(k)) \end{aligned} \tag{3.5}$$

where the residual $e = x_o - x$ converges to zero as k increases. A few observers have been developed for battery estimation. Klein et al. [60] applies a Luenberger observer to electrochemical model of the battery where the stability of the observer is not proved. Kim [56] develops a sliding mode observer for an equivalent circuit model of the battery. Moura et. al. [76] reduces the electrochemical model of the battery and then applies a back-stepping observer for the SoC estimation.

3. **Challenge**: The proposed algorithms are compared along with their features in Table 3.1. As mentioned, the model-based algorithms present the most promising algorithms for advanced BMS. Nevertheless, there are still a number of challenging issues regarding the accuracy, complexity, computational load and universality of the proposed algorithms. Some of the existing challenges are reviewed in the following:

   (a) The electrochemical model (EM) of the battery presents the most accurate model of the battery, however the complexity of partial differential equations (PDE) involved, pose many challenges for available estimation techniques. In fact, the literature in the control community dealing with PDEs is rather limited and narrow, where most of the observer or filter design methods are basically developed for systems described by a set of ordinary of differential equations (ODE). Hence, most of the work have been centred around reduction of the PDEs to ODEs and deriving a state space model (Eq.3.4) [33, 101] or simplification of PDEs such that limited existing tools for systems described by PDEs would be applicable [76].

   (b) Most of the work in the area of battery modeling and estimation, particularly algorithms using EM, is developed for a battery electrode and single cell. In reality, and for vehicle applications, we have to deal with battery modules and

packs. Battery module is a set of battery cells connected in series or parallel and battery pack is then assembled by connecting modules together, again either in series or parallel or a mix of both to deliver the desired voltage, capacity, or power density.

A number of issues such as large number of cells, spatial distribution of cells and their implication on the modeling, or temperature distribution in a battery module/pack, present new challenges and add another dimension to the battery modeling and estimation that needs to be investigated. The work developed in this chapter falls under the category of "Indirect Model-based Method" where unlike Kalman filter methods, reduction of battery equations are not required.

Table 3.1: Comparison of the SOC estimation methods.

Methods	Category	Advantages	Disadvantages
Coulomb (A-h) counting	Direct Method	Easy to implement	Inaccurate due to error accumulation unless the initial SoC is exactly known
Open-Circuit Voltage	Indirect Data-based Method	Accurate, Low computational load	Offline (needs the battery to be in the resting mode before measurement)
Impedance Spectroscopy	Indirect Data-based Method	Accurate, Complete information about battery conditions	Difficult to implement, Expensive method, Offline
Intelligent Method (Fuzzy - Neural Network)	Indirect Data-based Method	Doesn't need model, Easy to implement	Accuracy is strongly dependent to the richness of training data, chemistry-specific and not universal
Kalman Filter	Indirect Model-based Method	Accurate (if the model is accurate)	High computational load, needs reduction of electrochemical models to be implemented
Observer Design	Indirect Model-based Method	Accurate (if the model is accurate)	Nonlinear, Not easy to implement

3.2.2 Estimation of SoH

As mentioned in Section 3.1.2 , SoH determination has not found an established framework in the literature. This metric generally refers to deterioration of the battery condition with respect to its nominal condition. In general, different parameters that have a strong correlation to performance fade of battery are utilized for this purpose. Hence, different laboratory methods have been developed and used for measuring the health of a battery. X-ray methods, Voltammetry, Impedance spectroscopy, Galvanostatic intermittent method,

voltage or current pulse, are to name but a few [38, 80]. However, most of these methods are not suitable for real-time monitoring of a battery and thus not appropriate for practical use. A common practice in this field has been impedance measurement method [98, 36]. Despite its good accuracy, this method is not appropriate for online monitoring and requires off-line operation of the battery where a frequency rich test signal is applied and extensive measurements are taken.

Recent approaches for online monitoring of battery are mostly based on equivalent circuit model of the battery [57], or an empirical model [88], and they exploit estimation techniques to evaluate the state of the health of the battery. In the proposed methods, some parameter in the battery model are attributed to SoH, and parameter estimation methods are employed to determine the SoH. For instance, monitoring of a particular resistance or capacitance in equivalent circuit model is associated with SoH prediction [57]. Different algorithms such as least-square methods [77, 96] and Kalman filter [88] have been employed for this purpose. Considering a dynamic for the SoH and augmenting it to the battery model and employing state estimation techniques is also examined in [57]. However, the parameters of empirical or equivalent circuits do not necessarily represent any physical quantity but may only point to a phenomena within the battery. Hence, monitoring of the electrochemical model parameters can provide a more comprehensive framework for SoH determination. In this regard, Moura et. al. [77] has developed a parameter estimation technique of a reduced-order electrochemical model.

Development of appropriate models that could incorporate the battery's aging process is promising for health monitoring of the battery and deserves further research. This topic is explored with more details in Chapter 5.

3.3 Proposed Methodology

3.3.1 State Estimation

As discussed in Section 2.2.3, the focus of this Thesis is to employ the EM model for monitoring and estimation due to its desirable features such as accuracy, scalability and physics-based significance of the parameters in comparison with ECM and EPM models. There have been some attempts in recent years to use EM model for battery estimation by applying Kalman filtering (KF) or observer design techniques. Nevertheless, still most of these works resort to a simplified model (e.g. Single-Particle model) [101, 102] for estimation where spatial distribution of Li concentration and current density in the battery is not being engaged in the equations. The operating range over which the model is valid is also limited. Observer-design is also hindered by some issues affecting the observability of the system when both electrodes are considered [33].

Santhanagopalan and White [101, 102] apply both EKF and UKF to single particle (SP) model of the battery to estimate the SoC. However, as reported by [101], SP model is valid

for a limited range of charge/discharge rates. Moreover, voltage and current density are basically dependent on solid and electrolyte potentials where the corresponding equations are not considered in SP model. Hence, the applied filter needs to resort to numerical calculation of output derivatives which could be a source of error accumulation and impractical in a noisy environment. The work in [33] presented a more accurate model, namely average model, where the spatial dependence of Butler-Volmer current is still ignored. Based on this model, an EKF is applied for state of charge estimation. This algorithm is limited to a confined range of operation in terms of charge/discharge rate and temperature as well.

In this Thesis, we have proposed new estimation methodology for SoC based on particle filtering method. Particle filter (PF) has emerged as a powerful estimation technique where it removes the restrictive assumptions imposed on dynamic and form of conditional density (e.g. the requirement for it to be Gaussian) by Kalman filtering methods. In fact, PF presents an implementation of the Bayes Filter that can approximate the posterior distribution of the states with a set of weighted samples. This property introduces PF as an appealing estimator candidate to handle a wide range of general, non-Gaussian and nonlinear processes. Recent works have demonstrated the superiority of PF over Kalman based variants in dealing with nonlinear systems [95]. More importantly, the enticing feature of PF for us is that it is not necessary to simplify the partial differential equations describing the battery dynamics to a similar-state space model to be KF- applicable. Particle filters are applicable to any kind of equations without the need to change them. Hence, it can provide us with the desired feature of tracking the system in its entire range.

3.3.2 State and Parameter Estimation

Another area of concern in battery monitoring is SoH monitoring. This Thesis present a method for parameter estimation of the battery where the result can be helpful in assessment of the degradation of the battery. In fact, battery degradation reflects on battery parameters' variations over time. In this capacity, the proposed method can be viewed as a significant contribution towards the estimation of SoH.

To date most of the research works on battery estimation consider the model parameters to be known and constant for the estimation purposes. However, it is well known that batteries degrade over time and thus the parameters of the batteries slowly change over time. This consideration has been missing in most of the works in the area of battery estimation.

There are few works that have considered parameter estimation for the lithium-ion battery. Santhanagopalan et. al. [103] have made the most contribution to this field. They have presented a framework for estimation of the battery parameters using the Levenberg-Marquardt method. This method, however powerful, has two drawbacks. First, it needs calculation of Jacobian of the output with respect to the battery parameters, where in the complicated structure of battery dynamics, as shown in Section 2.3, this is a troublesome

task. Second, this method is an offline method or at least requires an accurate set of data in advance. Moura et. al. [77] recently tackled this problem from another angle by proposing an interesting PDE estimation technique using PDE swapping identifiers and least square methods. To implement this, however, they simplified the battery model significantly where many parameters do not appear in the battery model. Moreover, [77] assumes full-state measurements which is not a realistic assumption unless the parameter estimation and state estimation are being merged in one framework.

In present work, we approach the problem by proposing a simultaneous state and parameter estimation in a Bayesian framework. In this framework, the parameters and states of the system can be estimated in an online manner where full electrochemical model of the battery is taken into account. This algorithm provides an appropriate framework for study of battery degradation as well. Considering the fact that parameters are changing in a slower time-scale than the states, the algorithm introduces a multi-rate estimation framework in which the states and parameters are being estimated on different time scales.

3.4 An Electrochemical Model-Based Particle Filter Approach for Lithium-ion Battery Estimation

The objective is to estimate the state of charge of battery using the electrochemical model. A particle-filter approach is developed for this purpose. In this work, the reduced-order model (see Section 2.3.2) is considered for simulations, however, the developed algorithm would be well extendible to the full electrochemical model of the battery, albeit with much higher computational load.

The parameter of interest in estimation is often the SoC of the battery for which Bulk SoC and Surface SoC (Eqs.(3.1),(3.2)) were defined. Since the reduced order model is employed, surface SoC (3.2) is considered for estimation where $c_{s,surf,j}(x,t) = c_{se,j}(x,t)$, and $c_{se,j}$ is given in (2.24). The particle filter algorithm is presented in the following subsection.

3.4.1 An Overview on State Estimation Problem

Before discussing the particle filter algorithm, the state estimation problem in a probabilistic framework is briefly reviewed. The basic statement of state estimation problem is to determine an estimate of the system states given its model and a sequence of noisy observations (measurements) from the system. This implies that the complete solution to the estimation problem is provided by the probability density function $p(x_t|Y_s)$[1], where x_t represent the states of the system at time t, and $Y_s = \{y_1, ..., y_s\}$ the observation vector up

[1]Probability density function $p(a|b)$ means the relative likelihood for the random variable a to take on a given value, if the value of b is known.

to time s. This density function contains all available information about the state variable. Depending on the relation between t and s in $p(x_t|Y_s)$, three different estimation problems are obtained. When we have $t = s$ a filtering problem, when $t > s$ a prediction problem, and when $t < s$ a smoothing problem. Let the model of the system be generally defined as:

$$\begin{aligned} x_{t+1} &\sim p(x_{t+1}|x_t) \\ y_t &\sim p(y_t|x_t) \end{aligned} \tag{3.6}$$

Development of the probability density functions of interest is established based on the Bayes Theorem and the Markov property. Bayes Theorem describes the conditional probability densities of two stochastic variables ψ and φ as follows:

$$p(\psi|\varphi) = \frac{p(\varphi|\psi)p(\psi)}{p(\varphi)} = \frac{p(\varphi,\psi)}{p(\varphi)} \tag{3.7}$$

Moreover, a stochastic process has Markov property if the conditional probability distribution of future states of the process (conditional on both past and present values) depends only upon the present state, not on the sequence of events that preceded it. Now, the filtering density can be written as:

$$\begin{aligned} p(x_t|Y_t) = p(x_t|y_t, Y_{t-1}) &= \frac{p(y_t|x_t, Y_{t-1})p(x_t|Y_{t-1})}{p(y_t|Y_{t-1})} \\ &= \frac{p(y_t|x_t)p(x_t|Y_{t-1})}{p(y_t|Y_{t-1})} \end{aligned} \tag{3.8}$$

where $p(y_t|Y_{t-1})$ can be calculated according to:

$$\begin{aligned} p(y_t|Y_{t-1}) &= \int_{\mathbb{R}^{n_x}} p(y_t, x_t|Y_{t-1})dx_t = \int_{\mathbb{R}^{n_x}} p(y_t|x_t, Y_{t-1})p(x_t|Y_{t-1})dx_t \\ &= \int_{\mathbb{R}^{n_x}} p(y_t|x_t)p(x_t|Y_{t-1})dx_t \end{aligned} \tag{3.9}$$

where, $\mathbb{R}^{n_x}$ denotes the n_x-dimensional vector space over the field of real numbers. Similarly, one step-ahead density $p(x_{t+1}|Y_t)$ and smoothing density $p(x_t|Y_N)$ expressions could be derived [105]. The main results are collected in Theorem 1.

Theorem 1. *If the dynamic model is given by (3.6), the filter density $p(x_t|Y_t)$, the one step ahead density $p(x_{t+1}|Y_t)$, and the marginal smoothing density $p(x_t|Y_N)$ are given by:*

$$p(x_t|Y_t) = \frac{p(y_t|x_t)p(x_t|Y_{t-1})}{p(y_t|Y_{t-1})} \tag{3.10}$$

$$p(x_{t+1}|Y_t) = \int_{\mathbb{R}^{n_x}} p(x_{t+1}|x_t)p(x_t|Y_t)dx_t \tag{3.11}$$

$$p(x_t|Y_N) = p(x_t|Y_t) \int_{\mathbb{R}^{n_x}} \frac{p(x_{t+1}|x_t)p(x_{t+1}|Y_N)}{p(x_{t+1}|Y_t)} dx_{t+1} \tag{3.12}$$

where

$$p(y_t|Y_{t-1}) = \int_{\mathbb{R}^{n_x}} p(y_t|x_t)p(x_t|Y_{t-1})dx_t$$

Proof. See [105]. □

Deriving an analytical solution to the multidimensional integrals involved in Theorem 1 is not possible but in a few special cases. The most important special case is when the dynamic model is linear and the involved stochastic variables are normal, which has been extensively discussed in the literature and the optimal solution to the estimation problem would be Kalman Filter [53]. However, most of the real-world applications do not lend themselves to linear algorithms. Therefore, a number of solutions for state estimation problem of nonlinear systems are presented in literature. Extended Kalman Filter (EKF), Unscented Kalman Filter (UKF), Moving Horizon Estimation (MHE), Particle Filter (PF) are some of the prominent solutions proposed for this problem. As discussed earlier, our focus would be on particle filter in this thesis due to its attractive features.

Unlike most other nonlinear filtering methods, particle filter does not assume a fixed shape for densities (e.g. Kalman-based methods assume a Gaussian distribution). Instead, in particle filtering the densities of interest are approximated via a set of evolving samples or particles as:

$$p(x(t)) \approx \Sigma_{i=1}^{N_p} q^i(t)\delta(x(t) - x^i(t)) \tag{3.13}$$

where, N_p indicates the number of particles or samples in the approximation, x^i the sample location and q^i the sample weight. Thus PF can effectively capture the time-varying nature of distributions commonly encountered in nonlinear dynamic problems. Furthermore, this sampling based approach can solve the estimation problem in a recursive manner without resorting to model approximation. This method is also identified as "Sequential Monte Carlo method (SMC)" and has recently received a great deal of interest in the literature [95]. SMC is discussed in more detail in the next section.

3.4.2 Sequential Monte Carlo Methods-Particle Filtering

Problem Statement

The internal state of the system (not measurable) $\{x_t, t \in \mathbb{N}\}$, is modeled as a Markov process with initial distribution $p(x_0)$ and transition equation $p(x_t|x_{t-1})$. The observations $\{y_t, t \in \mathbb{N}\}$, are assumed to be conditionally independent given the process $\{x_t, t \in \mathbb{N}\}$ and of marginal distribution $p(y_t|x_t)$. The cumulative state and observations (measurements) are

denoted by $x_{0:t} \triangleq \{x_0, \ldots, x_t\}$ and $y_{1:t} \triangleq \{y_1, \ldots, y_t\}$, respectively, up to time t. According to the Bayesian approach, we are interested in recursive estimation of posterior probability density function (pdf): $p(x_{0:t}|y_{1:t})$.

Following Theorem 1, the recursive formula for the joint distribution $p(x_{0:t}|y_{1:t})$ could be simply derived as:

$$p(x_{0:t+1}|y_{1:t+1}) = p(x_{0:t}|y_{1:t}) \frac{p(y_{t+1}|x_{t+1})p(x_{t+1}|x_t)}{p(y_{t+1}|y_{1:t})} \tag{3.14}$$

where, $p(x_{0:t}|y_{1:t}) = \frac{p(y_{1:t}|x_{0:t})p(x_{0:t})}{\int p(y_{1:t}|x_{0:t})p(x_{0:t})dx_{0:t}}$. The marginal distribution $p(x_t|y_{1:t})$ also satisfies the following recursion:

$$\textit{Prediction:} \qquad p(x_t|y_{1:t-1}) = \int p(x_t|x_{t-1})p(x_{t-1}|y_{1:t-1})dx_{t-1} \tag{3.15}$$

$$\textit{Updating:} \qquad p(x_{0:t}|y_{1:t}) = \frac{p(y_t|x_t)p(x_t|y_{1:t-1})}{\int p(y_t|x_t)p(x_t|y_{1:t-1})dx_t} \tag{3.16}$$

In this recursion, prediction step uses both the knowledge of the previous state estimate and the process model to generate the a priori state pdf estimate for the next time instant. On the other hand, the updating (also called filtering) step applies the Bayes Formula to generate the posterior state pdf. As mentioned earlier, the evaluation of complex high-dimensional integrals in these expressions is analytically intractable in most cases. Thus, applying Monte Carlo (MC) methods is inevitable to reach a favorable solution which is not subject to constraints such as linearity or Gaussianity. The key idea underlying the Monte Carlo methods is to represent the probability density function (pdf) by a set of samples (particles) and their associated weights.

The density function $p(x_t|y_{1:s})$ is approximated with an empirical density function:

$$p(x_t|y_{1:s}) \approx \Sigma_{i=1}^{N_p} w_t^i \delta(x_t - x_{t|s}^i) \tag{3.17}$$

where N_p denotes the number of particles, w_t^i the associated weight of particle $x_{t|s}^i$ while normalized as $\Sigma_{i=1}^{N_p} w_t^i = 1$, and $\delta(.)$ is the Kronecker delta function. As the number of samples becomes very large, this MC characterization becomes an equivalent representation to the usual functional description of the posterior pdf, and the obtained filter approaches the optimal Bayesian estimate.

Particle Filter Algorithm

Different recursive algorithms are proposed to implement the above technique. They are generally categorized as particle filters or sequential Monte Carlo methods. They are also known as bootstrap filtering [43], condensation algorithm [71], and survival of the fittest

[54]. In this Thesis we review the "sampling importance resampling (SIR)" algorithm. SIR is organized in four basic steps:

1. *Initialization:*
   In the initialization stage, a finite number of particles are selected. Each particle is randomly initialized within an acceptable range wherein x_0 (i.e. initial state of the system) has the chance to sit. The number of particles is determined by a compromise between the desired accuracy and computational load. The other steps of the algorithm would run recursively.

2. *Prediction (time update):*
   This step considers the evolution of the system over time. It uses the stochastic model of the system to generate a possible future state for each sample. In other words, for all particles, the posterior system states are calculated.

3. *Correction (measurement update):*
   In this stage, each sample is weighted by the likelihood of seeing the observations in the (updated) state represented by the sample. Consequently, the samples that predict the observations well would have high weight, and samples that are unlikely to generate the observations would have low weight.

4. *Resampling:*
   This stage produces a uniformly weighted posterior. The key idea of resampling step is to eliminate the particles with low importance weights and to replicate particles with high importance weights.Therefore, the probability that a new sample is a copy of a particular sample s is proportional to the weight of s, so high-weight samples may be replaced by several samples, and low-weight samples may disappear

The above algorithm is represented as follows:

Algorithm 1 SIR Particle Filter

1. *Initialization:*
   For $i = 1, \ldots, N_p$, sample x_0^i from the prior distribution $p(x_0)$ at $t = 0$ and then set $t = 1$.

2. *Prediction and Correction:*

   - For $i = 1, \ldots, N_p$, sample $\tilde{x}_t^i \sim p(x_t|x_{t-1}^i)$.
   - For $i = 1, \ldots, N_p$, evaluate the importance weights according to $\tilde{w}_t^i \sim p(y_t|\tilde{x}_t^i)$.
   - Normalize the weights

3. *Resampling:*
   Resample N_p new particles $\{x_t^i, i = 1, \ldots, N_p\}$ with replacement from the set $\{\tilde{x}_t^i, i = 1, \ldots, N_p\}$ according to the importance weights. A new sample x_t^i is a copy of a particular particle $\tilde{x}_t^i$ with a probability proportional to the weight of $\tilde{x}_t^i$. Interested reader can consult with [105, 5] on different algorithms proposed for resampling.

4. Set $t = t + 1$ and go to step 2.

The block-diagram of this algorithm is illustrated in Figure(3.1). The interested reader is referred to [34, 5] for more details about the theories behind this PF algorithm and other variants of this algorithm.

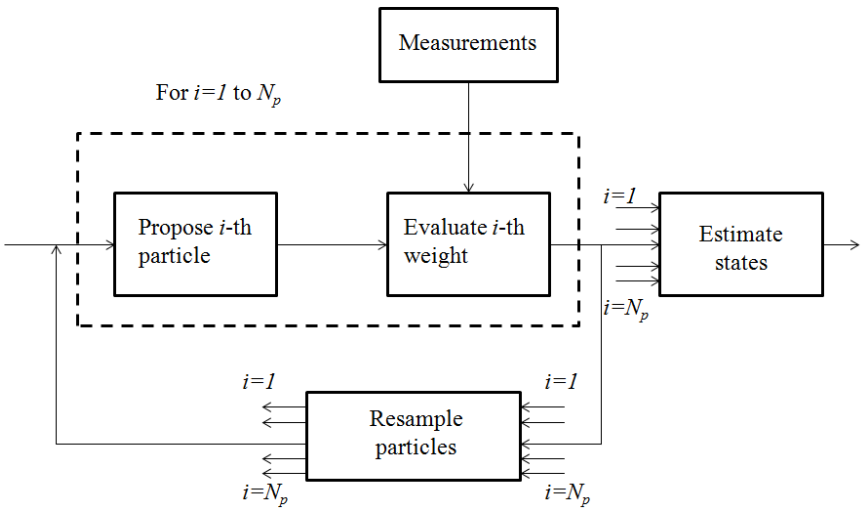

Figure 3.1: The major computational steps of a particle filter algorithm is shown in this block diagram.

3.4.3 Application of PF to the Battery Equations

The PF algorithm (Algorithm 1) was applied for battery estimation. The particles represent the concentration at the surface of the electrode (i.e. $c_{se,j}$). The particles are updated through the transition distribution, $p(x_t|x_{t-1})$, and posterior pdf is calculated. The predicted output for each particle $\tilde{y_t}^i$ is calculated and compared with the measured output y_t. The weight associated with each particle is determined as follows:

$$\begin{cases} e_t^i = y_t - \tilde{y_t}^i \\ \tilde{w}_t^i = exp((e_t^i)^2/2\zeta_y)/\sqrt{2\pi\zeta_y} \end{cases}, \; i = 1, \ldots, N_p \tag{3.18}$$

where, ζ_y is the variance of observation noise. The weights are normalized, the states of the interest are determined and the particles are resampled to produce a priori distribution for the next time step. The schematic of the procedure is shown in Figure (3.2).

3.5 Online State and Parameter Estimation of the Li-ion Battery

The objective is to develop an algorithm capable of simultaneous estimation of the states and parameters of the system in a Bayesian framework. The proposed estimation method is based on a particle filter proposed by [69] and [24] for simultaneous joint parameter and state estimation.

3.5.1 Combined Parameter and State Estimation

Dynamic Model and Analysis Perspective

Assume a Markovian dynamic model for sequentially observed data vectors $y_{1:t}$ in which the state vector at time t is x_t and the parameter vector is θ_t. The state equation defined by transition density as $p(x_t|x_{t-1}, \theta_t)$, and the observation equation is defined by the observation density as $p(y_t|x_t, \theta_t)$. Similar to SMC algorithm (Section 3.4.2), it is assumed that each $y_{1:t}$ is conditionally independent of past states and observations given the current state x_t and the parameter θ_t, and also, x_t is conditionally independent of past states and observations given x_{t-1} and θ_t.

The objective is to develop a sequential Monte Carlo method to sequentially update Monte Carlo sample approximations to the sequences of posterior distributions $p(x_t, \theta_t|y_{1:t})$. The main focus of this Thesis would be on a modification of Auxiliary Particle Filter as proposed by [69] and [24] to tackle the problem.

If both states and model parameters are to be estimated, Bayes's rule gives the following joint posterior distribution:

$$p(x_t, \theta_t|y_{1:t}) \propto p(y_t|x_t, \theta_t)p(x_t|\theta_t, y_{1:t-1})p(\theta_t|y_{1:t-1}) \tag{3.19}$$

Joint state and parameter estimation is achieved through the augmentation of the state space with the parameter vector. If the parameters are considered as constant, a Gaussian random walk is considered for the parameters as follows:

$$\begin{aligned} \theta_t &= \theta_{t-1} + \zeta_t \\ \zeta_t &= G(0, W_t) \end{aligned} \tag{3.20}$$

This strategy has been widely adopted in conventional state and parameter estimation techniques, such as the EKF [59]. However, as noted by some researchers [69], the random walk implies an increase in the magnitude of the covariance, resulting in posterior distributions that are more diffuse than they should be [24]. Hence, "Kernel Smoothing" is applied to alleviate this problem [69].

Kernel Smoothing

Let $\bar{\theta}_{t-1}$ and Λ_{t-1} be the Monte Carlo mean and covariance matrices computed from all the particles with weights, $\{\theta^i_{t-1}, w^i_{t-1}, i = 1, \ldots, N_p\}$. It is noted that the distribution $p(\theta_t|y_{1:t-1}) \approx \Sigma_{i=1}^{N_p} w^i_{t-1} G(\theta_t|\theta^i_{t-1}, W_t)$ would have a mean of θ_{t-1} and covariance matrix $\Lambda_{t-1} + W_t$. Thus, to reduce the covariance the kernel smoothing with smoothing factor $0 < h < 1$ is employed as:

$$p(\theta_t|y_{1:t-1}) \approx \Sigma_{i=1}^{N_p} w^i_{t-1} G(\theta_t|m^i_{t-1}, h^2\Lambda_{t-1}) \tag{3.21}$$

where, the kernel locations m^i_{t-1} are specified by a shrinkage rule that forces the particles to be closer to their mean [24]:

$$m^i_{t-1} = (\sqrt{1-h^2})\theta^i_{t-1} + (1 - \sqrt{1-h^2})\bar{\theta}_{t-1} \tag{3.22}$$

As a consequence, the probability in Eq.(3.21) would have the mean of $\bar{\theta}_{t-1}$ and covariance matrix Λ_{t-1}.

The parameter h is the manipulating parameter to deal with the changes of unknown parameters. Small values of h (e.g. $0 < h < 0.2$) are utilized for a fixed or slowly-varying unknown parameter where large values (e.g. $0.8 < h < 1$) are being employed for parameters with significant changes over time [24].

Auxiliary Particle Filter for State and Parameter Estimation

The importance function $p(x_t|x_{t-1})$ used in Algorithm 1 has an obvious defect in the sense that the state-space is explored without direct knowledge of the measurement y_t. The idea of incorporating this information in the importance function is explored in the Auxiliary Particle Filter (APF) introduced by Pitt and Shephard (1999) [86]. The combined state and parameter estimation particle filter presented here is in fact a modification of this algorithm presented by [24]. The interested reader is referred to [86] for more details about APF. The algorithm is presented as following:

Algorithm 2 Auxiliary SIR Particle Filter for State and Parameter Estimation

1. *Initialization:*
   For $i = 1, \ldots, N_p$, initialize the particles $\{x_0^i, \theta_0^i\}$ with equal weights of $\{w_0^i = 1/N_p\}$ and then set $t = 1$.

2. *Find the prior point estimates:*

   (a) For $i = 1, \ldots, N_p$,

      i. Calculate $\mu_t^i = E(x_t|x_{t-1}^i, \theta_{t-1}^i)$ and $m_{t-1}^i = (\sqrt{1-h^2})\theta_{t-1}^i + (1 - \sqrt{1-h^2})\bar{\theta}_{t-1}$

      ii. Calculate $w_t^i \propto p(y_t|\mu_t^i, m_{t-1}^i)w_{t-1}^i$

   (b) Normalize the weights

   (c) Resample N_p new particles $\{x_{t-1}^{parent(i)}, m_{t-1}^{parent(i)}, \mu_t^{parent(i)}, i = 1, \ldots, N_p\}$ with replacement from the set $\{x_{t-1}^i, m_{t-1}^i, \mu_t^i, i = 1, \ldots, N_p\}$ according to the importance weights w_t^i.

3. *Prediction and Correction:*

   (a) For $i = 1, \ldots, N_p$, draw θ_t^i from Gaussian distribution $G(.|m_{t-1}^{parent(i)}, h^2\Lambda_{t-1})$

   (b) Draw x_t^i from $p(x_t|x_{t-1}^{parent(i)}, \theta_t^i)$

   (c) Assign weights according to $w_t^i = \frac{p(y_t|x_t^i, \theta_t^i)}{p(y_t|\mu_t^{parent(i)}, m_{t-1}^{parent(i)})}$

   (d) Normalize the weights

4. Set $t = t + 1$ and go back to 2.

The particles μ^i serve as an auxiliary variable for deriving the importance density. By utilizing them, the new particles are generated from particles at the previous time step, conditional on the current measurement y_t, which will be closer to the true states. Conceptually, in contrast to standard particle filter, the auxiliary particle filter can be interpreted as a look ahead method, which at time $t-1$ predicts which samples will be in regions of

high likelihood at time t. As a result, the cost of sampling particles from regions of very low likelihoods is reduced [40].

3.5.2 Multi-Rate APF for State and Parameter Estimation of the Battery

In order to address the computational load of this algorithm, a multi-rate particle filter is proposed in this Thesis, where parameters are estimated in a slower time-scale than states. Provided that a sufficient number of particles is being used for estimation, the stability of the filter is guaranteed. The parameter estimation stage is stopped whenever the variance of estimated parameters at consecutive time steps is dropped below a certain threshold (V_{th}) which means that the parameter estimate has converged to its value.

In other words, we have two time scales T_{s1}, and T_{s2} used for state and combined state and parameter estimation, respectively. At sample times k' that $mod(t = kT_{s1} = k'T_{s2}, T_{s2}) = 0$, the parameter particles vector is initialized and the combined particle filter is performed. This continues with T_{s1} until the parameter vector converges (the stopping condition is considered as the variance of the parameters in a window of 10 time steps). Thereafter, we only perform the state parameter estimation given in Algorithm 1 until the next sample time is reached.

Applying this filter helps to reduce a great deal of computational load. Given the fact that parameters of the battery are slowly changing, this makes sense to perform state and parameter estimation at different rates. The proposed algorithm is given in Algorithm 3.

Algorithm 3 Multi-Rate Particle Filter Algorithm for Combined State and Parameter Estimation

for $t = 0 : T_{s1} : t_{end}$ **do**
  if $t = 0$ **or** $mod(t, T_{s2}) = 0$ **then**
    Initialize parameter particles
    $\hat{t} \leftarrow t$
    Run Algorithm 2
  else if $var\{\theta_\tau\}_{\tau=t-10T_{s1}}^{t} > V_{th}$ **then**
    Run Algorithm 2
  else
    Run Algorithm 1
  end if
end for

3.6 Simulation Studies

In two separate studies the effectiveness of the proposed algorithms are examined for Li-ion battery estimation. The Li-ion battery parameters used in simulations are adopted from the work in [51] and are given in Table 3.2.

The dynamic state evolution of the battery is obtained by discretizing the PDE equations (Eqs.(2.22)-(2.28)) by applying finite difference method choosing a proper step-length for time and position. This set of differential equations along with the algebraic equation corresponding to surface concentration (2.24) and volumetric rate (2.8) constitute a DAE set of equations that need to be solved at each time instant. The algorithms are applied and estimated values are compared with actual values obtained from solving the full dynamic model of the battery. The impact of different factors such as number of particles, and noise level present in the system are also studied on the performance of the algorithms. The performance results show that the proposed algorithms are effectively capable of tracking the SoC of the battery as well as desired parameters. They can also estimate other battery quantity variables that are often absent in the current monitoring approaches.

3.6.1 SoC Estimation of Li-ion Battery

The effectiveness of Algorithm 1 is investigated through the SoC estimation of a Li-ion cell. The current profile exerted for simulation tests is the one considered in [33] corresponding to FreedomCAR test procedure [124]. The particle filter is initiated with 100 particles corresponding to initial concentration of Lithium at solid phase (see Figure (3.2)). The number of particles is selected based on a study on the impact of number of particles on the accuracy that will follow. The results are shown in Figure (3.3). It is apparent that after a very short transient the proposed algorithm is capable of finding the correct SoC and tracks the correct value (3.3b). The SoC estimation error $|SoC - \hat{SoC}|/SoC$ is shown in Figure (3.3c) for a few first time steps to demonstrate how the algorithm converges toward the correct value. Normally, if the set of initial particles is diverse enough such that the exact value of interest have some representatives in the initial particles, then PF is very fast to catch up with the exact value of SoC. It is however very important to maintain the diversity of the particles at some reasonable level by injecting artificial noise, or other methods to prevent the sample impoverishment problem [5].

The beauty of PF algorithm is that in addition to SoC which is the main parameter of concern for all battery estimation algorithms, the spatial distribution of other parameters would also be obtainable. Figure (3.4) demonstrate this ability of PF algorithm. The mean squared error (MSE) error (i.e. $MSE = 1/N \sum_{i=1}^{M} e_i^2$) of $\phi_{se} = \phi_s - \phi_e$ with respect to x ,at negative and positive electrode, is calculated as: $MSE^-(t) = 1/L_n \int_{0^-}^{L^-} (\phi_{se}(t) - \phi_{se}(t))^2 dt$ and $MSE^+(t) = 1/L_p \int_{0^+}^{L^+} (\phi_{se}(t) - \phi_{se}(t))^2 dt$ and shown in Figure (3.4a) versus time.

Table 3.2: Li-ion Battery Parameters

Symbol	Value	Unit
$c_{s,p,max}$	22860	$[mol\ m^{-3}]$
$c_{s,n,max}$	26390	$[mol\ m^{-3}]$
c_e	2000	$[mol\ m^{-3}]$
$D_{s,p}$	1.0×10^{-13}	$[m^2 s^{-1}]$
$D_{s,n}$	3.9×10^{-14}	$[m^2 s^{-1}]$
D_e	7.5×10^{-11}	$[m^2 s^{-1}]$
F	96485.3365	$[C\ mol^{-1}]$
k_p	2.3×10^{-11}	$[mol/m^2 s/(mol/m^3)^{1.5}]$
k_n	2.3×10^{-11}	$[mol/m^2 s/(mol/m^3)^{1.5}]$
L_p	183	$[\mu m]$
L_s	52	$[\mu m]$
L_n	100	$[\mu m]$
p	1.5	
R	8.3144621	$[JK^{-1}mol^{-1}]$
$R_{s,p}$	8	$[\mu m]$
$R_{s,n}$	12.5	$[\mu m]$
α_a , α_n	0.5	
σ_p	3.8	$[\Omega^{-1}m^{-1}]$
σ_n	100	$[\Omega^{-1}m^{-1}]$
$\epsilon_{s,p}$	0.444	
$\epsilon_{s,n}$	0.357	
ϵ_e	1	
U_p	$= 4.199 + 0.0566 tanh(-14.555\theta_p + 8.609) - 0.0275[(0.998 - \theta_p)^{-0.492} - 1.901]$ $-0.157 exp(-0.0474\theta_p^8) + 0.81 exp[-40(\theta_p - 0.134)],\ \theta_p = c_{se,p}/c_{s,p,max}$	
$U_n = -0.16 + 1.32 exp(-3\theta_n) + 10.0 exp(-2000\theta_n)),\ \theta_n = c_{se,n}/c_{s,n,max}$		
$\kappa_{eff,j}$	$= (4.1253 \times 10^{-2} + 5.007 \times 10^{-4} c_e - 4.7212 \times 10^{-7} c_e^2 + 1.5094 \times 10^{-10} c_e^3$ $-1.6018 \times 10^{-14} c_e^4) \epsilon_{s,j}^p,\ j = n, e, p$	

Figure (3.4b) illustrates the spatial distribution of lithium ions in active material at the negative electrode. It is shown at three time instances versus $x \in [0^-, L^-]$.

Estimation of other battery quantities such as solid and electrolyte potential, or spatial distribution of Lithium ion concentration is specifically advantageous in health monitoring and fault diagnostics of the battery. Many degradation mechanisms in the battery manifest themselves through unexpected values for these quantities, or deviation of the their spatial distribution from its normal profile. Chapter 5.1 elaborates more on this point and discusses the effectiveness of these algorithms on fault monitoring of Li-ion batteries. In the following, the impact of number of particles, and observation noise level is studied.

Impact of Number of Particles

To study the impact of number of particles on the algorithm performance, the MSE error due to SoC estimation is tabulated in Table 3.3. The results demonstrate that as the number of particles increases the accuracy of the algorithm gets improved. However, there is always a compromise between the desired accuracy and computational load. Hence, our simulations were carried out with 100 particles which also provides good results.

Table 3.3: The impact of number of particles on the accuracy of estimation

Number of Particles	MSE
20	1.568×10^{-4}
50	1.4619×10^{-4}
100	7.8041×10^{-5}
250	5.6214×10^{-5}
350	4.5390×10^{-5}

Impact of Noise

The robustness of the algorithm is studied by increasing the noise and observing the MSE error for different noise levels. A normal Gaussian observation noise with different standard deviation (SD) is applied to the system for this purpose. Table 3.4 summarizes the results. In this study the number of particles is considered as $N = 50$. The results show that although generally the accuracy drops as the noise SD level goes up, the algorithm remains robust by providing a good accuracy. Also, comparing the results for SD values of 0.01 and 0.02, or 0.1 proves the robustness of algorithm and shows that the change in accuracy is not necessarily due to noise level. In other words, the filter can reject the noise in the system to a good extent. The difference between MSE values of $SD = 0.01$, and $SD = 0.02$ is partly due to the random initialization of the filter. Decrease in the accuracy in the high noisy environment is however inevitable.

Table 3.4: The impact of observation noise on the performance of the algorithm

Observation Noise SD	MSE
0.001	7.369×10^{-5}
0.01	1.9702×10^{-4}
0.02	3.8070×10^{-5}
0.05	6.4098×10^{-5}
0.1	1.8412×10^{-5}
0.2	3.2074×10^{-4}

A main feature of PF algorithms is that, unlike Kalman-based methods, they are insensitive to the type of the noise. Hence, to study this feature, the performance of the

algorithm with respect to colored noise is investigated in the following. The colored noise is generated as follows:

$$v_c[n] = 0.5 \times v_c[n-1] + v[n] \tag{3.23}$$

where v_c represents the colored noise and v the white Gaussian noise with variance of ζ_v^2. Therefore, the variance of the colored noise can be determined as: $\zeta_v^2/(1-0.5^2)$. The results are shown for noise SD of 0.02 in Figure (3.5). The inset in Figure (3.5b) shows that the error percentage (i.e. $EP(\%) = 100 \times \mid SoC - \hat{SoC} \mid / SoC(\%)$) remains in a 0.2% band which demonstrates a very good performance and also insensitivity of PF algorithm to the noise type.

3.6.2 State and Parameter Estimation of Li-ion Battery

For simulation studies, the estimation of parameters of diffusion coefficient (i.e. $D_{s,j}$) and the volume fraction of active material (i.e. $\epsilon_{s,j}$) at negative electrode ($j = n$) are selected. These parameters are selected due to the fact that some of the common degradation mechanisms that affect the lithium mobility in lattice of active material, or lead to loss of active area would impose a direct impact on these parameters and thus their estimation is desired to predict and detect the battery faults (The principles of degradation processes are discussed in Chapter 5). Changes to this set of parameters would also consequently affect the accuracy of the SoC estimation. Hence, these coefficients are being estimated along with the SoC of the negative electrode.

Figure (3.6) shows the results when the Algorithm 3 is employed for separate estimation of $D_{s,n}$ and $\epsilon_{s,n}$. The results are achieved with filters consisting of 100 particles. It can be seen that parameters can track the true values (Figure (3.6)). The parameter estimation is stopped when the estimated parameter converged and from thereon only the state estimation continues.

3.7 Summary and Discussion

This Chapter discussed the battery monitoring methodologies. First, the literature about battery monitoring, parameters of concern, and existing challenges were briefly reviewed. Then, a Bayesian approach towards battery monitoring was proposed as a novel solution that can address some of the current challenges. This approach can open a new window towards battery monitoring by considering the electrochemical model of the battery. The proposed methods are capable of estimating of both states and parameters of the battery. Moreover, in addition to state of charge of the battery, other parameters such as solid and electrolyte potential, and distribution profile of lithium concentration in the battery are also estimable through this methodology which makes it unique. Considering the electro-

chemical model in battery estimation is also itself desirable since its parameters possess physical significance, and thus their estimation provides some necessary information for fault diagnostics of the battery.

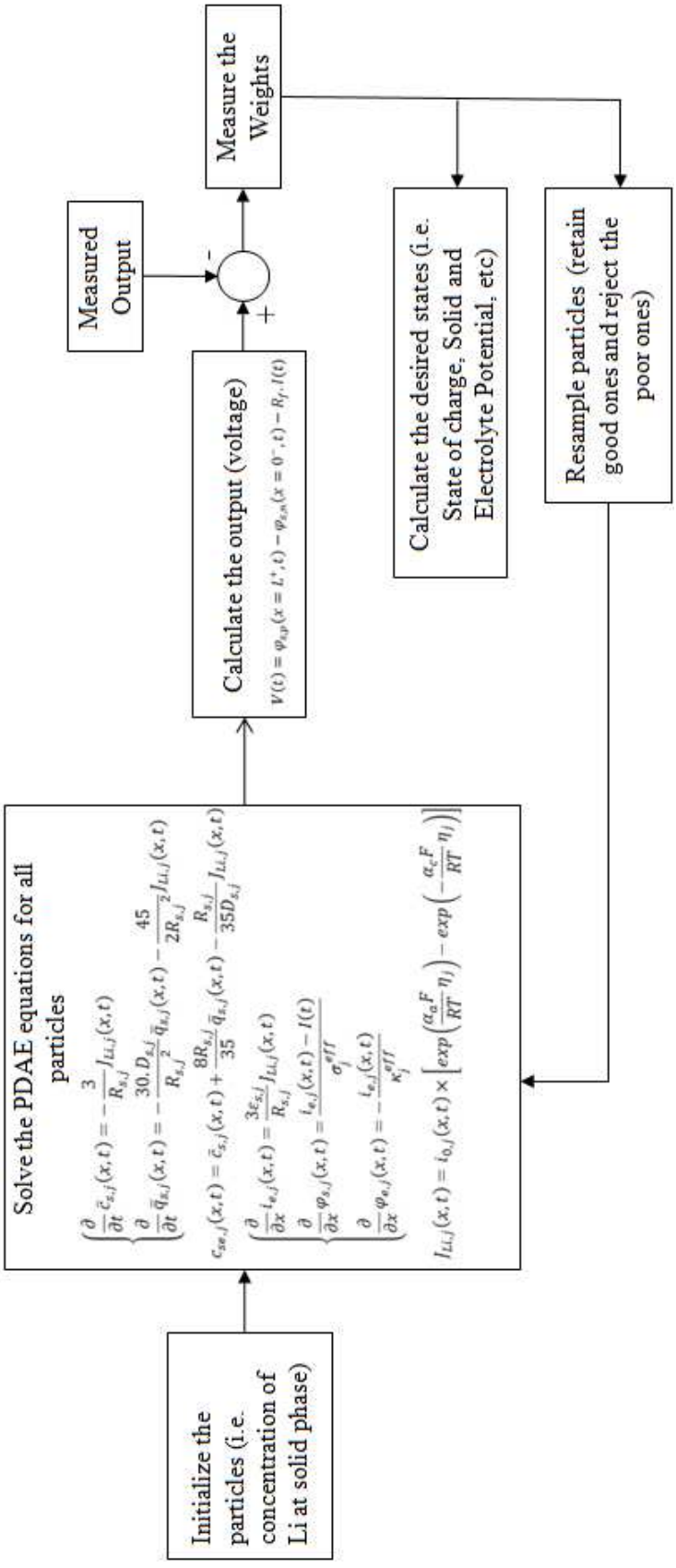

Figure 3.2: Schematic of the application of PF to battery estimation.

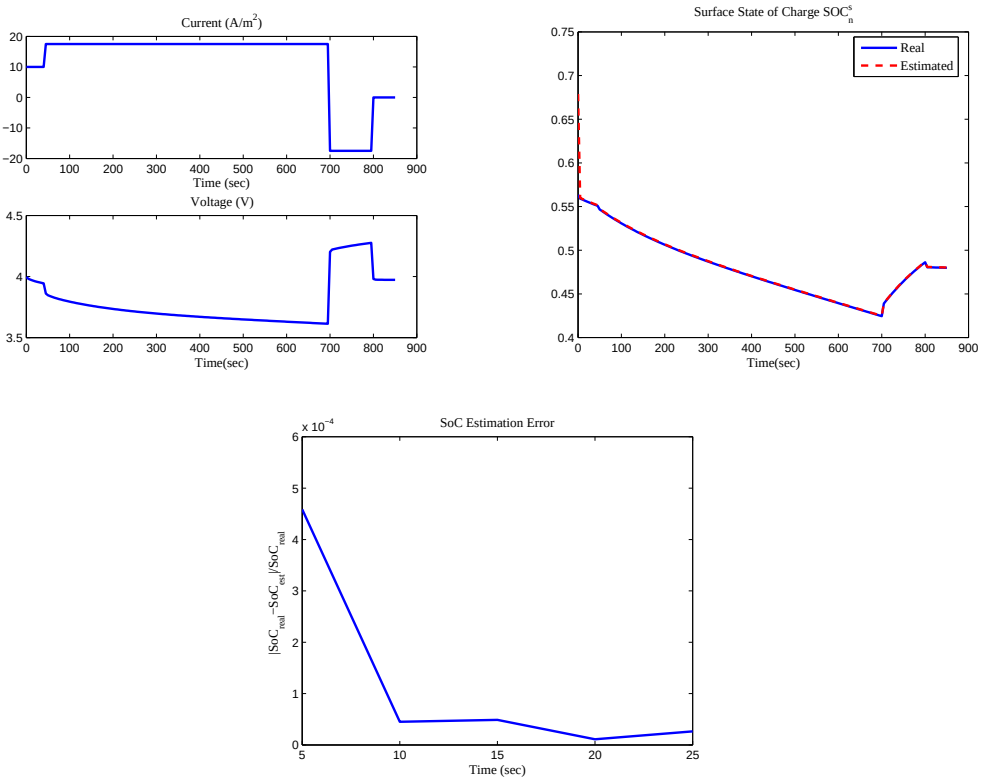

Figure 3.3: Performance of the PF algorithm for battery SoC estimation (a) Input and output of the system (b) Surface state of charge (c)Convergence of SoC Estimation

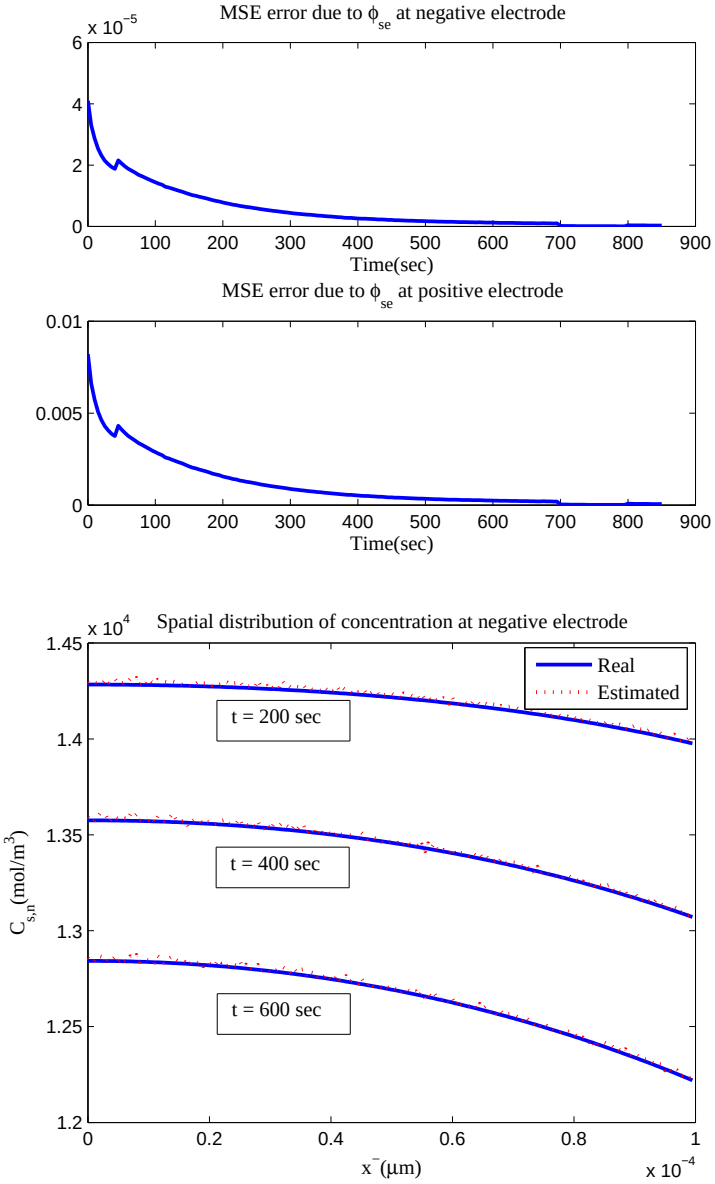

Figure 3.4: Performance of the PF algorithm in estimation of other parameters with spatial distribution. (a) MSE spatial error of ϕ_{se} versus time (b) Spatial distribution of lithium ions in active material at negative electrode versus position at three different time instants.

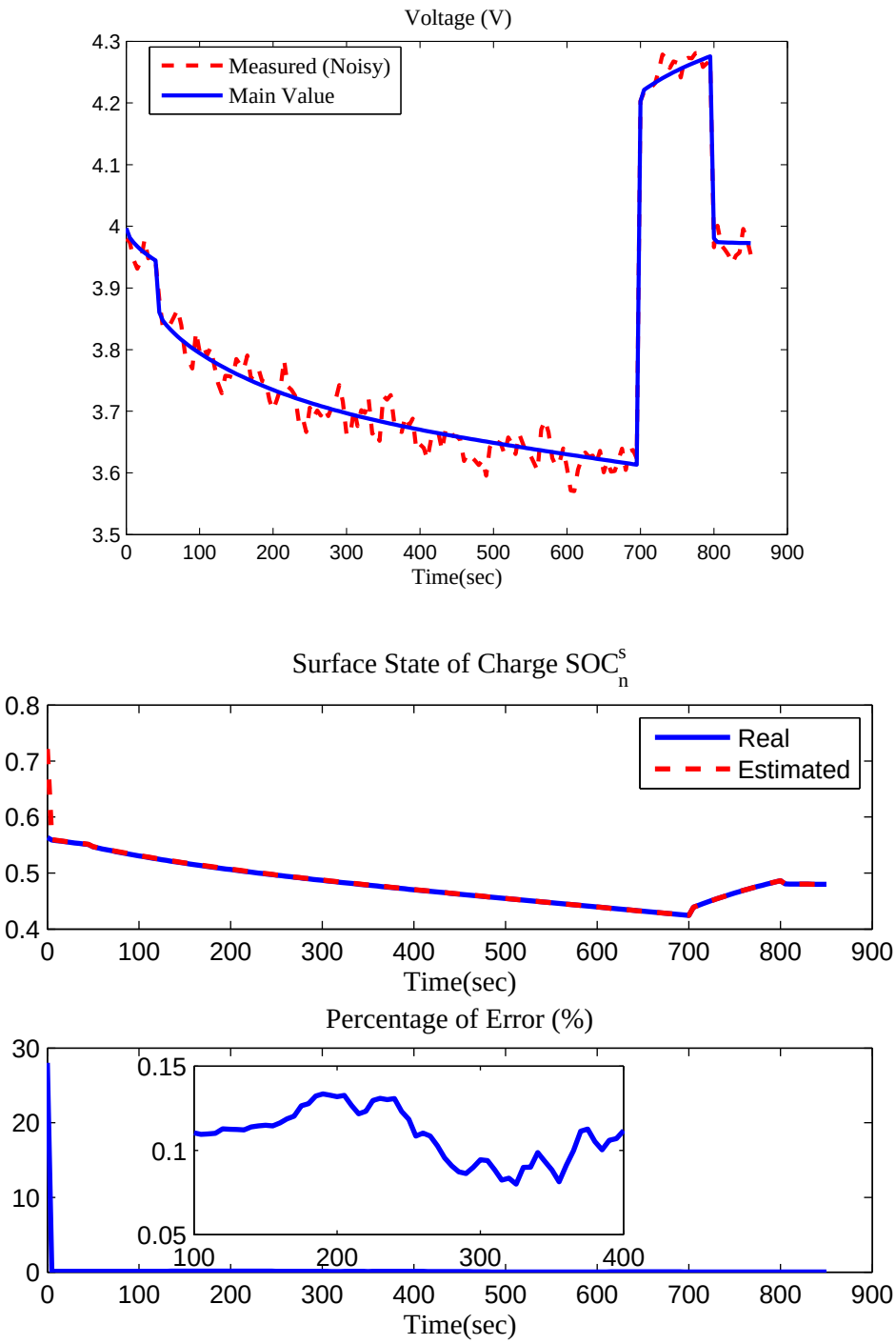

Figure 3.5: Performance of the PF algorithm in presence of colored noise. (a) The measured (noisy) voltage versus the main voltage (b) state of charge estimation and percentage of error. The inset shows the error percentage for $t \in [100, 400]$.

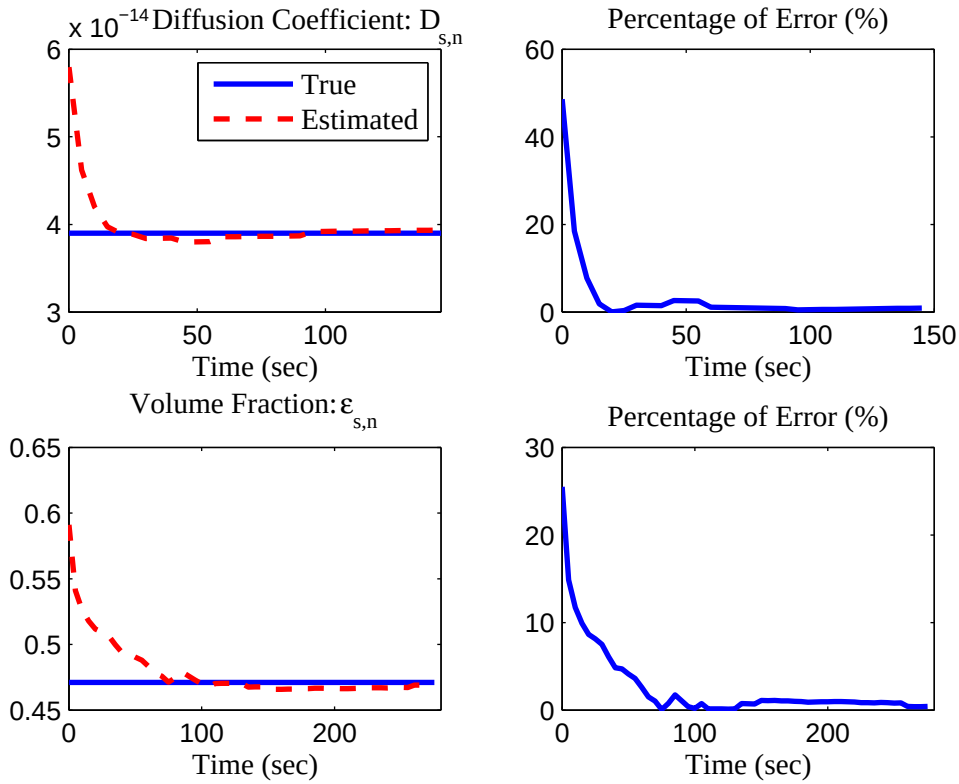

Figure 3.6: Parameter Estimation of $D_{s,n}$ and $\epsilon_{s,n}$. The parameters are estimated in independent runs with a PF with $N = 100$ particles.

Chapter 4

Data-Based Approaches to Battery Monitoring

4.1 Introduction

Model-based approaches to battery monitoring was discussed in the last chapter. The proposed particle-filtering-based algorithms present a universal methodology to battery monitoring. However, they suffer from the high computational load of the algorithm that make them not the best choice for real-time monitoring. In this chapter, two new methodologies that are inherently data-based and empirical also but take into account the physics of the battery are considered.

In section 4.2, a new methodology based on Takagi-Sugeno (T-S) fuzzy modeling is presented. This work attempts to establish a bridge between the complicated partial differential equations of the electrochemical model (see section 2.3) with linear like state-space models by proposing a Takagi-Sugeno (T-S) fuzzy system. In fact, fundamental EM model is approximated using multiple state space models using a data-based approach. The key idea is to solve the basic EM model using finite volume method (section 2.3.1) in the range of normal battery operation and then fit a T-S fuzzy model to the provided data. The proposed T-S fuzzy model provides a multiple state-space model and then a T-S observer fuzzy model is applied to estimate the unknown states.

In section 4.3, a new concept of "dynamic resistance" is introduced and is intended to provide a novel framework for battery monitoring where state estimation and aging effect are considered. This methodology has the potential to estimate both SoC and SoH in a unified framework. It is shown through extensive experiments that the introduced parameter of dynamic resistance is strongly dependent to the battery SoC and charge/discharge cycle number or aging. Hence, this parameter carries important information about the degradation and capacity fading of the battery. Moreover, it presents a viable and simple method to monitor the degradation of the battery whereas most of the previously proposed

methods are based on non-physical quantities, or destructive methods to gain access to the state of battery materials.

An appealing feature of the methods presented in this chapter is their extremely low computational load which makes them an appropriate choice for real-time monitoring of the battery.

4.2 Takagi-Sugeno Fuzzy Model

A Takagi-Sugeno (T-S) fuzzy model which is essentially an empirical model and attempts to include advantages of both ease-of-calculation of experimental models and accuracy of electrochemical models is proposed and developed in this section. The input space is decomposed into a set of fuzzy spaces and the output space is represented with multiple linear state space models. The main advantage is that while the inherent nonlinearity of the model is preserved, each local model is a linear model for which development of control and estimation strategy is straightforward. Moreover, the reliability range of the model can also be increased by consideration of the multiple models each of which representing a different region of the battery operation. A data-approach is adopted to identify the T-S model where the data is collected from extensive simulation of EM to have a fair extended range of data. By virtue of local state-space linear models, many of the available control/estimation strategies would be applicable to battery equations. A Luneberger-based fuzzy observer is developed to estimate the SoC in this section. For a good review of TS based modeling and control theory see [39].

4.2.1 T-S Fuzzy Modelling and Identification

The proposed TS model is composed of c fuzzy inference rules where each one is associated with one local state-space model. The l^{th} rule can be described as:

$$\begin{aligned} R_l: \quad IF \quad & z_{1,k}\, is\, F_{l,1}\, and \ldots and\, z_{q,k}\, is\, F_{l,q} \\ THEN \quad & x(k+1) = A_l x(k) + B_l u(k) + \vartheta_l \\ & y(k) = C_l x(k) + D_l u(k) \end{aligned} \tag{4.1}$$

where, $z_{1:q,k}$ denotes the premise variables which include the previous states and current input, i.e. $x(k)$ and $u(k)$, of the system and $F_{l,1:q}$ the fuzzy sets. The vectors $x(k) \in \mathbb{R}^n$ represents the state vector, $u(k) \in \mathbb{R}^m$ the input vector, $y(k) \in \mathbb{R}$ the output vector, respectively. Matrices $(A_l, B_l, \vartheta_l, C_l, D_l)$ represent the l^{th} local affine state-space model. Applying singleton fuzzifier, product fuzzy inference and center-average defuzzifier, the T-S fuzzy model can be expressed as:

$$\begin{aligned} x(k+1) &= A(\mu)x(k) + B(\mu)u(k) + \vartheta(\mu) \\ y(k) &= C(\mu)x(k) + D(\mu)u(k) \end{aligned} \tag{4.2}$$

where

$$(A, B, \vartheta, C, D)(\mu) = \sum_{l=1}^{c} \mu_l (A_l, B_l, \vartheta_l, C_l, D_l). \tag{4.3}$$

$\mu_l(z) \geq 0$ is the normalized membership function defined as:

$$\mu_l(z) = \frac{\beta_l(z)}{\sum_{i=1}^{c} \beta_i(z)}, \quad \beta_i(z) = \prod_{j=1}^{q} F_{i,j}(z), \tag{4.4}$$

where $F_{i,j}(z)$ is the grade of membership of z and β_i is the degree of fulfillment of i^{th} rule. The fuzzy sets $F_{i,j}$, are represented by Gaussian membership functions as follows:

$$F_{i,j}(z_{j,k}) = exp\left(-\frac{1}{2}\frac{(z_{j,k} - v_{i,j})^2}{\sigma_{i,j}^2}\right) \tag{4.5}$$

where $v_{i,j}$ denotes the center and $\sigma_{i,j}^2$ the variance of the Gaussian membership functions.

The applied data-based method for the generation of a TS fuzzy model (4.1) is based on Levenberg-Marquardt (LM) and fuzzy clustering. It is adopted from [1], [39] and modified by adoption of LM method for the estimation of local model parameters and eigenvalue decomposition for simplification of fuzzy-rule database. The proposed method is discussed in the following.

Model Identification

The objective is to identify both the membership functions and the local affine model parameters. The number of rules (i.e. c) could be considered as pre-set or determined within an iterative procedure where the identification begins from a minimum number of rules and it is increased until a certain stopping criteria is reached. The key idea of identification of membership functions is based on clustering and partitioning the identification data. The clustering is established based on the minimization of an objective function, V, which includes two basic terms, i.e. the sum of weighted squared distances between data points, z_k and the cluster prototypes (η), and estimation error of the local linear models (e).

$$\min_{\eta} V: \qquad V(\mathbf{z}, U, \eta) = \min_{\eta} \sum_{i=1}^{c} \sum_{j=1}^{N} (\mu_{i,k}) D_{i,k}^2$$

$$\text{where} \qquad D_{i,k}^2(\mathbf{z}_k, \eta_i) = \omega_i \cdot \prod_{j=1}^{n} exp(-\frac{1}{2}\frac{(z_{j,k} - v_{i,j})^2}{\sigma_{i,j}^2}.\frac{exp(-e^T.e)}{\sqrt{2\pi\sigma_i^2}}$$

$$e = y_k - g(z, \theta) \tag{4.6}$$

where ω_i represents the weight of each rule, $v_{i,j}$ and $\sigma^2_{i,j}$ the centers and standard deviation of the Gaussian membership functions, respectively, y^f_k the output of the fuzzy system and e is the modelling error.

The above optimization problem can be solved with different methods. The popular Alternating Optimization (AO) method is adopted here [1]. The main algorithm is summarized in Algorithm 4.

The minimization problem (4.8) is solved using a nonlinear least-squares regression technique called Levenberg-Marquardt method [75, 94]. LM is in fact a parameter learning method that adaptively averages between Gauss-Newton and gradient-descent methods. The objective is to estimate the parameters, θ, of a model such as $y = g(x, \theta)$, provided the observed values of dependent variable, y^*. This algorithm is reviewed in Algorithm 5.

Using algorithms 4 and 5, a T-S fuzzy model with c number of rules is developed. Now, the question is how to select the set of most important fuzzy rules. To improve the generalization ability of the model as well as its compactness, it is better to remove the redundant or less important fuzzy rules. To achieve this goal, a modified version of *"eigenvalue decomposition (ED) method"* introduced by [135] and [81] is adopted in this Thesis.

Simplifying T-S Model using Eigenvalue Decomposition (ED)

The main idea is to apply the eigenvalue decomposition to the partition matrix, and hence the rule space, and employ a measure index to rule out the redundant or less important rules.

Based on the partition matrix, $U = [\mu_{i,k}] \in \mathbb{R}^{c \times N}$, the correlation matrix is defined as: $\Phi_{uu} \triangleq UU^T \in \mathbb{R}^{c \times c}$. Applying eigenvalue decomposition on Φ_{uu} gives:

$$\Phi_{uu} = \Psi \Lambda \Psi^T \tag{4.14}$$

where $\Lambda = diag(\lambda_1, \lambda_2, ..., \lambda_c) \in \mathbb{R}^{c \times c}$ is a diagonal matrix whose diagonal entries are eignvalues of Φ_{uu}, and $\Psi = [\psi_1, \psi_2, \dots, \psi_c] \in \mathbb{R}^{c \times c}$ is an orthogonal matrix whose columns are the corresponding eigenvector. The matrix Φ_{uu} is symmetric and $\Phi_{uu} \geq 0$ and thus all of its eigenvalues are real and non-negative. Therefore, all eigenvalues can be arranged in a descending-order, i.e. $\lambda_1 \geq \lambda_2 \geq \ldots \geq \lambda_c \geq 0$, and all eigenvectors are arranged accordingly. The number of first r largest eigenvalues indicates the number of fuzzy rules that should be retained. The number of preserved rules, r, is either pre-determined or it can be determined as the number of eigenvalues that are not less than some certain threshold.

In order to determine which rules should be discarded, a measure index vector $I_{ED} \in \mathbb{R}^c$ is defined as:

Algorithm 4 T-S Fuzzy Model Identification

1. Choose a weighting exponent $m > 1$, a termination threshold $\epsilon > 0$ and a set of initial membership values $U^0 = [\mu_{i,k}]_{c \times N}$ such that $\mu_{i,k} > 0$ and $\sum_{i=1}^{c} \mu_{i,k} = 1$. Set $l = 1$.

2. Calculate the prototypes of clusters (i.e center and standard deviation) as follows:

$$\begin{aligned} \mathbf{v}_i{}^{(l)} &= \frac{\sum_{k=1}^{N} \mu_{i,k}^{(l-1)} \mathbf{z}_k}{\sum_{k=1}^{N} \mu_{i,k}^{(l-1)}}, \\ \sigma_{i,j}^{2\ (l)} &= \frac{\sum_{k=1}^{N} \mu_{i,k}^{(l-1)} (z_{j,k} - v_{j,k})^2}{\sum_{k=1}^{N} \mu_{i,k}^{(l-1)}},\ 1 \leq i \leq c \end{aligned} \tag{4.7}$$

   where $\mathbf{v}_i{}^{(l)} = [v_{i,1}, v_{i,2}, \ldots, v_{i,q}]$ and $\mathbf{z} = [z_1, z_2, \ldots, z_N]^T$.

3. Estimate the parameters of local models $(g_i, 1 \leq i \leq c)$ using Levenberg-Marquardt (LM) method. The parameters of each local model is estimated by solving the following minimization problem:

$$\min_{\theta_i} = \|\mathbf{y} - g_i(\mathbf{z}, \theta_i)\|^2 \cdot \zeta_i = \|\mathbf{y}\sqrt{\zeta_i} - g_i(\mathbf{z}, \theta_i)\sqrt{\zeta_i}\|^2 \tag{4.8}$$

   where $g_i(\mathbf{z}, \theta_i)$ designates the output of the local fuzzy model for $\mathbf{z} = [z_1, z_2, \ldots, z_N]^T$, and $\mathbf{y} = [y_1, y_2, \ldots, y_N]^T$, and ζ_i denote a diagonal matrix having membership degrees as follows:

$$\zeta_i = \begin{bmatrix} \mu_{i,1} & 0 & \ldots & 0 \\ 0 & \mu_{i,2} & \ldots & 0 \\ \vdots & \vdots & \ddots & \vdots \\ 0 & 0 & \ldots & \mu_{i,N} \end{bmatrix}$$

   The standard deviation of the modeling error is given as:

$$\sigma_i^{2(l)} = \frac{\sum_{k=1}^{N} (y_k - g_i(\mathbf{z}, \theta_i))^T (y_k - g_i(\mathbf{z}, \theta_i)) \cdot \mu_{i,k}^{(l-1)}}{\sum_{k=1}^{N} \mu_{i,k}^{(l-1)}} \tag{4.9}$$

   The probability of the cluster and the impact of rules are also defined as:

$$p(\eta_i) = \frac{1}{N} \sum_{k=1}^{N} \mu_{i,k},\ \omega_i = p(\eta_i) \prod_{j=1}^{n} \frac{1}{\sqrt{(2\pi\sigma_{i,j}^2)}} \tag{4.10}$$

4. Compute the distance measure $D_{i,k}^2(z_k, \eta_i)$ (4.6)

5. Update $U^{(l-1)} \to U^{(l)}$ according to

$$\mu_{i,k}^{(l)} = \frac{1}{\sum_{j=1}^{c} (\frac{D_{i,k}(z_k, \eta_i)}{D_{j,k}(z_k, \eta_j)})^{2/(m-1)}}, 1 \leq i \leq c, 1 \leq k \leq N \tag{4.11}$$

6. If $\|U^{(l)} - U^{(l-1)}\| < \epsilon$ stop, else $l = l + 1$ and go back to Step 2.

Algorithm 5 LM Method for Model Parameters Identification

1. Initialize the parameter vector, $\theta^{(0)}$ and the damping factor γ. Choose the thresholds of the stop conditions, ϵ_1 and ϵ_2.
   Calculate the chi-square error criterion for $m = 0$:

$$\begin{aligned}\chi^{(m)}(\theta^{(m)}) &= \sum_{i=1}^{N}\left[\frac{(y_i^* - y_i(\theta^{(m)})}{w_i}\right]^2 \\ &= \Big(Y^* - Y(\theta^{(m)})\Big)^T W \Big(Y^* - Y(\theta^{(m)})\Big)\end{aligned} \tag{4.12}$$

   where W is the weighting diagonal matrix with $W_{ii} = 1/w_i^2$. The value of w_i is a measure of the error in measurement y_i.
   For $m = 1, 2, \ldots$ follow steps 2-5.

2. Find the Jacobian matrix:

$$J = \frac{\partial g(x, \theta)}{\partial \theta}$$

3. Find the correction vector $\Delta\theta$:

$$\Delta\theta = \left(J^T W J + \gamma\, diag(J^T W J)\right)^{-1} J^T W (Y^* - Y) \tag{4.13}$$

4. Update the parameter vector:

$$\theta^{(m)} = \theta^{(m-1)} + \Delta\theta$$

5. Find $\chi^{(m)}$ (4.12) and do the following:

   (a) If $\|\chi^{(m)} - \chi^{(m-1)}\| < \epsilon_1$, or $\|\theta^{(m)} - \theta^{(m-1)}\| < \epsilon_2$: Stop.

   (b) Otherwise: If $\chi^{(m)} > \chi^{(m-1)}$, reduce γ (e.g. $\gamma = \gamma/4$). Else, keep the old parameters: $\theta^{(m)}$=$\theta^{(m-1)}$ and increase γ (e.g. $\gamma = 2\gamma$).

$$I_{ED} = diag(\Psi_r \Psi_r^T) = diag(\psi_1 \psi_1^T + \psi_2 \psi_2^T + \ldots + \psi_r \psi_r^T) \tag{4.15}$$

where $\Psi_r = [\psi_1, \psi_2, \ldots, \psi_r] \in \mathbb{R}^{c \times r}$ includes the first r columns of Ψ, i.e. the eigenvectors corresponding to the r biggest eigenvalues. The position of r largest indexes in I_{ED} determines the r rules that should be retained. The rest of $c - r$ rules are removed, and the T-S state model parameters are estimated using a LM method.

Algorithm 6 Eigenvalue Decomposition Algorithm for T-S Model Reduction

1. Compute the eigenvalue decomposition of Φ_{uu} (4.14) and sort out the eigenvalue, and corresponding eigenvectors in a descending order in matrices Λ and Ψ, respectively. Determine the number of fuzzy rules that should be retained: r.
2. Partition Ψ into $\Psi = [\Psi_r, \Psi_{c-r}]$ where Ψ_r corresponds to the first r columns of Ψ.
3. Compute the measure index I_{ED} (4.15) . Find the r largest indexes in I_{ED}. Their position indicates those rules that should be retained.
4. Keep the r rules with indexes found in Step 3 and estimate the parameters of local state space models corresponding to r rules using a LM method. Note that the membership functions are already determined in Algorithm 4.

4.2.2 Observer Synthesis

The SoC is not directly measurable in Li-ion battery and the main objective of this modeling exercise is in fact to find a systematic model-based approach to estimate the all important SoC. Given the type of the model used, different observers have been employed to estimate SoC. In the past works, Kalman filter and its variants [122, 102, 89, 88] have received the most attention in this regard for both ECM and EPM. Given the freedom that ECMs provide, due to the availability of state-space model, other observers such as sliding model observers [56] are also proposed. Luenberger observer [60], Extended Kalman filter [33], [101], and Particle filter [100] are also exploited for the Electrochemical model of the battery. There are however some issues with observer design for electrochemical model of the battery. Observability of the general system is an important issue, and also, the stability and robustness of the observers are other challenging issues that need to be addressed properly. In the case of the filters, i.e. Extended Kalman or Particle filter, stability remains to be a concern. There are however a few observer design cases for reduced EM models [76, 32, 132].

In this section, we discuss the design of an appropriate observer for the TS model (4.1) identified using Algorithms 4-6. The simple Luenberger type observer and a generalized H_2 observer design is adopted for this system to address the robustness of the observer. The advantage of the applied observers is that the observer gains are selected such that the

stability and robustness of observer is analytically proved using Lyapunov Theorem. The observer designs are adopted from [39]. The fuzzy observer for TS model (4.1) is designed as a TS fuzzy system with the same number of rules (i.e. $l \in M := \{1, 2, \dots, r\}$).

Consider the T-S fuzzy model 4.1 where the noise is also considered:

$$\begin{aligned} R_l: \quad IF \quad & z_{1,k}\, is\, F_{l,1}\, and \dots and\, z_{q,k}\, is\, F_{l,q} \\ & x(k+1) = A_l x(k) + B_l u(k) + \vartheta_l + E_l w(k) \\ THEN \quad & y(k) = C_l x(k) + D_l u(k) + G_l w(t) \\ & q(k) = Hx(k) \end{aligned} \tag{4.16}$$

where, q is a linear combination of the state variables to be estimated, and w denotes the noise variable that belongs to $l_2[0, \infty)$. The fuzzy observer for TS model (4.16) is designed as a TS fuzzy system with the same number of rules (i.e. $l \in M := \{1, 2, \dots, r\}$) as follows:

$$\begin{aligned} R_o^{(l)}: \quad IF \quad & z_{1,k}\, is\, F_{l,1}\, and \dots and\, z_{q,k}\, is\, F_{l,q} \\ & \hat{x}(k+1) = A_l \hat{x}(k) + B_l u(k) + \vartheta_l + L_l(\hat{y}(k) - y(k)) \\ THEN \quad & \hat{y}(k) = C_l \hat{x}(k) + D_l u(k) \\ & \hat{q}(k) = H\hat{x}(k). \end{aligned} \tag{4.17}$$

where $\hat{x}$ and $\hat{y}$ are the estimated state and output matrices, respectively. The vectors $L_l, l \in M$ are the observer gains to be determined. Therefore, the fuzzy observer error dynamic equation derived from (4.16) and (4.17) can be written as:

$$\begin{aligned} \tilde{x}(k+1) &= \sum_{j=1}^{r}\sum_{l=1}^{r} \mu_j \mu_l (A_l + L_l C_j)\tilde{x}(k) \\ &\quad - \sum_{j=1}^{r}\sum_{l=1}^{r} \mu_j \mu_l (E_l + L_l G_j) w(k) \\ \tilde{q}(k) &= H\tilde{x}(t) \end{aligned} \tag{4.18}$$

where $\tilde{x}(k) = \hat{x}(k) - x(k)$, and $\tilde{q}(k) = \hat{q}(k) - q(k)$ are the observer errors. Provided error dynamics (4.18) , the objective is to design the observer such that the two conditions are satisfied:

1. The observer error system is globally exponentially stable.
2. The observer error system has a prescribed level ζ in the generalized H_2 sense under the zero initial condition.

$$\Xi := sup\{\|\hat{q}(T_f) - q(T_f)\| | \tilde{x}(0) = 0, T_f \geq 0, \Sigma_{t=0}^{T_f} w^T w \leq 1\} < \zeta \tag{4.19}$$

It means that the observer error system is globally exponentially stable and the induced l_2-norm of the operator from w to the observer error, $\hat{q} - q$, is less than ζ under zero initial condition for all nonzero $w \in l_2[0, \infty)$.

The following Theorem helps to design the observer's gains.

Theorem 2. *[39] Given a constant $\zeta > 0$, the observer error system (4.18) is globally exponentially stable with generalized H_2 performance ζ, if there exists a positive definite matrix P, a matrix R, and a set of matrices $Q_l, l \in M$, such that the following LMIs are satisfied:*

$$\begin{bmatrix} P & H^T \\ H & \zeta^2 I \end{bmatrix} > 0, \tag{4.20}$$

$$\begin{bmatrix} P - R - R^T & RA_l + Q_l C_j & -RE_l - Q_l G_j \\ A_l^T R^T + C_j^T Q_l^T & -P & 0 \\ -E_l^T R^T - G_j^T Q_l^T & 0 & -I \end{bmatrix} < 0, \ l, j \in M. \tag{4.21}$$

Furthermore, the observer gains are determined as:

$$L_l = R^{-1} Q_l, \ \ l \in M. \tag{4.22}$$

Proof. See [39]. □

The performance index ζ described above is also optimized using the following convex optimization problem.

Algorithm 7

$\min\limits_{P,R,Q_l} \zeta^2$, subject to LMIs (4.20) and (4.21).

The simple Luenberger observer is also designed using the following Theorem. In this design, noise is not considered, and thus, no robustness performance index is considered for this observer.

Theorem 3. *In the absence of noise, the fuzzy observer error system (4.18) is globally exponentially stable if there exists a positive definite matrix P and a set of matrices $Q_l, l \in M$ such that the following LMIs are satisfied:*

$$\begin{bmatrix} -P & A_l^T P + C_j^T Q_l^T \\ PA_l + Q_l C_j & -P \end{bmatrix} < 0, \ \ l, j \in M. \tag{4.23}$$

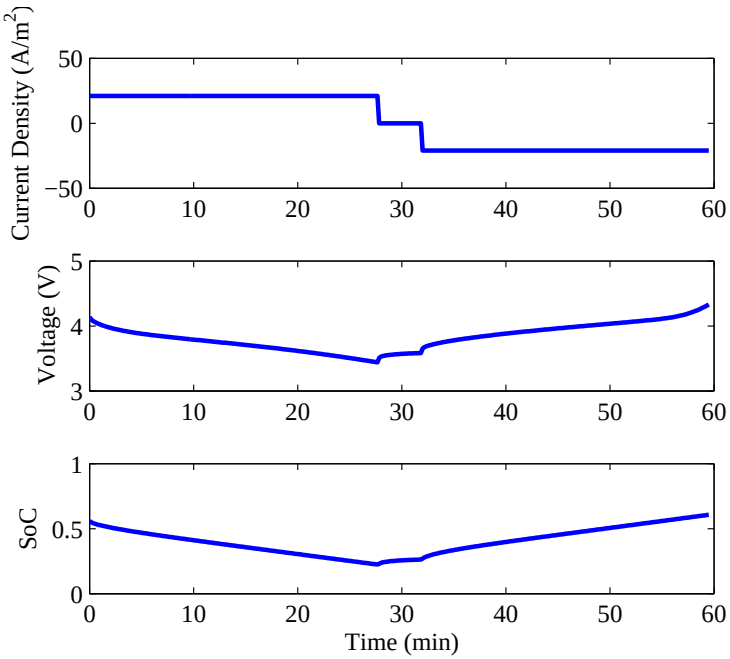

Figure 4.1: A typical charge-rest-discharge cycle for $I = 21A/m^2$ and $T = 293°K$.

Furthermore, the observer gains are determined as:

$$L_l = P^{-1}Q_l, \;\; l \in M. \tag{4.24}$$

Proof. See [39]. □

4.2.3 Simulation Studies

A Li-ion battery with the parameters given in Table 3.2 is considered. The battery equations are solved using COMSOL package for temperature range of $[244 - 303]°K$ and current in the interval of $[17.5 - 35]A/m^2$. The range of operation can easily be extended to any other region. A typical voltage and SoC profile for one cycle is shown in Figure (4.1).

For the modeling purposes, the state, input and voltage vectors are considered as follows:

$$x(k) = SoC(k), \; u(k) = [I(k), T(k)]^T, \; y(k) = V(k). \tag{4.25}$$

where $V(k)$ denotes the battery voltage, $I(k)$ the current, and $T(k)$ the temperature, where $I(k) < 0$ is considered for charge and $I(k) > 0$ for discharge. The SoC estimation is carried out using the T-S fuzzy systems with different number of rules (i.e. c). The modeling performance of the T-S models is shown in Figure (4.2) where the developed T-S model is not specifically trained for this current and temperature profile but they are within the range for which the model is trained. The percentage error due to each fuzzy system is

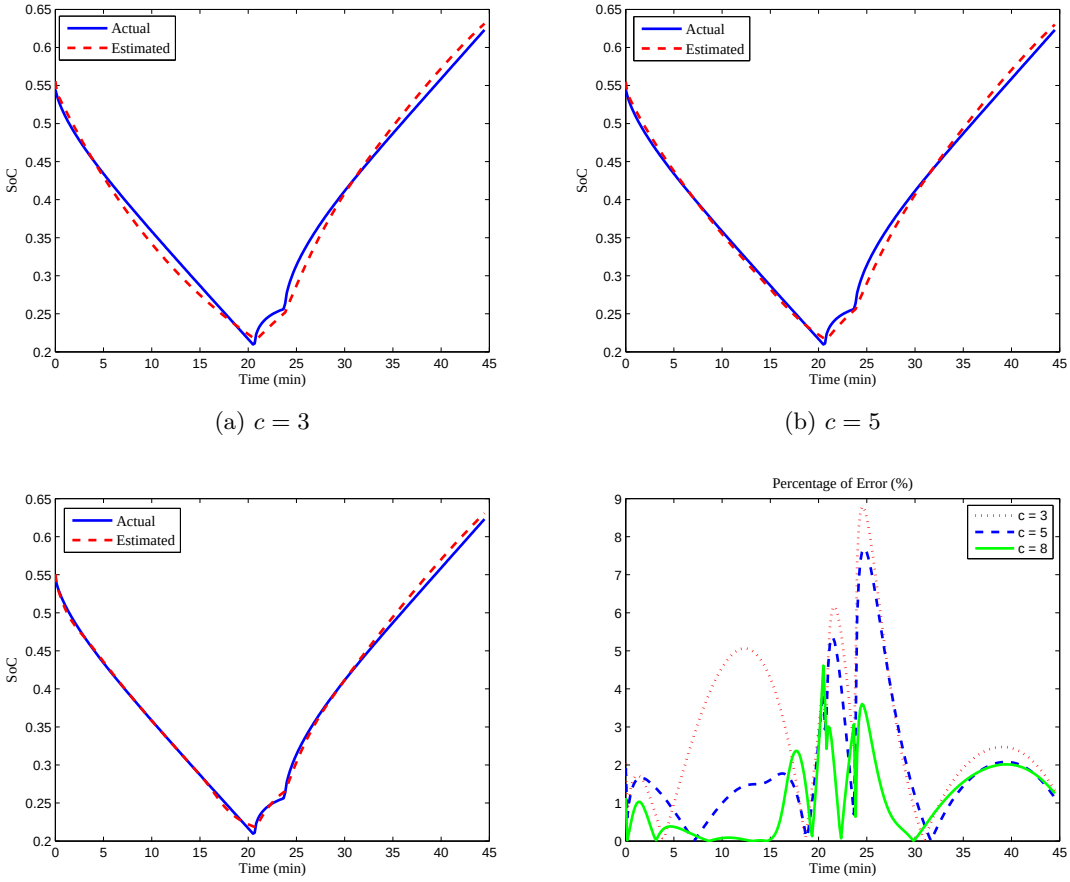

(a) $c = 3$ (b) $c = 5$

(c) $c = 8$ (d)

Figure 4.2: Performance of the T-S model for the Li-ion battery dynamics for $I = 28A/m^2$ and $T = 273°K$.

compared in Figure (4.2d). The Mean-Squared-Error (MSE) error corresponding to this set of test-data is given in Table 4.1 . Figure (4.2d) and Table 4.1 confirm that, as expected, the accuracy of the model will increase as the number of rules are increased. However, too many rules might cause generalization problem as it is discussed in the next section. The impact of T-S model simplification using ED is also demonstrated in Figure (4.3). The error percentage corresponding to a fuzzy system with $c = 5$ rules and a simplified version of the same system with $r = 3$ rules are compared.

The performance of the T-S model is quite convincing to be considered as an accurate model for control design objectives. In fact, the relative flexibility and much lower computational load that it provides to implement control schemes can justify its employment versus electrochemical model.

Table 4.1: MSE error versus number of rules for a typical cycle

No. of rules (c)	3	5	8
MSE	1.45×10^{-4}	7.99×10^{-5}	3.4×10^{-5}

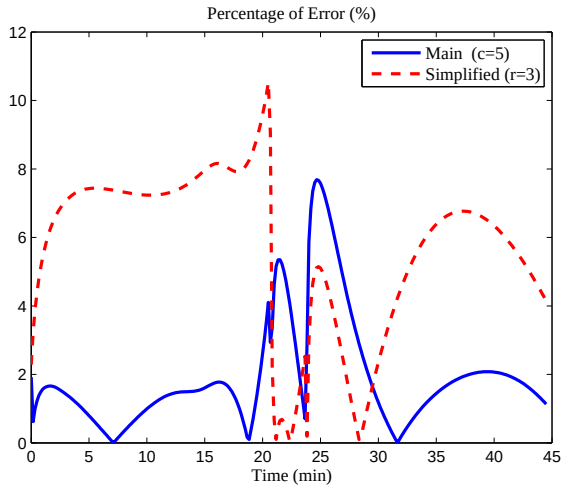

Figure 4.3: Percentage of error for a fuzzy system with $c = 5$ and its simplified counterpart with $r = 3$.

Observer Design

Provided the model developed in Section 4.2, the LMI problems derived in (4.21) and (4.23) are solved to find the observer gains L_l of local models. For this purpose, *"**cvx**"* which is a Matlab software for disciplined convex programming is used to solve the LMI problems [44]. The performance of H_2 observer and Luenberger observer is investigated and compared in Figure(4.4) for a TS-fuzzy model with $c = 3$ rules. The two cases of no noise and noise injection of $\sigma_w = 0.2$ on the output ($E_l = 0, G_l = I$) are considered to highlight the performance of H_2 observer in a noisy environment. The performance index obtained by solving the optimization problem (7) is $\zeta = 0.0142$. Since this high performance provide a very slow observer dynamics, the convergence speed of the observe is enhanced by imposing a decay rate on the observer ([123, 136]). Note that based on (4.25), the (A_l, C_l) cannot be unobservable unless one of them is zero which would never happen in model identification. It is also assumed that the whole T-S model is observable.

Remark 1. As noted by [3], without the zero initial condition assumption (in system (4.18): $x(0) = (\hat{x})(0)$), it is impossible to derive the LMIs in theorems (2 and 3). This assumption is typically made in design of H_∞ and H_2 observers. However, it should be noted that this is a sufficient condition. Simulation evidence verifies that the system is robust enough to the nonzero initial condition as well.

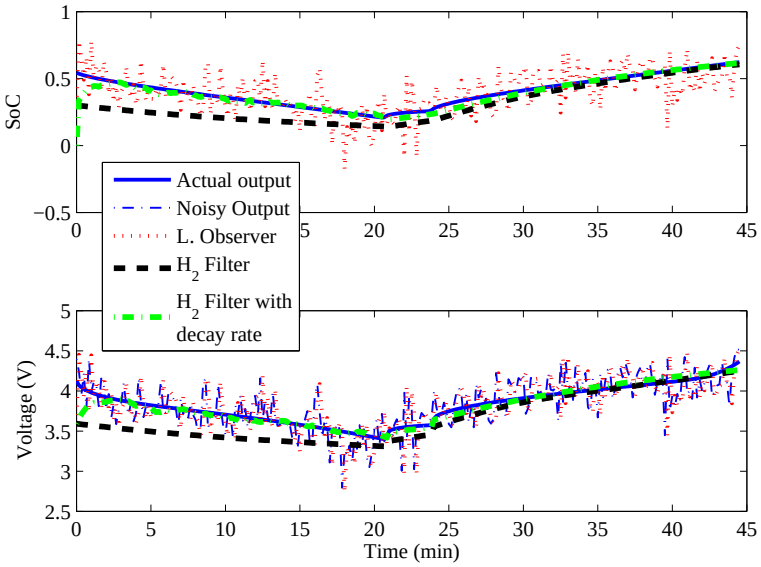

Figure 4.4: Performance of the T-S Luenberger and H_2 observers for $c = 3$ rules.

Pulse Modulation

To demonstrate the generalization ability of the developed model, a pulse modulation of the input is considered. The input is a continuation of different currents with multiple periods, however, the magnitude of the current is within the trained region. An observer for each case is designed and the performance of the estimation is shown in Figure (4.5) where Figure (4.5a) shows the applied current to the system.

Figures (4.5b) and (4.5b) demonstrate the SoC estimation and percentage of error of different T-S fuzzy systems. The results show that increasing the number of rules might lead to overestimation and will decrease the generalization ability of the model. Figure (4.5b) illustrates that the performance of the system with $c = 3$ is remarkably better than the systems with $c = 5$ and $c = 8$ rules, and also the system with $c = 5$ rules shows a relatively better performance than $c = 8$. Looking at the Figure, it appears that the main problem lies at the positive edge of each pulse. The fuzzy observer with $c = 3$ rules is however able to track the actual SoC with less than 2% error reasonably quick after each positive edge of the input. Moreover, considering the data with similar pulse input profile in the training data set would address this problem. The here aim was however to study the generalization ability of the model, and thereby no such data were present in the training data set.

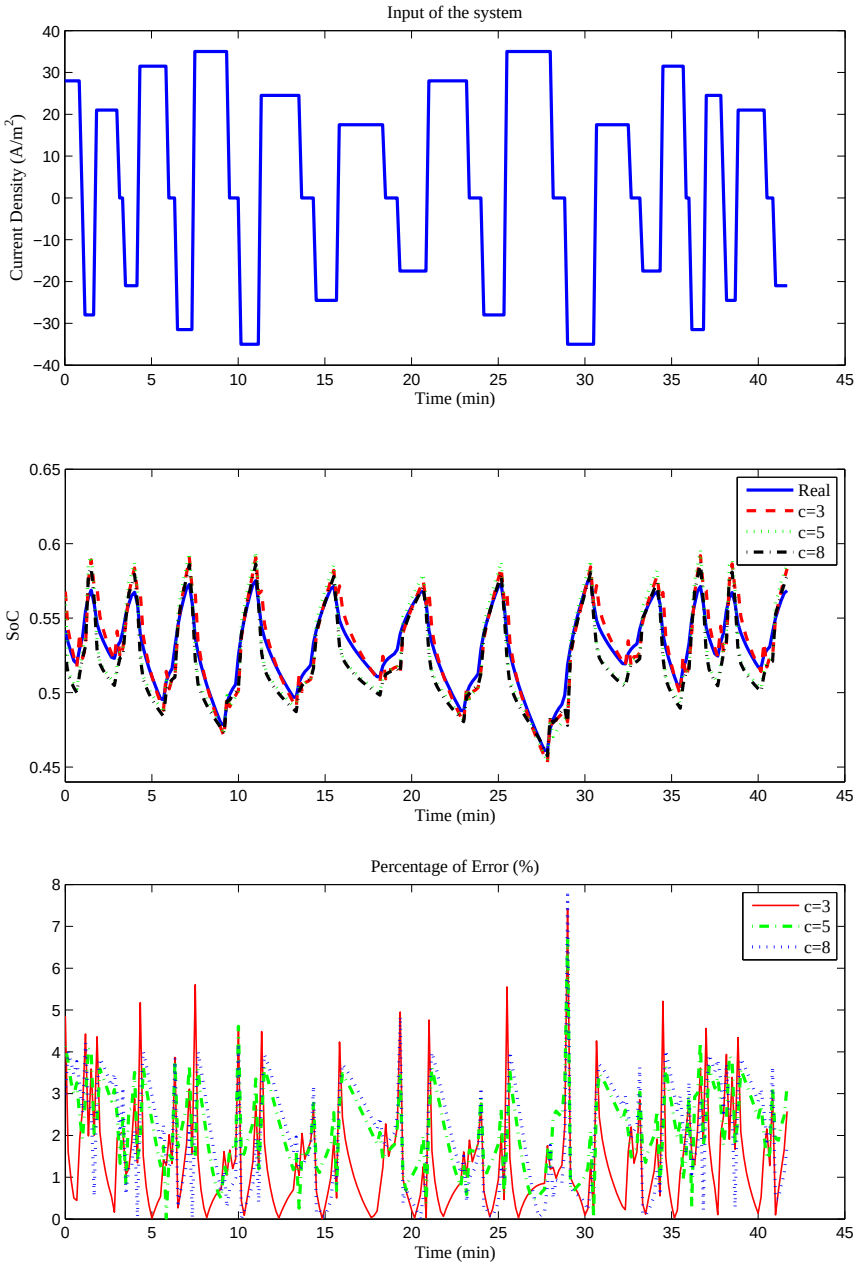

Figure 4.5: Generalization performance of the method. (a) The applied input to the system (b) *SoC* estimation performance of the T-S fuzzy system with different number of rules. (c) Comparison between the percentage of error between different systems.

4.3 Dynamic Resistance

Most of the battery model parameters are usually a nonlinear function of SoC. Nevertheless, this fact is usually disregarded in many of the battery modeling and simulation approaches due to the complexity of processes with a battery under load. For instance, most of the parameters involved in electrochemical model of the battery such as diffusion coefficients or changes in active materials resistance are functions of state of charge [46, 74, 85, 128]. On the other hand, most of EM-based simulation and estimation schemes apply constant parameters as a simplifying measure. Moreover, model parameters are also time dependent, changing with time and are a function of the cycle number and aging of the battery. To Measure battery parameters associated with active materials destructive methods are needed and hence not practical for real-time monitoring. Also, there are no models that can appropriately take into account the relationship between the parameters and cycle number. Thus, the problem that arises with model-based monitoring using constant parameters is that the estimation precision degrades as the battery cycles. Additionally, there is no clear understanding of the cycle life of the battery in the monitoring process of the battery. Hence, there is a need to consider battery cycle number, and parameters degradation due to aging, in battery modeling to be able to provide a more realistic picture for battery health monitoring within an appropriate framework.

In this Thesis, we have introduced *"Dynamic Resistance"* as a resistance which is a function of cycle number and state of charge of battery that can be easily monitored during the normal operation of the battery. Moreover, dynamic resistance shows different profiles for "charge" or "discharge" cycles of the battery that can include the intrinsic hysteresis phenomenon of voltage profile during charge-discharge processes. Unlike impedance spectroscopy which is a known methodology to measure the health of the battery and needs application of a frequency-rich signal [47, 98], the proposed technique does not need extra circuitry and would not need application of external signals to the battery-in-use.

4.3.1 Methodology

In this subsection, measurement of dynamic resistance is discussed. At a particular SoC, a current pulse of ΔI is applied to the battery and the voltage variation (i.e. ΔV) is measured. The electronic resistance and capacitive response can then be calculated. The response of the battery to the applied pulse is composed of different components whereas each component is triggered due to different processes occurring inside the battery. Figure (4.6) shows a typical pulse response where IR_e is spontaneous response related to electronic resistance and capacitive charging, and IR_d is the response of diffusion related processes, including the dominant Lithium diffusion in active materials. Each resistance can be decomposed as:

$$R_e = R_a + R_c + R_{SEI} + R_{el} + R_{contacts} \tag{4.26}$$

$$R_d = R_{act} + R_{ct} + R_{diffusion} + R_{concentration} \tag{4.27}$$

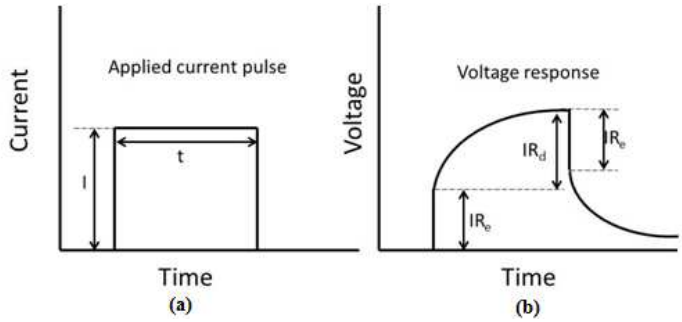

Figure 4.6: Battery response to applied current pulse (a) The current pulse of I with length of t. (b) Voltage response is composed of two components, IR_e and IR_d.

where R_e represents the overall electronic resistance, including electronic resistance of the anode R_a, electronic resistance of the cathode R_c, electronic resistance of surface layers formed on electrodes due to electrolyte decomposition (solid electrolyte interface) R_{SEI}, electronic resistance at the electrode / current collector interface R_{el}, and contact resistances at the battery tabs $R_{contacts}$. The R_d indicates the overall diffusion-related resistance components involving transport of ions and proceeding chemical reactions, such as activation resistance R_{act}, charge transfer resistance R_{ct}, and Lithium ion diffusion in solid phase that dominates the ionic resistances $R_{diffusion}$, and resistance due to concentration polarization at the electrode/electrolyte interfaces impeding ion diffusion processes $R_{concentration}$.

The system demonstrates different responses with respect to R_e and R_d. The electronic resistances show an immediate response to the applied current and voltage pulses. However, the diffusion related processes leading to resistances, R_d, are slow with longer relaxation time. There is also an intrinsic relation between the R_e and R_d which is material dependent.

In this work, the length of the pulses, t, is small (i.e. $t = 10\ sec$) and thus the immediate change in resistance at the beginning of pulse application that manifest electronic resistance (i.e. R_e) is measured. The electronic resistance in the cell follows Ohm's law as:

$$R_e = \frac{\Delta V}{\Delta I} \tag{4.28}$$

4.3.2 Feasibility of Technology in Vehicle Application

Implementation of this methodology on vehicle for battery monitoring would not require excessive development of the current battery management system design. Application of current pulse during the charge cycle can be simply implemented by reducing/increasing

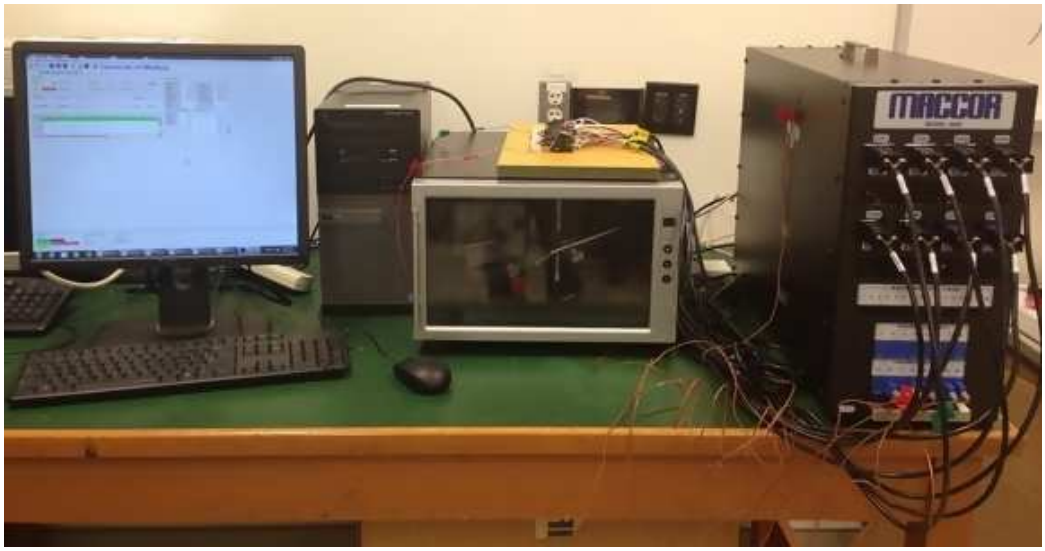

Figure 4.7: Experimental Setup: Maccor Battery Cycler and Tester (Maccor 4300) and temperature chamber.

the current for short periods of time whenever the measurement of SoC or SoH is desired. Moreover, it should be noted that although the notion of dynamic resistance was explained and simulated by applying a pulse to the battery, however during the discharge cycle, the driving cycle can itself provide the necessary information to deduce the dynamic resistance. Change of the vehicle speed leads to different loads on the battery and thus the battery current would change accordingly. Hence, in contrast to other methods such as impedance spectroscopy [47, 98] or resistance measurement methods [58], no extra circuitry is needed and also the proposed technique possess the real-time feasibility which can also provide important information about the conditions of the battery-in-use.

4.3.3 Experiment

A prismatic 2 Ah cell with graphite anode and nickel-cobalt aluminum oxide (NCA) cathode chemistry was used to collect data for model validation. The tests were carried out with a Maccor Battery Cycler (Maccor 4300) (Figure (4.7)). The current pulses of 0.1 A magnitude and duration of 10 sec was mounted on the main charge/discharge current of 0.5 A. A sample charge/discharge cycle with the applied pulse is shown in Figure (4.8). The voltage response due to applied current pulse was analyzed to evaluate "dynamic resistance" of the cells as a function of state of charge. The pulse current - voltage measurements are performed to obtain voltage profile hysteresis during charge and discharge processes (see Figure (4.9)). The dynamic voltage-current profiles are analyzed to obtain cell characteristics, mainly the SoC, and SoH.

Figure (4.10) shows the dynamic resistance versus SoC for different cycle numbers and also different charge - discharge cycles. The dependency of R_e on SoC and cycle number

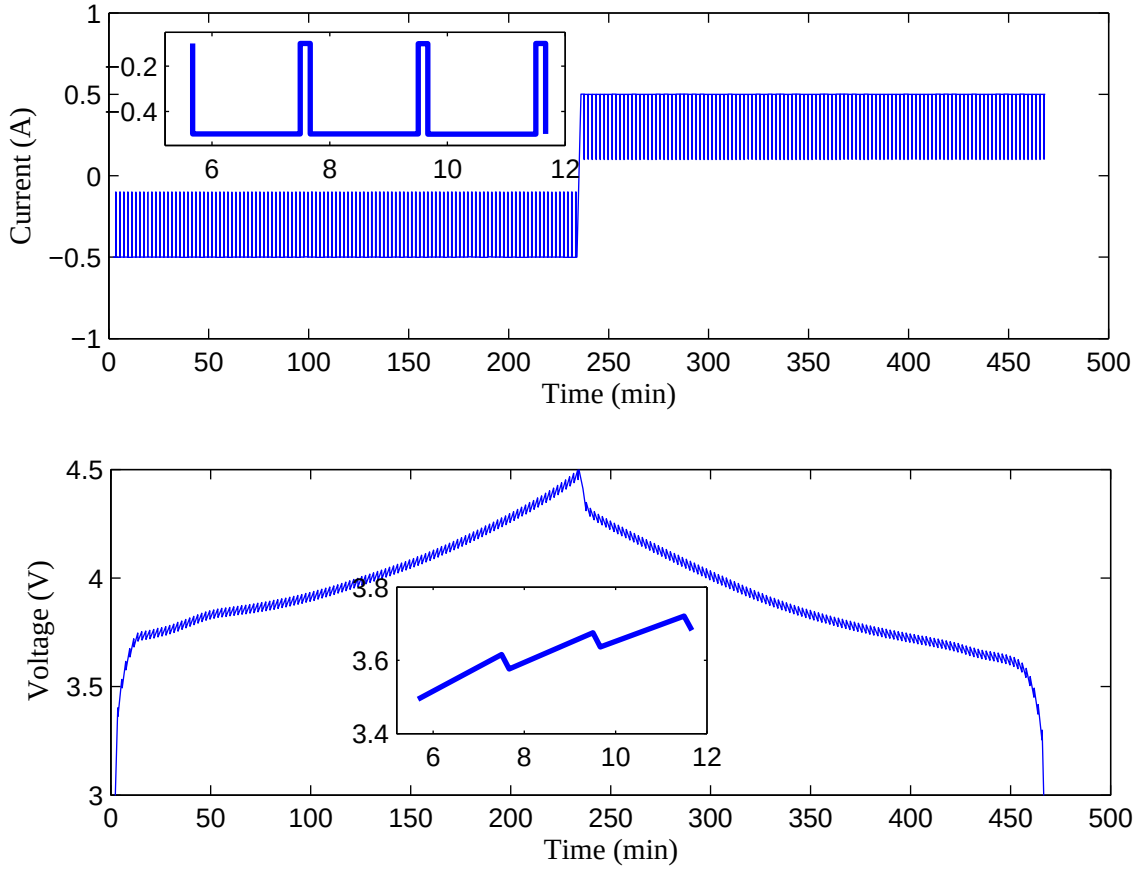

Figure 4.8: A charge/discharge cycle with short pulses mounted on the main charge/discharge current. The inset show the current and voltage for a few minutes to provide a more clear graph of the pulses and their response.

can be well observed in Figure (4.10). Results clearly show significant variation of cell resistances as a function of SoC and cycle number. In the following we will discuss an approach employed for modeling of dynamic resistance versus SoC.

4.3.4 Modeling

The objective is to find a model that can describe SoC in terms of R_e and cycle number. However, often the cycle number of the battery used is not available. Moreover, the cycle number alone without any knowledge about the history usage is not a good indicator of the current condition of the battery. For example, two identical batteries that experience different usage patterns would exhibit different characteristics at the same cycle number. Hence, a more practical parameter is the total power throughput, P_{tot}, of the battery and that is considered to account for cycle number and different battery usage patterns in this work.

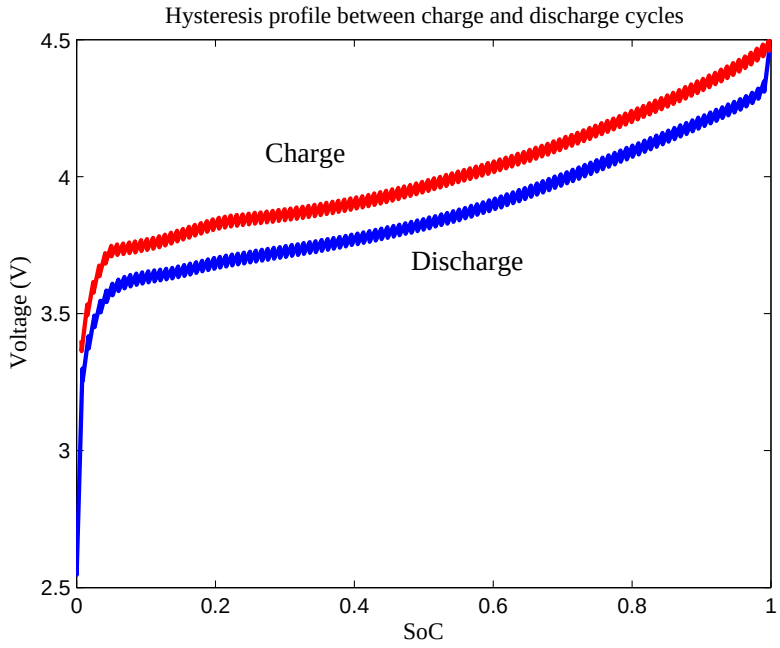

Figure 4.9: The hysteresis phenomenon is clear between charge/discharge cycles. The introduced method would also take care of this fact by consideration of two different models for charge/discharge cycles.

For the purpose of modeling, a particular neural network that can provide a fixed mathematical model description of the mapping between output and input is exploited. The main idea is to try different combination of mathematical functions in the network's topology and choose the best fit as the output of the network. The basic principles of this network are discussed in the following.

GMDH Neural network using heuristic self-organization method

Consider the following model

$$y(t) = f(x_1(t), x_2(t), \dots, x_N(t)) \tag{4.29}$$

where $x_i (i = 1, \dots, N)$ are the inputs and $y(t)$ is the output of the nonlinear system of interest. The problem is to determine the unknown model f using the available data, i.e. $[X, Y]$.

Group Method of Data Handling (GMDH) algorithm provides a solution to the posed problem using a nonlinear system identification method which employs an inductive learning scheme to construct a description of the system using heuristic self organizing map [72]. The identification process is fulfilled through a neural network where the topology of the network is self-organized using some heuristic rules [61, 82]. The proposed network has

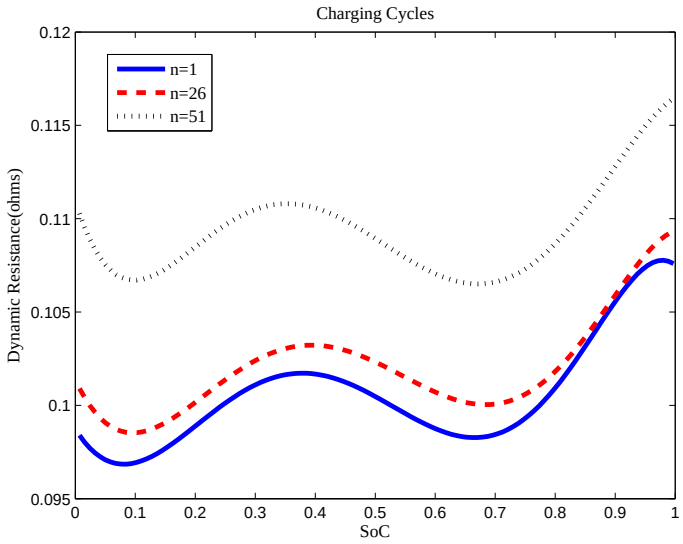

(a)

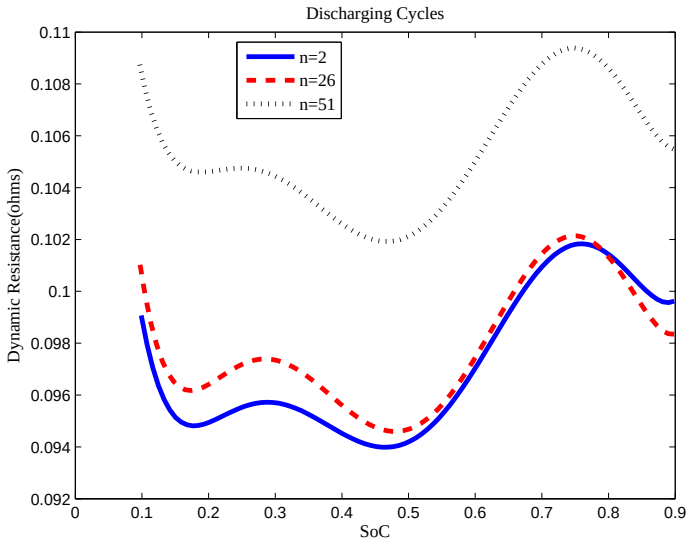

(b)

Figure 4.10: 2D dependence of dynamic resistance versus state of charge for different cycle numbers. (a) Charging Cycles (b) Discharging Cycles.

a multilayer perceptron-type structure in which the inputs of previous layer construct the possible combinations of the inputs in the next layer. The best results are chosen in this layer from which the next layer will be constructed. This process is continued to reach a certain level of accuracy at some layer. The final result is a mathematical description of output y in terms of $x_i (i = 1, \ldots, N)$ that is built in the network.

The mathematical model built via GMDH algorithm is in fact a combination of partial descriptions (PDs) of data. The partial description of data is formed through a base function involving two or more number of inputs. The Kolmogorov-Gabor polynomial is commonly used as the function to form the PD as following:

$$Y_{PD}(x_1, x_2, ..., x_p) = a_0 + \Sigma_{i=1}^{p} a_i x_i + \Sigma_{i=1}^{p} \Sigma_{j=1}^{p} a_{ij} x_i x_j + \Sigma_{i=1}^{p} \Sigma_{j=1}^{p} \Sigma_{k=1}^{p} a_{ijk} x_i x_j x_k + \ldots + a_{12\ldots p} x_1^{n_1} x_2^{n_2} \ldots x_p^{n_p} + \ldots \quad (4.30)$$

Y_{PD} is a partial description of inputs $(x_1, x_2, x_3, \ldots, x_p)$ which is a subset of the total number of inputs. A PD of order r possesses all possible terms generated from $(x_1, x_2, x_3, \ldots, x_p)$ where $n_1 + n_2 + \ldots + n_p \leq r$ for all terms. For instance, a PD of order 3 from input variables x_i and x_j using Kolmogorov-Gabor polynomial is constituted as:

$$PD = a_0 + a_1 x_i + a_2 x_j + a_3 x_i x_j + a_4 x_i^2 + a_5 x_j^2 + a_6 x_i^2 x_j + a_7 x_i x_j^2 + a_8 x_i^3 + a_9 x_j^3$$

The successive generation of PDs at different layers will gradually converge to the optimal structure of network that can predict the output with a desired precision. The algorithmic procedure of construction of GMDH neural network for a set of input-output data is described as following.

Procedure of constructing the GMDH neural network:

Step 1 Select the input variables $x_i (i = 1, \ldots, N)$ and choose the structure of network. The number of input variables for each PD, i.e. p, the order of polynomials for each PD, i.e. r, and the number of neurons in each layer, i.e. L, are chosen in this step. The available data are divided to two training and validation sets. Training data set is used to train the network and validation data set is used to validate the prediction performance of network.

Step 2 Calculate the PD corresponding to each set of input variables (z_m). Each PD is recorded in a neuron at the first layer. If the number of input variables for each PD is p, $\binom{n}{p}$ would be the total number of neurons in the current layer.

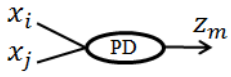

The coefficients of PD is derived by minimizing the mean squared error between the Y_{PD} and actual output y, using regression analysis as follows:

$$Y = XA \tag{4.31}$$

$$A = (X^T X)^{-1} X^T Y \tag{4.32}$$

where A represents the vector of coefficients of each PD, Y denotes the output data from the training data set and X is a matrix of the values of all terms (e.g. $x_i x_j$, $x_i^2 x_j$, ...) calculated using the training data set.

Step 3 Determine the prediction error of each neuron (i.e. m) using both the training and validation data as follows.

$$E_m = \sqrt{\frac{1}{M} \Sigma_{i=1}^{M} (y_i - z_{mi})^2} \tag{4.33}$$

where M is equal to the total number of validation and training data. z_{mi} is calculated using the coefficients estimated in step 2 for each PD.

Step 4 Keep the L neuron with best predictive capability and discard the rest.

Step 5 If the current layer is the first layer, continue to the next layer and go to 2.

Step 6 If the minimum value of prediction error is not decreased from previous layer stop the algorithm. Otherwise go to 2 and constitute the next layer.

Once the algorithm is stopped, the node (neuron) characterized by the best performance (i.e. minimum prediction error) is selected as the output node. All the remaining nodes in that layer (and probably next layers) are discarded. This node is traced back to the first layer and all the nodes that have no contribution to this node will be discarded from previous layers as well. The resulting network is shown in Figure (4.11). The mathematical description of input/output can be extracted from the network using the mathematical description of each contributed PD.

4.3.5 Simulation Studies

A fresh Li-ion battery cell, with the characteristics described in 4.3.3, was extensively cycled to collect enough information about cycling of the battery. An impulse current of $0.1-0.5(A)$ and length of $10(sec)$ was applied to the system to measure the dynamic resistance of battery based on Eq.(4.28). The state of charge of battery is measured based on a coulomb-counting method as follows.

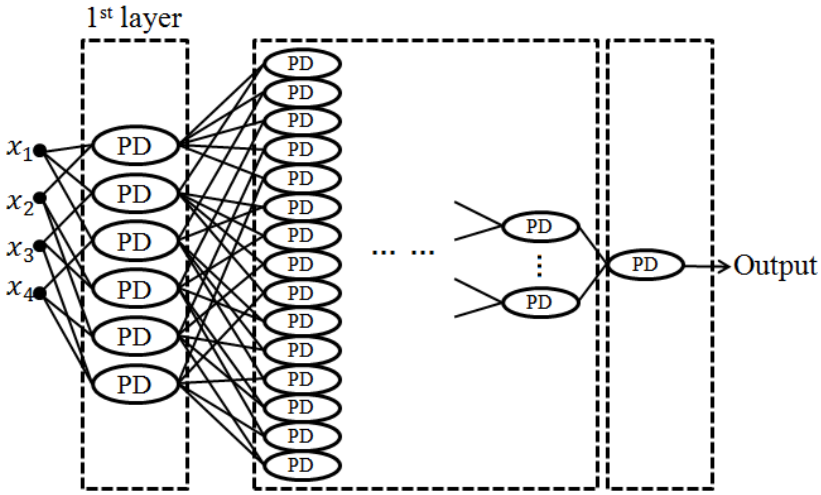

Figure 4.11: Schematic view of the GMDH neural network

$$SoC(t) = SoC(t_0) - \frac{1}{Q}\int_{t_0}^{t} I(\tau)d\tau \tag{4.34}$$

where $Q(Ah)$ denotes the nominal capacity of the battery and I is the current of the battery where $I < 0$ is conventionally considered for charging. It is worthwhile mentioning that since the battery was fully charged and discharged in experiments, the $SoC(t_0)$ is known based on the abrupt drop of voltage when the battery is fully discharged (i.e. $SoC = 0$) at each cycle.

The acquired data are smoothed using a Savitzky-Golay filter [104] in order to suppress the impact of varying temperature and other measurement and environment noises inherent in the system during the cycling tests.

As mentioned, the effect of cycle number is incorporated to the model via the total power throughput of the battery (P_{tot}). The battery power is considered as $P(t) = I(t)V(t)$, where I represent the current, V the voltage and the total power throughput is evaluated as the integration of P over the usage time, $P_{tot}(t) = \int_0^t P\ dt$. All of this data are readily available in a vehicle battery management system and can be easily embedded in the proposed framework.

SoC estimation

In this work, dynamic resistance R_e, current voltage V and square root of total power throughput $\sqrt{P_{tot}}$ are considered as the inputs of the first layer of GMDH neural network and the output is considered as the SoC of the battery. The following measure, $\sqrt{P_{tot}}$ is considered instead of P_{tot} since it reduces the variation range of the variable and shows better estimation performance. Hence, $X = [R_e(t), V(t), \sqrt{P_{tot}}]$ and $y = SoC(t)$. A GMDH

neural network is considered to model the nonlinear function of $y = f(X)$. The result of the network is a closed-form polynomial function that expresses $y = SoC$ in terms of x_1, x_2, and x_3. For the sake of brevity, the long equation of $y = f(x_1, x_2, x_3)$ is not listed here. Table 4.2 show the mean square error (MSE) of SoC estimation for a few different cycles. The acquired results show the effectiveness of this approach.

Table 4.2: MSE of SoC estimation using GMDH neural network for a few random samples.

Cycle number	15	57	97	197	251	296
MSE	0.0145	0.0232	0.0124	0.0150	0.0140	0.0128

SoH estimation

As discussed in 3.1.2, SoH is generally referred to deterioration of the battery conditions with respect to its nominal conditions. It is also mentioned that for HEV and EV applications, the end of battery life is considered to be the condition that battery can only deliver 80% of initial capacity. Monitoring of the dynamic resistance and comparison with dynamic resistance of a fresh cell is proposed as a new technique for SoH monitoring. It is a real-time technique that is easily implementable on the current BMS technology. Figure (4.12) shows the strong correlation between the average dynamic resistance and capacity fade. The average dynamic resistance is calculated as the average of dynamic resistance versus SoC within one cycle (i.e. charge or discharge) (Eq. 4.35). Capacity fade is calculated as the difference between maximum useable capacity of each cycle (i.e. C_n) and the fresh cell capacity (i.e. C_0) (Eq. 4.36).

$$R_e^{ave} = \int_0^1 R_e(SoC)\, dSoC \tag{4.35}$$

$$\Delta C\% = \frac{C_n - C_0}{C_0} \times 100\% \tag{4.36}$$

4.4 Summary

This Chapter dealt with data-based methods for battery estimation and monitoring. The main purpose of the developed methods are to provide methodologies that can address the real-time implementation of monitoring algorithms while also taking the physics of the system into account. In this regard, two different approaches were considered: i) Fuzzy Modeling of Battery System, ii) Monitoring Using Dynamic Resistance

In the first work, a Takagi-Sugeno Fuzzy model was developed for the battery system where the data were extracted from the electrochemical model of the battery. The nonlinear behaviour of the battery dynamics is dealt with clustering the data and fitting a linear state-

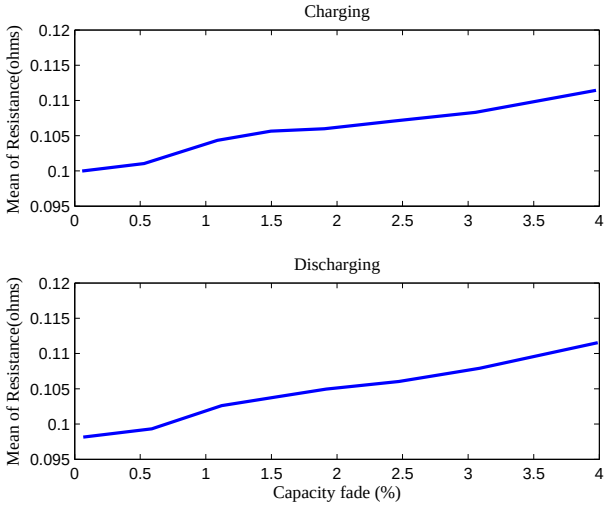

Figure 4.12: Correlation of capacity fade versus average dynamic resistance for 50 cycles.

space model to each cluster. The final response of the system is then a fuzzy mixture of all local linear models. It was shown that this strategy can provide a tools to effectively address the battery modeling. This would also obviate the need for look-up tables in battery model parameters which are usually required if the reliability of the model in a wide range of operation is concerned. The other feature of this model is that it facilitates the application of control theory algorithms to the system. A robust observer design was conducted in this regard.

In another work, the parameter "dynamic resistance" was introduced as a new means to monitor the battery behaviour. This parameter is dependent on SoC as well as battery aging conditions. Therefore, it provides a framework to incorporate the aging in SoC monitoring of the battery. The dynamic resistance was modeled versus SoC and power throughput as an indicator of aging condition, using a neural network model. Monitoring of dynamic resistance is also very advantageous from SoH monitoring standpoint since as it was investigated, this parameter shows a one-to-one relationship with SoH of the battery. The beauty of the proposed methodology is that it is implementable using the data collected during the normal operation of the battery.

Chapter 5

Diagnostics of Lithium-Ion Batteries

5.1 Introduction

As discussed in Section 2.4, fault detection and diagnosis is one of the main tasks of an advanced BMS. However, battery diagnostics is an area that is less developed, particularly from an industrial point-of view. Nevertheless, developing a robust fault diagnosis system for electric-based transportation is a crucial step in improving performance, reliability, and high margin of safety for a sustainable HEV and EV markets. Complicated nature of failure processes, lack of enough experimental evidence and hence lack of understanding of the physics of the problem and sheer size of the corresponding mathematical models are perhaps the major barriers to developing appropriate algorithms for diagnostics of the battery. This Chapter presents a model-based approach towards the diagnostic problem of the battery. The physics of the problem including the degradation and failure mechanisms are reviewed and also, some physics-based models that have been presented for modeling of some degradation mechanisms of the battery are briefly discussed. Finally, particle filtering-based algorithms for fault-detection of the battery is developed for a few common degradation processes.

5.2 Degradation

In this Thesis, degradation and aging of the battery refers to "irreversible" changes in the normal battery properties. They are also referred to as "failure" mechanisms in this Thesis. Failures in a battery can be classified as incipient or gradual and abrupt faults. Under the class of gradual faults, battery normally perform but in a degraded mode, whereas abrupt faults affect the battery performance in such a way that the normal operation of battery would be no longer possible. Although battery aging is inevitable, an intelligent BMS could

manage the battery's utilization and charge-discharge process so that the battery life is elongated. Besides, aging effects should be estimated in order to have a valid prediction of the life of the battery and modify the state of charge estimation of the battery.

Abrupt faults, in contrast to gradual faults are avoidable by careful monitoring of the battery. Some of them could be the result of aging mechanisms that gradually result in a big shut-down, for instance stress build-up at the electrode / current collector interface may cause sudden delamination and disconnect of active materials from current collector. Hence, if aging mechanisms are controlled effectively, these faults can be avoided. However, in the case of their occurrence, they should be detected as quickly as possible and corrective actions should be taken before damaging other equipment.

Due to the advantages of model-based control and fault detection strategy in a battery system, it is very important to have a good understanding of the aging phenomena and its relationship to the battery's electrochemical model. Some of the faults manifest themselves in certain parameters in the model of the battery while others could follow specific dynamic models that should be incorporated into a model-based analysis of the battery. It should be noted that development of appropriate models that could incorporate the battery's aging process is an area that requires much more research. Darling and Newman [29], and more comprehensively, Ramadass and his colleagues [93, 90], originally initiated modeling of aging processes from a first-principles point of view. Most of the other works [12, 18, 13, 118], however, present empirical models for this purpose, and hence, are battery specific, and cannot be generalized for all battery systems. The major challenge here is a lack of deep understanding of various phenomenon including degradation and failures of various types within the battery system. In addition, many of the aging processes are chemistry dependent, and may significantly vary from one class of battery to the next. In the following, a list of well-known failure mechanisms in Li-ion batteries is provided. Modeling of these mechanisms is also discussed briefly.

5.2.1 Degradation and Failure Mechanisms

i. *Formation of resistive films on the active particle surface, solid/electrolyte interface (SEI) layer:*

Principally, SEI is the solid electrolyte interphase which refers to a protective layer that is formed in the initial charge-discharge cycles and is permeable for lithium ion transport but rather impermeable to other electrolyte components and electrons [30]. Conventionally, however, SEI term has been used for all sorts of protective layers regardless of the functionality and formation procedure of the layer.

Different chemical processes, i.e. side reactions, can lead to film formation on the surface of electrode particles. Passivation of the negative electrode, cell oxidation and deposition of metallic lithium onto the negative electrode due to overcharge are the

main examples. Note that metallic lithium deposition, due to its particular significance is discussed in a separate part individually.

Electrode passivation refers to passive film formation on the electrodes. Reduction of solvent (for the electrolyte) is the main reaction accountable for passive film formation [93]. Although, formation of elastic flexible passive film on the anode is vital for stability of the cell [7], it is also a source of degradation of the battery which increases the impedance of the battery. Hence, in order to have a valid estimation of the performance of the battery, this process needs to be considered while studying the degradation processes.

Electrolyte oxidation, on the other hand, leads to build up of surface film on both positive and negative electrodes. In negative electrode, electrolyte may react with negative electrode and cause delithiation (oxidation) of lithiated carbon ($Li_xC_6 \longrightarrow ye^- + yLi^+ + Li_{x-y}C_6$) and result in deposition of Li_2CO_3, polymeric film, Li_2O, and LiF on the negative electrode [14]. In the positive electrode, experimental evidence shows that by increasing the potential at the positive electrode/electrolyte interface, electrolyte oxidation may occur which could be detected by noticing the increase of the surface resistance [137].

As battery ages, growth of SEI and passivation layer can further penetrate the pores of electrode and clog them and may also penetrate into the pores of separator. As a consequence, this will lead to decrease of active surface area of the electrode [130, 17]. In effect, it will decrease the charging capability (particularly in negative electrode) of the battery.

The reduction and oxidation of electrolyte components deteriorate the performance of the battery. Electrolyte decomposition is the cause of several degradation mechanisms taking place in the battery. It could also be considered as a contributing process accountable for self-discharge of the battery.

Electrode decomposition leads to electrolyte loss and further SEI formation (at electrode/electrolyte interface). Moreover, as a result of electrolyte decomposition (i.e. reduction), gaseous products may also be released. These gaseous products will increase the internal pressure of the cell for which exceeding the pressure over a certain limit will cause severe safety problems in the cell.

From a modeling point of view, each side-reaction is represented by a physical model. Moreover, this mechanism has a major influence on the internal parameters of the generic battery model, e.g. loss of rate capability, decrease of electrolyte conductivity, and loss of cell capacity [4].

ii. *Deposition:*
Surface films on the electrodes are composed of lithium ion conducting materials. Ap-

plying an electrical field to electrodes results in Li dissolution or deposition on the surface films. The lithium deposition in the form of metallic lithium occurs when the rate of lithium ion diffusion in the bulk of electrode is less than the rate of incoming lithium. This phenomenon often takes place at high charge rates. Hence, lithium deposition is basically a parasitic side reaction occurring during high rate charging. This problem is more pronounced at low temperatures as the diffusion of lithium in bulk of electrode is lower.

a. Plating: Refers to a rather uniform metallic lithium deposition.

b. Dendrite Formation: Non-uniform deposition which could be assumed as the major failure of Li electrodes at the anodes. Deposition and dissolution of Li inherently leads to morphological change of Li surface. When the surface film cannot accommodate these changes, it will result in breakdown of the surface films and consequently highly non-uniform deposition of Lithium. Dendrite formation can lead to severe safety issues such as shorting (dendritic growth through separator), formation of high area reactive lithium, etc [7].

iii. *Positive electrode dissolution:*
This mechanism is related to the dissolution of metal ions from electrode lattice into the electrolyte and is the primary reason for capacity loss of positive electrode. In addition to the chemical nature of the positive electrode (i.e. positive electrodes containing Mn), structural defects in the positive active material, reactive impurities, and high charging potentials are the main reasons leading to metal dissolution [4, 92]. Electrode dissolution might result in metal deposition (e.g. manganese dissolution in $LiMn_2O_4$ electrodes, or cobalt leaching from $LiCoO_2$ electrodes) which eventually leads to loss of active material, deposition on and clogging of the negative electrode pores, and dendrite formation. Generally, overvoltage and high temperature promote the rate of metal dissolution.

iv. *Loss of active material:*
There are several reasons that have been identified causing loss of active material, including: dissolution at the positive electrode, volume change of carbon electrode, and particle isolation in the both negative and positive electrodes. In the positive electrode, dissolution is the main reason that leads to active material loss and consequently capacity loss (see part iii). In the negative electrode, during insertion of lithium into solid particles, the volume of the carbon electrode increases (about 10%) and causes the degradation of surface film where it consumes lithium to repair the surface layers and hence loss of active material occurs [126].

Particle isolation as another factor of loss of active material may also occur in both negative and positive electrodes [26]. In positive electrode, oxidation of solvent at

high potentials forms a film that electronically isolates the active material, whereas in negative electrode, isolation occurs due to accumulation of electrolyte decomposition products on the surface of the particles [26, 55].

v. *Growth of large inactive materials:*
Different side reactions taking place in a battery may lead to inactive mass formation on the electrodes (particularly on the cathode) and volume of inactive materials will increase as the battery ages. This phenomenon could be modeled by considering the side reactions occurring in the battery and is more pronounced at elevated temperatures. It essentially leads to capacity fading of electrodes.

vi. *Current collector corrosion:*
Corrosion here is mostly regarded as pitting corrosion which refers to local creation of small holes in the surface of metal. It usually results from a chemical reaction between the electrolyte and electrodes. Pitting corrosion may initiate from surface defect sites, local surface impurities, or due to surface adsorption of aggressive ions or polar molecules. Current collector corrosion is a major cause of self-discharge process occurring in some batteries [139]. In critical case, corrosion of the current collector may induce a short-circuit, affecting battery's safety, particularly in batteries with bi-polar electrode design [78]. This problem is however more pronounced for positive current collector (Al). Overcharge and overdischarge are the main factors causing this mechanism. The reader is referred to [78, 15, 10] for more on electrochemical analysis of corrosion process in both positive and negative current collectors.

vii. *Loss of electrical contact between metallic grids and active materials:*
This failure refers to electronic isolation of active mass from current collector occurring due to expansion-contraction of active material during charge-discharge process, and surface film formation. As the electrode expands, it generates new surfaces that may react with electrolyte and form insulation surface film. This fault is more significant in anode side, where formation of thick layers of solvent reduction products can lead to electric isolation of graphite particles and consequently, their deactivation [7]. This mechanism depends on the morphology of the particles (i.e. graphite particles) and possible gas formation between the reactive electrode's surface and solution species [8].

Furthermore, volume changes of the active negative electrode material can cause mechanical disintegration and delimitation of the composite electrode which eventually may lead to loss of electrical contact between current collector and the electrode active material (i.e. carbon) [130]. The loss of active materials due to mechanical disintegration is more severe in high capacity silicon anode, where the lattice expansion due to $Li - Si$ alloy formation may exceed 300%.

viii. *Electrode distortion, disorder or fracture in lattice structure of electrodes:*
Fast charging/discharging of a battery can lead to fracture in the crystallites structure of the electrode. This phenomenon is more prominent during fast charging. It can lead to non-uniform charging of surface to bulk and may create stress at the interface of fully charged portion of the particle and the charge deficient part. Both cracking and structural damage might occur on the carbon electrode due to structural changes during lithium uptake (i.e. insertion of Lithium in the graphite lattice) that will create mechanical stress. In the other side, lithium ion insertion in the positive electrode which leads to molar volume changes, or phase transitions, can cause lattice distortion and mechanical stress. This in turn leads to change of the capacity ratio of the individual electrodes and imbalance of the electrode capacity.

ix. *Electrochemical grinding and pulverization of active materials:*
The electrode particles, particularly oxide particles (in the positive electrode), pulverize into finer powders under chemical and mechanical stress. This crushing process is termed "electrochemical grinding" [25]. The two originating factors for stress build-up in the cell are mainly volume changes in the lattice and phase transformation, i.e. coexistence of different phases such as lithium deficient and lithium rich phase [97]. Particle fragmentation, i.e. crushing of the particles into finer powders, can increase the dissolution rate by increasing the surface area which can eventually lead to loss of contact between particles. It is noticeable that higher electric fields, i.e. high potential, can be a promoting factor for pulverization of the particles by increasing the mechanical stress and fatigue during multiple cycles [25].

x. *Loss of plate active surface area:*
This phenomenon is a consequence of repeated metal dissolution and recrystallization. For example, dissolved manganese (or other metals) formed as a result of positive electrode dissolution can be reduced at the negative electrode and blocks the pores and thus reduce the active surface area [4]. Partial delamination due to stress at electrode - current collector interface and formation of isolated islands also leads to loss of active surface area.

xi. *Porosity change of the electrode:*
Formation of the side-reaction products that block the pores with inactive materials leads to porosity change in the electrodes. This, in effect, will have impact on the capacity and power fade of the battery [108]. Another significant factor is the volume changes of the active material (due to lithium insertion/extraction) that can largely affect the electrode porosity as well [42]. Porosity change will lead to variation of surface area and diffusion rate in the electrode.

xii. *Change in the diffusion coefficient:*

Diffusion coefficient value is mainly related to the structure-composition of active materials and represents the lithium mobility in the lattice. A low value of the diffusion coefficient can limit charge and discharge rates and induce large concentration gradients in the electrolytic solution during cell operation. It consequently increases the polarization losses and boosts the side-reactions, thus advancing failure mechanism, as the battery cycles [108, 119]. It is important to note that diffusion coefficient in battery electrode is a dynamic component and varies significantly as the concentration of lithium in electrode active material changes during charge and discharge. In the negative electrode, disorder or fracture of the lattice, reduction of metal on the electrode, and other side reactions may lead to change of diffusion rate leading to slow charge-discharge process. In the positive electrode, electrochemical grinding of the oxide particles (see part ix) influence the diffusion coefficient in the lattice of cathode particles. This also affects the lithium mobility in positive electrode significantly [79].

xiii. *Battery swelling:*

Battery swelling occurs mainly due to gas evolution in the cell. Gas forms from the decomposition of electrolyte (i.e. reduction or oxidation of electrolytes at the electrodes). The effect of gas evolution is reduction of the interfacial area between active material and electrolyte and consequently pressure build up in the cell which eventually leads to mechanical stress within the electrodes [106]. The gas bubbles also may trap in electrode pores and have an impact on electrode porosity and loss of contact.

In rare cases, gas evolution could cause very high pressures which can eventually lead to explosion. This is however usually controlled by venting mechanisms in the battery (particularly in cylindrical cell design). Apart from side effects such as porosity change, loss of contact, etc, this process changes the transport properties in electrolyte such as diffusion rate and penetration of electrolyte in electrode pores [106].

xiv. *Increase of electrode's impedance:*

Formation of surface films, formation of cracks in the surface film, gradual thickening of surface layer due to repetitive breakdown and repair of the surface layers, fracture in lattice structure of electrodes (i.e. graphite), loss of contact, etc, leads to an unavoidable increase of the electrode's impedance. Thus, essentially, the resistance against Lithium ion transport gradually increases. This phenomenon has been identified with the effect of electrode's impedance increase on the degradation. The impedance rise may have components related to kinetic, ohmic, and concentration polarizations. In general, contribution of various degradation processes to impedance rise in the cell can be analyzed in time or frequency domain because they have different characteristic times. However, physics of those processes must be carefully studied first.

xv. *Binder degradation:*
The binder material (e.g. fluorine-containing polymers, PVdF) can react with the charged anode (i.e. forming LiF) which leads to decomposition of the binder. This process leads to loss of Lithium as well as loss of mechanical integrity of the coated electrode [130]. Role of binder in electrodes with significant volume breathing during charge-discharge is very important.

xvi. *Abrupt faults:*

A. Thermal runaway
In the event of exothermic reaction between electrode/electrolyte, the internal temperature in the cell would increase. If the cell cannot dissipate this temperature rise properly, it will lead to further acceleration of exothermic reactions and will finally result in thermal runaway and perhaps battery explosion [9]. This failure is often a consequence of battery abuse such as overcharge, exposure to high temperatures, short-circuit, nail penetration, and crushing of the cell [117].

B. Short-circuiting
Melting or destruction of separator, and the growth of dendrite through separator are the two main reasons that can lead to internal short-circuiting. Internal short-circuiting is itself a fault of the battery that may lead to thermal runaway and cause more damage to the battery [9, 138]. Manufacturing defects, impurities, and existence of conductive foreign object in electrode may also cause short circuit in the cell.

C. Case rupture
Pressure buildup in the cell due to gas evolution, or as a result of exothermic reactions, in the extreme cases, can lead to cell rupture. Chemical hazards such as leakage or venting of corrosive or toxic materials could be the dangerous results of cell case rupture. Besides its safety concern, it will have a severe and abrupt impact on the battery performance [9].

5.2.2 Modeling of Degradation Processes

In order to have a valid estimation of the health condition and life-time of a battery, it is imperative to assess the individual and mutual impact of different failure mechanisms on the performance of the battery. Hence, a scalable and systematic model-based approach which is applicable to different batteries with different usage histories is extremely appealing. For this, a good physical understanding of the processes that are occurring in the battery is needed.

There are however two big challenges to model-based approach. First, the physics of some of the failure mechanisms is not yet well understood, and has not yet been modeled

in terms of first principles (i.e. physical laws). Second, the mutual impact of different mechanisms on each other, makes it very difficult to track each single individual process. Besides, the run-time and complexity of a physics-based model which incorporate all relevant processes, is costly for real-time monitoring. Nevertheless, with the every-day advancements in computers technology and given the fact that SoH measurement needs not be as fast as SoC monitoring, this problem could be addressed by a model based approach.

In this section, we try to introduce some of the modeling efforts that have been made in this area. Some of the degradation and failure processes of a battery have been translated into physics-based mathematical models. The developed models of degradation processes are not exhaustive by any means; nonetheless, many of the major failure modes of the battery have been modeled.

Degradation mechanisms have different impacts on the normal battery model from a control point-of-view. Some of them will add a set of equations to the existing set of battery equations where other ones may manifest themselves through changing the parameters of the battery model. In the language of control theory, the first set of mechanisms add state equations to the model of the battery, whereas the second set, i.e. parameter changes, might be observed by suitably designed parameter estimation methods. Design of proper observers or filtering methodologies are the potential solutions that can address the model-based monitoring of the battery. In this regard, combination of the frequency analysis along with time-domain model analysis can provide a complete picture about the battery. Frequency analysis could be particularly promising in detection of failure mechanisms.

i. *Side-reactions:*

Many of the aforementioned degradation mechanisms correspond to different chemical side-reactions taking place in the battery. At least, the major side-reactions leading to degradation mechanism is known, and thus, considering the dynamics of the corresponding reaction is the key to model a failure. In order to model a reaction, it is sufficient to consider the conservation of mass and rate expression for each species involved in the reaction. The conservation of charge equation for each phase (i.e. solid and electrolyte phase) in porous electrodes will then couple the rate equations of the reactions. A Butler-Volmer equation is considered to determine the rate of each reaction where some parameters such as open-circuit potential of the reaction, and other kinetic rates need to be calculated from experimental data.

$$i_k = i_{0,k}\left[exp\left(\frac{\alpha_{ak}F}{RT}\eta_{s,k}\right) - exp\left(-\frac{\alpha_{ck}F}{RT}\eta_{s,k}\right)\right] \tag{5.1}$$

where k refers to reaction number. The exchange-current density, $i_{0,k}$, in general format can be expressed as:

$$i_{0,k} = \mu_k \prod_j \left[\frac{C_j}{C_j^0}\right]^{\gamma_j} \tag{5.2}$$

where j indicates the phase (i.e. solid or solution phase). The driving force of the reaction is the overpotential, $\eta_{s,k}$, which can be written as:

$$\eta_{s,k} = \phi_s - \phi_e - U_k \tag{5.3}$$

where U_k represents the open-circuit potential of the side-reaction which is a function of the concentration. The kinetic parameters α_{ak}, α_{ck}, μ_k, and γ_j should be calculated experimentally. Assuming independent reactions, the total current density at each electrode can be written as: $i = \Sigma_k i_k$.

In order to simplify the equation, while considering an irreversible side-reaction, which is true for most of the failure side-reactions, a Tafel expression can be replaced with Butler-Volmer equation (5.1) at higher rates as:

$$i_k = i_{0,k} exp\left(\frac{\alpha_{ak} F}{RT}\eta_{s,k}\right) \tag{5.4}$$

For concentration of species i, C_i, the material balance shall be written as [4]

$$\frac{\partial C_i}{\partial t} = -\nabla . N_i + R_i \tag{5.5}$$

where N_i the molar flux of species i is calculated using the concentrated solution theory as follows.

$$\begin{aligned} &\text{Flux of dilute nonionic component :} && N_i = -D_{0i}\nabla C_i \\ &\text{Flux of dilute ionic component :} && N_i = -D_{0i}\nabla C_i - z_i \frac{D_{0i}}{RT} F C_i \nabla\phi \end{aligned} \tag{5.6}$$

and R_i, the net rate production of species i is calculated using the porous electrode theory.

$$R_i = -\Sigma_k a_k \frac{s_{i,k}}{n_k F} i_k \tag{5.7}$$

For more details on modeling of a side-reaction see [4].

ii. *Film formation on the electrodes:*
Electrode/electrolyte interface is accountable for many of aging mechanisms particularly at the carbon electrode side. Hence, modeling of the side reactions occurring on

this interface is very important to keep track of the battery degradation processes. In this regard, amongst the degradation processes, the formation and growth of passive film on the anode side has attracted most of the efforts. The SEI formation on the anode and its dynamic growth during battery aging contribute to overall cell impedance which can also be correlated to the predicted SoH.

Film formation modeling is nothing but the modeling of the side-reactions that lead to growth of a surface film on the electrodes. Reference [93] considers the problem of growth of film on the negative electrode due to slow solvent diffusion/reductions in the charge mode. It is reasonable to assume less or no capacity fade during a discharge cycle in comparison to charge cycle due to the growth of film on the negative electrode. It is important to note that chemical reactivity of the lithiated graphite is a function of lithium concentration, and at high state of charge, the electrode is most reactive, even at open circuit condition (i.e. self discharge).

The basic current density, J_{Li}, that appeared in the basic EM-model of the battery (2.2,2.3,2.4,2.5) can be decomposed as $J_{Li} = J_m + J_{sd}$, where J_m represents the main Lithium insertion reaction current density and J_{sd} is the side reaction current density. Main reaction kinetics, J_m, as mentioned, was expressed using a Butler-Volmer equation (2.8). The irreversible kinetics of the side-reaction leading to film formation (on the anode side) can be approximated by a Tafel equation as follows.

$$J_{sd} = -i_{0,sd} a_n exp(-\frac{\alpha_{c,n} F}{RT} \eta_{sd}) \tag{5.8}$$

where the overpotential of the side reaction η_{sd}, is written as:

$$\eta_{sd} = \phi_s - \phi_e - U_{sd} - \frac{J_{Li}}{a_n} R_{film} \tag{5.9}$$

The rate of the growth of resistive film which is being created by the above side reaction can be estimated as:

$$\frac{\partial \delta_{sd}}{\partial t} = -\frac{J_{sd} M_p}{a_n \rho_p F} \tag{5.10}$$

This film adds up to the total resistance of the negative electrode by considering the following equation.

$$R_{film} = R_{SEI} + \frac{\delta_{sd}}{\kappa_p} \tag{5.11}$$

where κ_p is the conductivity of the film. Note that R_{SEI} refers to the resistance of the film layer that has been created in the very first few cycles. The value of R_{SEI} is often considered as known for most types of the battery chemistry.

iii. *Lithium Deposition:* Under overcharge conditions, or when high charging rate is applied, metallic lithium may be deposited on the negative electrode. The corresponding side reaction ($Li^+ + e^- \longrightarrow Li(sol)$) can be modeled in a similar manner to what was done about solvent reduction on the negative electrode. However, it is pointed out in [4] that lithium deposition reaction is a facile process, and the surface overpotential will be low and therefore can be approximated adequately by linearizing the Butler-Volmer equation.

$$J_d = -i_{0,d} a_n \frac{(\alpha_{a,n} + \alpha_{c,n})F}{RT} \eta_d \tag{5.12}$$

The film growth on the surface due to deposition can then be modeled as

$$\frac{\partial \delta_d}{\partial t} = -\frac{J_d M_p}{L_n a_n \rho_p F} \tag{5.13}$$

The dendrite formation which is due to non-uniform deposition on the electrode is more complicated in nature and needs more careful consideration. Due to non-uniformity of the dendrites, the spatial distribution of the deposited layer needs to be considered in modeling of this phenomenon.

Note that in order to incorporate the effect of film layers on the impedance of the electrode, the conductivity and dielectric constants of layers need to be known. For example, if conductivity is known, the resistance of the deposited layer can be determined as δ_d/κ_p. Furthermore, if the film layer has some porosity or if it is not a pure ion conductor, the diffusion limitations should also be taken into consideration in the model of the battery [125].

iv. *Loss of active area:*
As mentioned, different side reaction such as passivation of negative electrode, crystallization, etc, will lead to reduction of the active area that is available for electrochemical reactions. This phenomenon can be simply modeled by considering the volume fraction of the precipitated layer [131]

$$a = a^0 \left[1 - (\epsilon_{layer}/\epsilon_0)^{g_p}\right] \tag{5.14}$$

where ϵ_{layer} is the volume fraction of the passivated layer on the interface and ϵ_0 is the porosity of the electrode. The term g_p is a geometrical factor varying from 0 to 1 which indicates the shape of the precipitated layer and how it has blocked the active area.

v. *Loss of active material:*
Different processes and side-reactions are responsible for loss of active material on both electrodes. By considering the side-reactions, the current density corresponding to each of the reactions can be estimated with a Tafel equation because we are only interested in irreversible reactions that lead to irreversible loss of active material. The loss of active material can then be estimated as:

$$Q_{loss} = \int_{t=0}^{t} J_{sd} A_j dt, \quad j = n, p \tag{5.15}$$

vi. *Volume and porosity changes in the porous electrodes:*
Volume changes in electrode may affect both the dimensions and porosity of the electrode. Reference [42] developed a model for volume changes for three different type of electrodes. For Li-ion batteries, we will have the volume change both due to deposition of side-reaction products on electrode surface and insertion/extraction of Lithium into/out of porous electrodes. In total, we can write:

rate of change in porosity + rate of change of volume (i.e. electrode dimensions) =
rate of change due to product formation + volume change due to intercalation.

The components of this equation can be expressed mathematically as:

$$\text{rate of change in porosity} = \frac{1}{1-\epsilon}\left[\frac{\partial}{\partial t}(1-\epsilon) + \mathbf{u}.\nabla(1-\epsilon)\right]$$
$$\text{rate of change of volume} = \nabla.\mathbf{u}$$
$$\text{rate of change due to product formation} = -\frac{s\hat{V}}{nF}\frac{J}{1-\epsilon}$$
$$\text{volume change due to intercalation} = \frac{1}{V_p}\left[\frac{\partial V_p}{\partial t} + \mathbf{u}.\nabla V_p\right]$$

where $\mathbf{u}$ is the vector of local electrode velocity. Variable V_p indicates the volume of electrode particle, and $\hat{V}$ represents the molar volume reaction product. Parameter J is the local volumetric electrochemical reaction rate which is calculated from a Tafel equation. For more details on boundary conditions, and solution of this equation, see [42].

vii. *Stress analysis on the battery:*

Reference [97] models the effect of hydrostatic stress on diffusion of lithium by modifying the diffusion equation of lithium in solid phase as follows:

$$\frac{\partial}{\partial t}C_{s,j}(x,t) = \frac{1}{r^2}\frac{\partial}{\partial r}\left\{D_{s,j}\left[r^2\frac{\partial C_{s,j}}{\partial r} + \frac{C_{s,j}}{RT}\left(\bar{V}_{s,j} - \frac{M_j}{\rho_j}\right)r^2\frac{\partial \sigma_{h,j}}{\partial r}\right]\right\}, \quad j = n,p \quad (5.16)$$

where σ_h represents the hydrostatic stress, M the molecular mass, $\bar{V}_s$ is the partial molar volume of lithium in the intercalation material and ρ indicates the density of the particle.

In order to take into account the phase transformation during the process of insertion/extraction of lithium into electrode, the above diffusion equation should be written for both coexisting phases in the electrode particle. The movement of phase boundary is assumed to be controlled by the diffusion process in the adjacent phases. The equation can thus be written as:

$$\left(C^{\alpha}_{eq,j} - C^{\beta}_{eq,j}\right)\frac{dr_j}{dt} = D^{\alpha}_{s,j}\frac{\partial C^{\alpha}_{s,j}}{\partial r} - D^{\beta}_{s,j}\frac{\partial C^{\beta}_{s,j}}{\partial r}, \quad j = n,p \quad (5.17)$$

where α and β refers to two phases, i.e. lithium rich and lithium deficient phases. Terms $C^{\alpha}_{s,j}$ and $C^{\beta}_{s,j}$ represent the lithium concentrations, and $C^{\alpha}_{eq,j}$ and $C^{\beta}_{eq,j}$ the maximum soluble concentrations of Li in α and β phases, respectively. The boundary condition of diffusion equation (Eq. 2.3) can be modified as:

$$D^{i}_{s,j}\frac{\partial C^{i}_{s,j}}{\partial r}|_{r=R_j} = -\frac{J_j}{a_j F}, \quad j = n,p; i = \alpha,\beta \quad (5.18)$$

where it refers to lithium flux at particle/electrolyte interface and $i = \alpha,\beta$ during deintercalation/intercalation, respectively.

The stress distribution in intercalation particles arising due to diffusion process is modeled by relating the elastic deformation of the material to intercalation process. The following equations are presented to model the stress tensor components, where hydrostatic stress σ_h is the average of principal components as $\sigma_h = (\sigma_r + 2\sigma_t)/3$. Parameters σ_r and σ_t represent the radial and tangential components of the stress tensor, respectively.

$$
\begin{aligned}
&\frac{\partial \sigma^i_{r,j}}{\partial r} + \frac{2}{r}(\sigma_{r,j} - \sigma_{t,j}) = 0,\ j = n, p; i = \alpha, \beta \\
&\sigma^i_{r,j} = \frac{E^i_j}{(1+\nu^i_j)(1-2\nu^i_j)} \left[(1-\nu^i_j)\frac{\partial w_j}{\partial r} + 2\nu^i_j \frac{w_j}{r} - (1+\nu^i_j)\Omega^i_j C^i_{s,j} \right],\ j = n, p; i = \alpha, \beta \\
&\sigma^i_{t,j} = \frac{E^i_j}{(1+\nu^i_j)(1-2\nu^i_j)} \left[\nu^i_j \frac{\partial w_j}{\partial r} + \frac{w_j}{r} - (1+\nu^i_j)\Omega^i_j C^i_{s,j} \right],\ j = n, p; i = \alpha, \beta
\end{aligned}
\tag{5.19}
$$

where w_j is radial displacement in region j, E indicates the modulus of elasticity for the material, ν the Poisson's ratio, and Ω the expansion coefficient due to intercalation (i.e. $\Omega^i_j = \bar{V}^i_j/3$) . See [97] for more details.

viii. *Battery Swelling:*
The gas evolution in the battery affects the electrolyte volume fraction. The reduction in electrolyte volume fraction of the electrolyte can be modeled as [106]:

$$
\epsilon_e(x, t + \Delta t) = \epsilon_e(x, t) - \Delta\epsilon_{gas}(x, t) \tag{5.20}
$$

where $\Delta\epsilon_{gas}(x,t) = \Delta V_{gas}(y(x))/V_{cell}$ and y is the local state of charge. Change of ϵ_e will in turn change the effective diffusion coefficient and conductivity in electrolyte phase. The volume fraction of active material remains rather unchanged due to gas evolution. Thus, battery swelling does not affect the transport properties in solid phase. The volume fraction of inert materials (i.e. binder, conductive additives) increase by $\Delta\epsilon_{gas}$ as the result of swelling.

ix. *Frequency Analysis*
The aforementioned equations are all time-based equations that often express the spatial distribution of different states of the battery or some physical parameters of the battery. On the other hand, frequency response of a battery can also present valuable knowledge about the status of the battery and its degradation processes. Reference [111] presents the analytical impedance models of the battery. However, for deriving these models, the author resorts to some simplifying assumptions such as constant properties of the battery where it could not be a valid assumption in the study of state of health and degradation processes in battery systems. Given the varying nature of the battery and coupled set of partial differential equations involved in its model, deriving an analytical impedance response would not be feasible. Instead, a measured impedance response along with the model analysis (time domain analysis) can significantly help in analyzing the effect of each one of individual failure mechanisms.

Reference [126] characterized the degradation processes with an impedance spectroscopy. The method presented therein opens a window to the methodologies which apply impedance stereoscopy for real-time monitoring. This article exploits a parameter estimation method on an equivalent circuit model to identify the impedance response of the battery for different components of the battery. These impedance measurements are then used to measure the health of the battery. Alternatively, we propose to use the EM-model of the battery, the impedance response of battery components (i.e. porous electrodes, electrolyte) can be extracted and used for health monitoring of the battery.

5.3 Fault Detection Using Particle-Filtering

The diversity of different degradation mechanisms and complexity of the associated models are so abundant that it requires a number of research works to address all of them. In this section, it is shown that how the particle filtering methods can be employed for detection and estimation of the battery faults using the electrochemical model of the battery. For this purpose, "positive electrode dissolution" and "plating mechanism" as two types of the common degradation mechanisms are considered and appropriate monitoring approaches are developed. The particle filtering methods developed in Sections (3.4) and (3.5) are employed as the estimation engines in the developed fault detection algorithms.

5.3.1 Plating Mechanism

Plating is a common degradation process in Li-ion batteries and degrades the battery's life and durability [48]. To the best of our knowledge, there is no systematic modeling of plating mechanism. However, it is reported that lithium plating side reaction is likely to occur at the negative electrode surface when

$$\phi_s - \phi_e < U_k \tag{5.21}$$

where U_k corresponds to the equilibrium potential (i.e. open circuit potential) of the side reaction of lithium plating on the electrode surface and is considered as $U_k = 0$ [129, 112]. Therefore, during the charge of Li-ion battery the $\phi_{se} = \phi_s - \phi_e$ is estimated at the negative electrode surface and maintained positive to prevent the plating mechanism.

For this purpose, the state estimation algorithm proposed in Section (3.4.2) is employed and the solid/electrolyte phase potential difference at negative electrode/electrolyte interface $\phi_{se}(x = L^-)$ is estimated to insure the plating mechanism does not occur. A safety margin of 10 mV is considered, and whenever the $\phi_{se}(x = L^-)$ drops below this threshold, a fault alarm is made to control the charging rate and prevent the plating. Therefore, the proposed detection system consists of two stages as shown in fFigure (5.1): 1) estimation, 2) comparison and alarm generation.

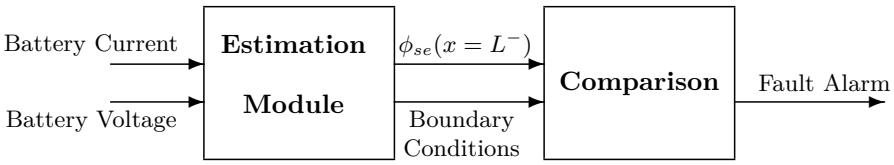

Figure 5.1: The proposed algorithm for the Plating Mechanism Detection

Simulation Studies

A battery with the characteristics given in Table 3.2 was used to investigate the performance of the algorithm. The plating condition is simulated by instantly increasing the charge rate by 4 times. The battery is being charged with the rate of 8.75 A when after 200 sec the current is instantly increased to 30 A. This can reproduce conditions under which plating is very likely to occur.

The application of PF for $\phi_{se}(x = L^-)$ estimation is shown in Figure (5.2). The straight line shows the simulation without any fault detection algorithm. It is clear that in this case, ϕ_{se} passes the margin of 0 V (i.e. dotted line) which can lead to plating that would degrade the performance as well as life of the battery. The dashed line shows the performance of the fault detection algorithm where a PF algorithm estimates the ϕ_{se} and as soon as it hits the margin of 10 mV (i.e. dash-dot line), a fault alarm is generated and the charging is stopped. A viable solution is to reduce the rate of charge sufficiently to give the negative electrode enough time to absorb all the Li-ions that are released from the positive electrode. The results show the effectiveness of the algorithm and its capability to detect the problem soon enough to prevent plating mechanism to begin.

Employment of the fault detection algorithms such as plating mechanism detection, not only prevents the hazardous conditions but also help to utilize the battery more efficiently by reducing the conservative margins that usually would be considered if no fault detection algorithm is placed.

5.3.2 Positive Electrode Dissolution

It was discussed in item (iii), Section (5.2.1), that Positive "Electrode Dissolution" is related to the dissolution of metal ions from electrode lattice into the electrolyte and is the primary reason for capacity loss of positive electrode. This process leads to decrease of the volume fraction of active material. Park et. al. [84] studies the impact of positive electrode dissolution in Li-ion batteries with $LiMn_2O_4$ as the cathode and shows that the following relationship describes the volume changes in cathode due to material loss.

$$V(t) = V_i \left(1 - \frac{0.304}{2} \frac{X_a}{X_a + 1}\right) \tag{5.22}$$

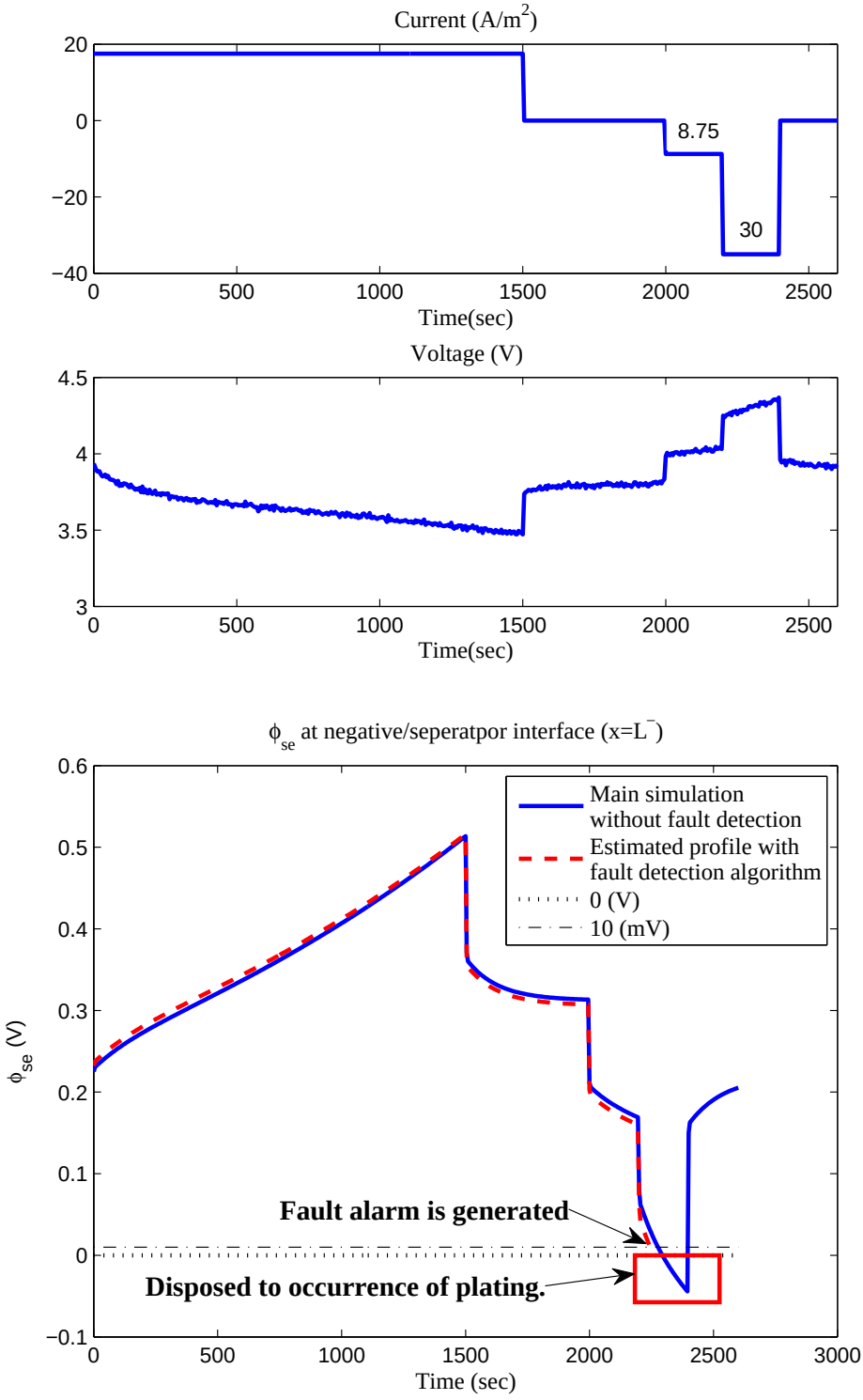

Figure 5.2: Performance of the fault detection algorithm. (a) Applied current and measured voltage (noisy) (b) Real and estimated values of $\phi_{se}(x = L^{-})$. A fault alarm is generated as soon as the estimated value hit the margin of 10 mV and the charging is stopped.

where, V_i represents the initial volume, and X_a the dissolution reaction. Therefore, the volume fraction of the cathode active material ($\epsilon_{s,p}$) is changed as:

$$\epsilon_{s,p} = \epsilon^i_{s,p}\left(1 - \frac{0.304}{2}\frac{X_a}{X_a + 1}\right) \tag{5.23}$$

where, $\epsilon^i_{s,p}$ is the initial volume fraction value of the cathode active material. The volume fraction changes in composite electrodes affect the specific interfacial area and the effective transport properties in the electrochemical model of Li-ion batteries as following:

$$a_p = 3\frac{\epsilon_{s,p}}{R_{s,p}} \tag{5.24}$$

$$\sigma_{eff,p} = \sigma\epsilon_{s,p} \tag{5.25}$$

Simulation Studies

It was shown that the dissolution of positive electrode would lead to decrease of the volume fraction of active material at positive electrode. Hence, a proper parameter estimation algorithm capable of estimation of the value of positive volume fraction ϵ_p can provide the framework for detection of this fault. In the proposed framework, certain thresholds shall be defined for ϵ_p and rate of its drop based on experimental results. Then, if the value of ϵ_p drops below that defined threshold, it means that the battery is approaching the end of its useful life. Also, if the rate of drop of ϵ_p is higher than a certain threshold, it can be either a sign of the end of life of the battery, or the battery might be under abuse and its usage pattern have to be changed; hence a fault alarm has to be generated. The schematic of the fault detection algorithm for positive electrode dissolution is depicted in Figure(5.3). However, a comprehensive experimental research study is required to relate the State of Life (SoL) of battery to the value of battery parameters and their associated rate of change.

The parameter estimation method developed in Section (3.5) is examined for two different values of $\epsilon_p = 0.29$ as the normal value and $\epsilon_p = 0.15$ as the degraded value. If it was possible to estimate the value of volume fraction, then one can relate the values to the SoL of the battery and extract a better prediction of the state of life of the battery. The results are shown in Figure(5.4) and (5.5). Figure(5.4b) and (5.5b) show that the error converges to a 2% error bound and stays there after a reasonable transient.

5.4 Summary and Discussion

This chapter presented a rather comprehensive survey of the different chemical and mechanical mechanisms that degrade the operation of a Li-ion battery. We have tried to collect all the major degradation or aging mechanisms of the battery in this list. However it is noted

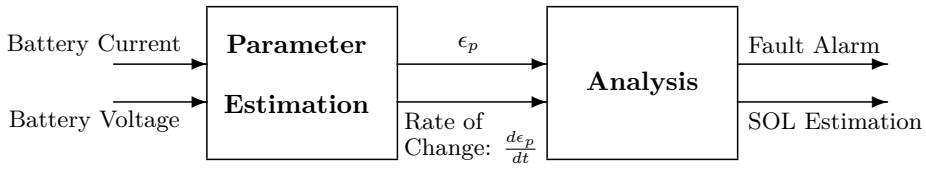

Figure 5.3: The schematic of fault detection framework for the positive electrode dissolution mechanism

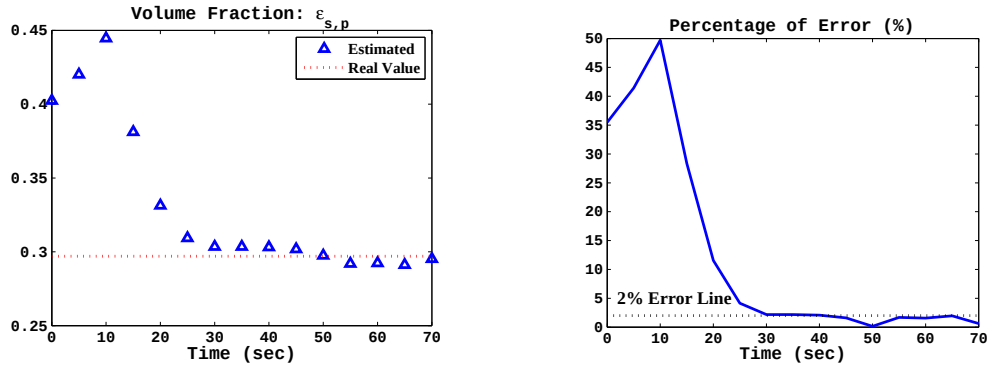

(a) (b)

Figure 5.4: Performance of the parameter estimation algorithm on ϵ_p. (a) Estimation of the normal value $\epsilon_p = 0.29$ due to fresh cell (b) Percentage of error

that what occurs as a fault in the battery might be originated from multiple mechanisms or a complex combination of them.

The degradation of Li-ion batteries was studied from a control theoretic perspective. In order to prepare the fundamentals for a model-based approach towards the diagnostics of battery, some physics-based models that have been presented for modeling of some degradation mechanisms of the battery are briefly reviewed. However, not all the degradation processes are yet modeled in the literature. This is, in fact, an area that needs much more research investigations to address all the problems in modeling of the degradation mechanisms within the battery. Understanding the physics of the degradation processes is a major challenge towards the modeling of them.

Incorporation of the main electrochemical model (EM) in the battery monitoring, and estimation of the model parameters can provide an appropriate framework for analyzing the degradation and failures of the battery. Therefore, the methodologies developed in Chapter (3) capable of dealing with EM are very instrumental in battery diagnostics. The degradation of the battery is however a colossal problem with enormous electrochemical complications.

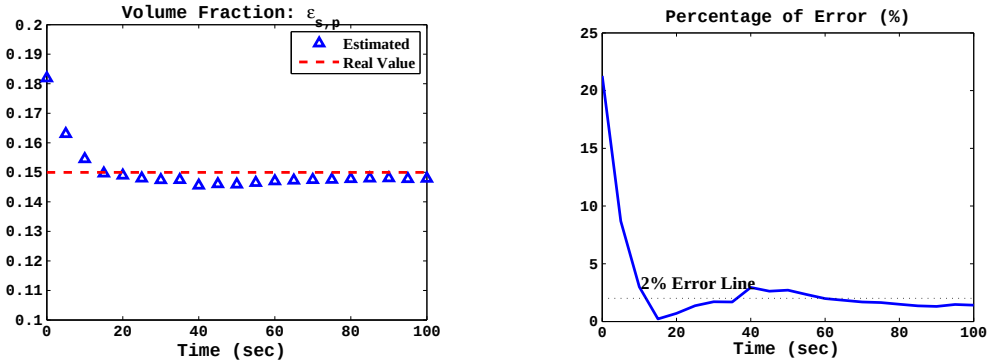

(a) (b)

Figure 5.5: Performance of the parameter estimation algorithm on ϵ_p. (a) Estimation of the degraded value $\epsilon_p = 0.15$ due to aged cell (b) Percentage of error

As a proof of concept, particle filtering based techniques developed in Chapter (3) were employed to estimate the onset of faults or measure the degree of degradation occurred in the battery. The estimated states/parameters acquired from the proposed methods can also be very helpful to attain an assessment of the state of life the battery. This however needs an independent electrochemical research study to relate the parameter variations to the state of life of the battery. To the best of our knowledge, this work is the first of its kind to analyze the diagnostics of the battery from a control theoretic point of view. Development of the analysis to other degradation mechanisms such as film formation on the anode, stress buildup, etc, and eventually embed all this information in a unified framework to study the state of life of the battery can be considered as a road map to battery diagnostics studies.

Chapter 6

Cell Balancing

6.1 Introduction

Although battery packs are integrated with batteries of the same type and specification, there exists certain discrepancies between cells' characteristics that would intensify as the battery pack ages. Different factors such as manufacturing variance in the battery characteristics from production, different aging processes, temperature distribution across the pack, etc, can cause and magnify the imbalance between cells. Due to existing mismatches, the cells do not necessarily possess the same amount of charge and thereby charging/discharging of the pack with the same rate might lead to overcharge/overdischarge of the cells with higher/lower SoC, respectively. Hence, "cell balancing" or "battery equalization" is introduced as a preventive measure to avoid over-charge/discharge of the battery cells by keeping the cells balanced at the same level of SoC. In contrast to Lead-acid and Nickel-based battery systems, the cell balancing problem is more crucial for Li-ion batteries from a safety perspective since they can not tolerate overcharge/overdischarge which could lead to serious cell damage.

Preventing the over-usage of cells would also contribute to health of the battery and help to enhance the life-span of the battery. An appropriate and reliable cell balancing circuit would also indirectly help to attain the maximum usable capacity of the battery by insuring the safety of the batteries, reducing the conservative safety margins and thus increasing the efficiency of the system.

Design of an efficient and effective cell balancing circuit is conducted at three levels: i) circuit design, ii) construction, and iii) control. From the circuit design point of view, the literature is rather rich and a multitude of appropriate circuit topologies are proposed for battery equalization [20, 28]. They can generally be divided to dissipative and non-dissipative categories. Dissipative methods simply try to balance the cells by extracting energy from the higher charged cells and dissipating it on shunts or resistors [20], or selectively disconnecting imbalanced cells from the battery pack [107]. Simple implementa-

tion, low production cost, and stable operations are the main advantages of these methods whereas energy dissipation poses a major drawback for these schemes. Hence, the main effort has been toward development of non-dissipative methods where the main idea is to transfer the charge between the cells and/or pack instead of dissipating it. Three types of charge-type, discharge-type, and charge- and discharge-type equalization methods are developed in this regard. In the charge-type, the energy extracted from the battery stack is transferred to the under-charged battery, whereas in the discharge-type the charge from the overcharged cell is transferred back to the battery stack or a few of battery cells. In this regard, different structures with capacitor, inductor or transformer as the medium for charge transfer are developed [20]. In the charge- and discharge-type, or bi-directional schemes, the equalizing currents flow from any over charged cells into other under charged cells via some sort of converter [83].

Although, design of optimal cell-balancing circuits is extensively discussed in power electronics community, the technical issues associated with implementing the designed circuits such as cost, speed, and technical difficulties with switches, has impeded the application of the circuits in an industrial scale. Therefore, the current BMS technology mostly rely on dissipative methods despite their inefficiency. More research efforts is required to address the existing technical issues and advance the cell balancing technology.

Control of balancing circuits also need further research. Most of the control schemes are developed based on the voltages of the cells and adopt a simple logic-based control algorithm to control the switches [116]. The parameters of the switches are usually fixed and a logic-based algorithm manages the switching between cells. There are however a few works that have tackled this problem using a control theory approach. Speltino et al. [116] implement a cell-balancing algorithm where the SoC is employed as the main decision variable of the algorithm. Lee and Cheng [66] address this problem by adopting a fuzzy controller where the voltage is considered as the balance indicator and the premise variables of the fuzzy rules are voltages of the cells. Yan et al. [134] improved the previous work by developing a fuzzy controller based on the SoC values. The sum of and difference between SoC values as well as total internal resistance are adopted as the inputs of the fuzzy system. Danielson et al. [27] opens an optimal control view into the problem where however the battery and balancing circuit dynamics are not considered in formulation.

This chapter tackles the problem of cell balancing within an optimal control framework. The control objectives are defined as a minimization problem and a control horizon is considered to cast the problem into a nonlinear model predictive control (NMPC) structure. The solution to the optimization problem, which involves hybrid system dynamics, is found using a gradient descent based algorithm. Moreover, in contrast to previous works, the model of the cells is completed by considering an equivalent circuit model. The cell-balancing circuit is a bi-directional topology composed of Cuk converter [67]. In the following, an equivalent circuit model of the battery employed in this work is reviewed and the cell balancing circuit

is analyzed. Then, the cell-balancing problem is formulated in a NMPC framework and the proposed solutions are discusses. Finally, the chapter is concluded with discussion of a simulation study.

6.2 Battery Model and Balancing Circuit Analysis

6.2.1 Li-ion Battery Model

In this work, an equivalent circuit model adopted from [63] is considered for battery simulation. This model is much more complete in comparison with previously considered models in balancing circuits. The model schemes is shown in Figure (6.1).

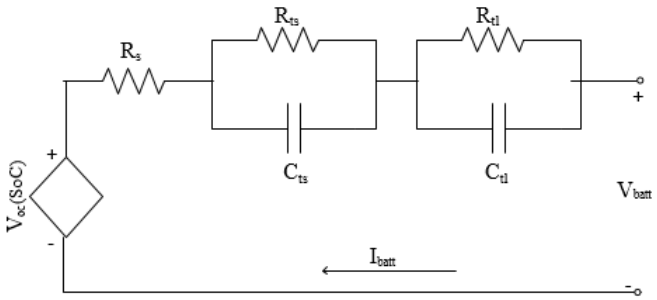

Figure 6.1: The equivalent circuit model of the battery.

The battery equations are given as:

$$\begin{cases} \dot{V}_{ts} &= \frac{1}{R_{ts}C_{ts}}\left(-V_{ts} + R_{ts}I_{batt}\right) \\ \dot{V}_{tl} &= \frac{1}{R_{tl}C_{tl}}\left(-V_{tl} + R_{tl}I_{batt}\right) \\ V_{batt} &= V_{oc} - R_sI_{batt} - V_{ts} - V_{tl} \end{cases} \tag{6.1}$$

where the open circuit voltage and circuit elements are functions of SoC as following:

$$\begin{aligned} V_{oc} &= -1.031e^{-35SoC} + 0.2156SoC \\ &\quad -0.1178SoC^2 + 0.3201SoC^3 + 3.685 \\ R_s &= 0.1562e^{-24.37SoC} + 0.07446 \\ R_{ts} &= 0.3208e^{-29.14SoC} + 0.04669 \\ C_{ts} &= -752.9e^{-13.51SoC} + 703.6 \\ R_{tl} &= 6.6038e^{-155.2SoC} + 0.04984 \\ C_{tl} &= -6056e^{-27.12SoC} + 4475 \end{aligned} \tag{6.2}$$

A coulomb counting method is adopted for SoC calculation. This method facilitates the formulation of the dynamics of the battery and balancing circuit in a state space format. However, other SoC estimation methodologies can also be incorporated in the proposed structure. The coulomb counting method can be represented as:

$$SoC(t) = SoC(t_0) - 1/Q \int_{t_0}^{t} I(\eta)d\eta \tag{6.3}$$

where Q (Ah) indicates the nominal capacity of the battery and I the charge/discharge current of the battery, where the convention of $I < 0$ is considered for discharge in formulations.

6.2.2 Balancing Circuit Principle and Analysis

In this work, a bidirectional balancing circuit is considered for analysis. In bi-directional configurations, the equalizing currents can flow from any over charged cells into other under charged cells via some sort of converter. This would present the most efficient and fastest non-dissipative balancing circuit topology. The balancing circuit in this work is adopted from [67, 66] where a Cuk converter is considered as the equalizing unit between each two cells in the battery string. The schematic of the cell balancing circuit is shown in Figure (6.2). The battery string continues from points A and B and each two adjacent cells are equalized via a similar topology.

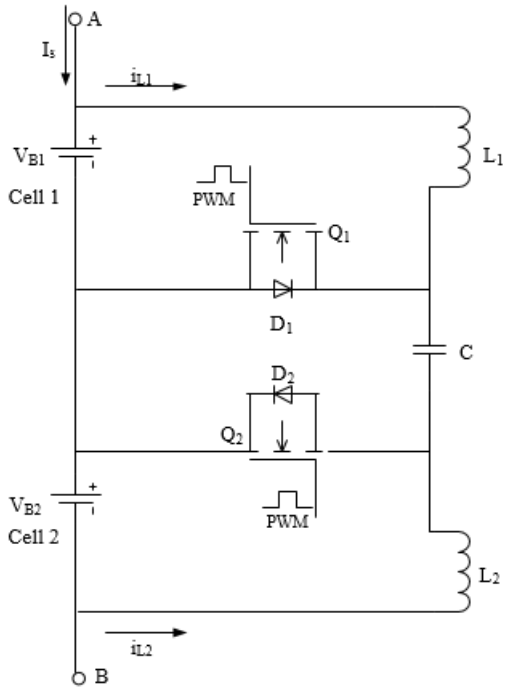

Figure 6.2: Schematic of cell balancing circuit using a modified Cuk converter.

The charge is transferred from the cell with the higher charge (i.e. higher SoC) through the two inductors and the energy-transferring capacitor. The MOSFETs with embodied diodes are the switches which control the balancing circuit. A PWM signal is applied to MOSFETs to control their on/off conditions.

For the circuit analysis, the two batteries are replaced with the equivalent circuit model shown in Figure (6.1). Without loss of generality, we assume that cell 1 has higher charge than cell 2. The frequency of the PWM signal is considered as f_s and thus the period of one control cycle is $T_s = 1/f_s$. The duty cycle is denoted as $D \in (0, 1)$ and the MOSFET Q_1 is on for $[0, T_0]$ and off for $(T_0, T_s]$ where $T_0 = D \times T_s$. For the circuit elements, the general hint is to select inductors L_1 and L_2 large enough to operate in "Continuous Inductor Current Mode (CICM)", where the inductor current never reaches zero during one switching cycle. In addition, the capacitor is also sufficiently small so it can be fully discharged during the switching period.

In the initial state, provided the appropriate values for circuit elements, the capacitor (C) is instantly charged to $V_C(t) = V_{B1}(t) + V_{B2}(t)$, where V_C denotes the voltage of capacitor C and V_{B1} and V_{B2} represent the voltages of cells 1 and 2. In the period $[0, T_0]$, Q_1 is on, $i_1 > 0$ and charge is transferred from cell 1 to L_1 and is stored in the inductor. In this period, C discharges to cell 2 and L_2 stores some of energy. During the conduction mode of Q_1, the state space equations are denoted as follows:

$$\begin{cases} \dot{i}_{L1} &= \frac{1}{L_1} V_{B1} \\ \dot{V}_C &= \frac{1}{C}(-i_{L2}) \qquad , 0 < t \leq T_0, \quad Q_1 : On \\ \dot{i}_{L2} &= \frac{1}{L_2}(V_C - V_{B2}) \end{cases} \tag{6.4}$$

The current that passes through cells is considered as $I_{batt_1} = I_s - i_{L1}$ and $I_{batt_2} = I_s + i_{L2}$, where I_s represents the current of battery string that is charged from source or discharged to the load. Substituting V_{B1} and V_{B2} from Eq. (6.1) in (6.4) and taking the derivative of both sides of Eq. (6.3) gives the state space equations $\dot{X} = f_1(X)$ for $0 < t \leq T_0$, where X the state vector and f_1 are given as:

$$X = [i_{L1}, V_C, i_{L2}, SoC_1, SoC_2, V_{ts_1}, V_{tl_1}, V_{ts_2}, V_{tl_2}]^T \tag{6.5}$$

$$f_1 = \begin{bmatrix} 1/L_1(V_{oc_1} - R_{s_1}(I_s - X(1)) - X(6) - X(7)) \\ 1/C(-X(3)) \\ 1/L_2(X(2) - (V_{oc_2} - R_{s_2}(I_s - X(1)) - X(8) - X(9))) \\ 1/Q(I_s - X(1)) \\ 1/Q(I_s + X(3)) \\ \frac{1}{R_{ts_1} C_{ts_1}}(-X(6) + R_{ts_1}(I_s - X(1))) \\ \frac{1}{R_{tl_1} C_{tl_1}}(-X(7) + R_{tl_1}(I_s - X(1))) \\ \frac{1}{R_{ts_2} C_{ts_2}}(-X(8) + R_{ts_2}(I_s + X(3))) \\ \frac{1}{R_{tl_2} C_{tl_2}}(-X(9) + R_{tl_2}(I_s + X(3))) \end{bmatrix} \tag{6.6}$$

The series resistors, R_{s_1}, R_{s_2}, and open circuit voltages, V_{oc_1}, V_{oc_2}, are themselves nonlinear functions of $X(4)$ and $X(5)$ as given in Eq. (6.2).

In the period $(T_0, T_s]$, Q_1 turns off and D_2 gets on. During this period, cell 1 continues to discharge its excess charge to L_1 inductor, and L_1 charge back the capacitor C using its stored energy. Note that the charge of capacitor has been decreased during the last period. On the other part, the inductor L_2 continuously charges cell 2 until its stored energy is totally transferred. The circuit will reach the steady state when $i_{L2} = 0$. While Q_1 is off, the circuit equations are described as:

$$\begin{cases} \dot{i}_{L1} &= \frac{1}{L_1}(V_{B1} - V_C) \\ \dot{V}_C &= \frac{1}{C} i_{L1} \qquad\qquad , T_0 < t \leq T_s, \quad Q : Off \\ \dot{i}_{L2} &= \frac{1}{L_2}(-V_{B2}) \end{cases} \tag{6.7}$$

Similar to (6.6), the state equations, $\dot{X} = f_2(X)$ are derived as following:

$$f_2 = \begin{bmatrix} 1/L_1(V_{oc_1} - R_{s_1}(I_s - X(1)) - X(6) - X(7) - X(2)) \\ 1/C\ X(1) \\ 1/L_2(-(V_{oc_2} - R_{s_2}(I_s - X(1)) - X(8) - X(9))) \\ 1/Q(I_s - X(1)) \\ 1/Q(I_s + X(3)) \\ \frac{1}{R_{ts_1}C_{ts_1}}(-X(6) + R_{ts_1}(I_s - X(1))) \\ \frac{1}{R_{tl_1}C_{tl_1}}(-X(7) + R_{tl_1}(I_s - X(1))) \\ \frac{1}{R_{ts_2}C_{ts_2}}(-X(8) + R_{ts_2}(I_s + X(3))) \\ \frac{1}{R_{tl_2}C_{tl_2}}(-X(9) + R_{tl_2}(I_s + X(3))) \end{bmatrix} \tag{6.8}$$

This sequence is repeated by the frequency of f_s until the cells 1 and 2 reach an approximately same level of charge (a 2% margin is usually considered as acceptable). It is worth noting that the currents i_{L1} and i_{L2} are limited to 0 by the diode D_2 if they get less than zero. This means that we might have three more state dynamics f_3, f_4, and f_5 which is similar to Eq.(6.8), except that i_{L1}, i_{L2} or both are zero, respectively. When $SoC_1 < SoC_2$, the analysis is similar, except that Q_2 and D_1 plays the main role in the balancing circuit.

The dynamics of the system present a hybrid system which has two type of switching or transitions, namely controlled (i.e. externally forced) and autonomous (i.e. internally forced). The controlled transitions refers to the transitions which are induced by an external control event, where autonomous transitions are specified by a certain guard condition on states. If the continuous state satisfies the guard condition, then the system transitions to a new dynamic mode. In this balancing circuit, the switching from f_1 to f_2 is induced by the duty cycle of PWM signal which is an external control event, and switching from f_2 to either f_3, f_4 and f_5 is imposed by states (i.e. $X(1)$ and $X(3)$) when they pass through a certain guard (i.e. $X(1) < 0$ and $X(3) < 0$) and thus is internally forced.

6.3 Problem Formulation and Methodology

6.3.1 Problem Formulation

There are two variables that can control the balancing circuit, namely the frequency f_s and duty cycle D of PWM signal, given the circuit elements are considered constant. Due to the implementation difficulties, the frequency is usually considered as constant, and the duty cycle is the only variable that is used to control the balancing circuit. We will also consider the duty cycle as the manipulating variable in this work while the proposed methodology also has the capacity to encapsulate the frequency of PWM as a manipulating variable as will be discussed.

The main objective is to balance two adjacent batteries while minimizing the energy loss. The charges drawn from Cell 1 are always larger than that filled into Cell 2. Hence, the ratio of i_{L2} to i_{L1} is used as an indicator of equalizing efficiency [134]. It is clear from equation (6.3) that as $I = i_{L1} + i_{L2}$ increases, the time required to balance the cells would decrease. Therefore, the inverse of total equalizing current, i.e. $1/(i_{L1} + i_{L2})$, is another objective in the defined cost function. This problem is cast into a nonlinear model predictive control (NMPC) framework as follows:

$$\begin{aligned} &\min_{\{D\}_1^H} J(\{D\}_1^H, X) = \min_{\{D\}_1^H} \int_{t_0}^{t_0+H\times T_s} \left[\Gamma_1 \frac{1}{X(1)+X(3)} + \Gamma_2 \left(1 - \frac{X(3)}{X(1)}\right)\right] dt \\ &\text{subject to} \begin{cases} \dot{X} = F(X, \{D\}_1^H),\ t \in [t_0, t_0 + HT_s] \\ \{D\}_1^H \in (0,1) \end{cases} \end{aligned} \tag{6.9}$$

where Γ_1 and Γ_2 are positive constants and indicate the weight of each objective in the cost function. They are selected adaptively based on the difference between the state of charge of the two cells (see section 6.4 for details). For the sake of simplicity the prediction and control horizon are assumed equal to H. The process dynamics which is essentially hybrid is represented by F. It is also noted that the system is an autonomous hybrid system since it does not explicitly depend on any independent variable (input) but only on switching times and initial condition. The cost function J, is defined as the integral of SoC difference and is minimized subject to the duty cycle of PWM signal in control horizon. The duty cycle as the minimization parameter is defined as

$$D = T_0/T_s \tag{6.10}$$

where T_0 is the duration in which the Q_1 is on.

The general practice in solving the power electronics control problems that involve converters has been to consider the average model and design the controller for the average model and small-signal model (e.g. [73]). However, in this problem, the voltage source and

load (as appears in Cuk converter circuits) are battery cells 1 and 2, respectively, which are two dynamic systems whose equations are changing with time and hence average model would not converge for this problem. This is also verified through simulation in MATLAB and POWERSIM, that the average model would not converge for this problem. Hence, we need to consider the complete hybrid system arrangement to solve this problem.

As mentioned, the PWM signal frequency and hence T_s, is considered as constant, therefore optimizing in terms of D is equal to optimizing in terms of T_0 (see Eq. (6.10)) which is the the switching time of MOSFET. In order to solve this problem, it is cast into an optimal control framework where optimization of the switching time of the hybrid system is considered in the control horizon.

In general, the system shows hybrid dynamics: (6.11) for $0 < t \leq HT_s$ where H is the control horizon. The switching of f_1 to f_2 is externally forced and always occurs at $T = D \cdot T_s$ within each T_s period, but other switchings are dependent on the value of T_0^h and initial values, and might occur or not within a cycle. When Q_1 is off, depending on the initial conditions, either of $X(1)$ or $X(3)$ might get less than zero first and the system switches to f_3 or f_4, respectively. Thereafter, if both are limited by diode to zero, the system switches to f_5. Therefore, the switching times τ_1^h and τ_2^h are internally forced and either of them could be equal to hT_s. The optimization problem (6.9) is solved subject to the switching times' vector $\{T_0\}_1^H = [T_0^1, T_0^2, \ldots, T_0^H]$, i.e. $\min_{\{T_0\}_1^H} J$. The optimal switching time of T_0^1 is applied and the control horizon window is moved forward in time. In the following we will discuss the proposed method for a solution of this problem.

$$\dot{X} = F(X) = \begin{cases} f_1(X) & t \in ((h-1)T_s, T_0^h] \\ f_2(X) & t \in (T_0^h, \tau_1^h] \\ \begin{cases} f_3(X) \\ f_4(X) \end{cases} & t \in (\tau_1^h, \tau_2^h] \\ f_5(X) & t \in (\tau_2^h, hT_s] \end{cases} \quad , h = 1, 2, \ldots, H. \tag{6.11}$$

6.3.2 Proposed Methodology

There is an extensive body of literature that deals with the switching time optimization in hybrid systems ([140] and references therein). In this regard, two types of "internally forced" switching (IFS) and "externally forced" switching (EFS) are generally distinguished. As mentioned, IFS is labelled by certain guard conditions on internal states of the system, where EFS refers to switching that occurs as a result of an external control event (e.g. a pre-determined switching time, external command). Algorithms are generally developed for systems with only IFS or only EFS. In this problem, however, both of the IFS and EFS are involved. Nevertheless, the system is autonomous and IFS times are a function of EFS times. In other words, once the EFS times (i.e. $\{T_0\}_1^H$) are known, the IFS times

(i.e. $\{\tau_1, \tau_2\}_1^H$) are also determined since there is no control action on the system. Hence, in the proposed methodology only $\{T_0\}_1^H$ is the minimization parameter of concern. The optimization problem is thereby formulated as following:

$$\begin{aligned} &\min_{\theta} J(\theta, X) \\ &\text{subject to} \begin{cases} \dot{X} = F(X, \theta),\ t \in [t_0, t_0 + HT_s] \\ \theta \in \Theta \end{cases} \end{aligned} \tag{6.12}$$

where J is defined in (6.9), $\theta = \{T_0\}_1^H = [T_0^1, T_0^2, \dots, T_0^H]$ and $\Theta = \{\theta \,|t_0 < T_0^1 < t_0 + T_s < T_0^2 < t_0 + 2T_s < \ldots < T_0^H < t_0 + HT_s\}$.

A gradient-descent based scheme is employed to solve this problem. The body of the algorithm is summarized at Algorithm 8.

Algorithm 8 Gradient-descent algorithm to find the optimal switching times

1. Set the iteration index $k = 0$. Choose an initial θ^k.
2. Find the gradient of cost function $\nabla(J) = \frac{\partial J}{\partial \theta}(\theta^k)$.
3. Find an appropriate step size ζ_k and a feasible direction $h(\theta^k)$ and update the θ^k to be $\theta^{k+1} = \theta^k + \zeta^k h(\theta^k)$. The feasible direction is defined as the projection of $(-\nabla J)$ on the $\Psi(\theta) = \{h(\theta) \in \mathbb{R}^H \,|\exists \hat{\zeta} > 0, \forall \zeta \in [0, \hat{\zeta}], \theta + \zeta h(\theta) \in \Theta\}$ where ζ denotes the Armijo step size.
4. Set $k = k + 1$ and return to step 2 if a predetermined termination condition is not satisfied. The termination condition can be defined based on the norm of feasible direction (h), the increment of θ, etc.

The Armijo stepsize ζ is defined as follows:

$$\begin{aligned} m = \min\{&m \geq 0 \mid \theta + \beta^m h(\theta) \in \Theta, \\ &J(\theta - \beta^m h(\theta)) - J(\theta) \leq \alpha \beta^m < h(\theta), \nabla J(\theta) >\} \in \mathbb{N} \\ \zeta = \beta^m& \end{aligned} \tag{6.13}$$

where $\alpha \in (0, 1)$, $\beta \in (0, 1)$ and $< .\ ,\ . >$ refers to the inner product of two vectors.

The main difficulty that arises in Algorithm 8 is due to calculation of the gradient of cost function with respect to the switching times, i.e. ∇J. The proposed method is adopted from [37] when a costate function is employed to calculate ∇J as follows.

Let the cost function be defined as $J = \int_0^T W(x)dt$ where $\dot{x} = f_i(x(t)), \text{for all } t \in [\tau_{i-1}, \tau_i],\ i = 1, \dots, N+1$ with the given initial condition $x(0) = 0$. The feasible set of

switching times is represented by $\Lambda := \{\bar{\tau} = (\tau_1, \dots, \tau_N)^T : 0 = \tau_0 \leq \tau_1 \leq \dots \tau_N \leq \tau_{N+1} = T\}$. For every $\bar{\tau} \in \Lambda$, the costate $p(t) \in \mathbb{R}^n$ is defined backwards according to the following differential equation:

$$\dot{p} = -\left(\frac{\partial f_{i+1}}{\partial x}(x,t)\right)^T p - \left(\frac{\partial W}{\partial x}(x)\right)^T, \quad t \in [\tau_i, \tau_{i+1}],\ i = N, N-1, \dots, 0 \tag{6.14}$$

with the boundary condition $p(T) = 0$. Then the following proposition is given for calculation of ∇J [37].

Proposition 1. *Suppose that L and $\{f_i\}_{i=1}^{N+1}$ satisfy the following assumptions:*

i. The functions are twice continuously differentiable.

ii. There exists a constant $K > 0$ such that, for every $x \in \mathbb{R}^n$, and for all $i \in \{1, \dots, N\}$:

$$\|f_i(x)\| \leq K(\|x\| + 1) \tag{6.15}$$

For every point $\bar{\tau}$ in the Λ, and for all $i = 1, \dots, N+1$, the derivative $(dJ/d\tau_i)(\bar{\tau})$ is given by:

$$\frac{dJ}{d\tau_i}(\bar{\tau}) = p(\tau_i)^T \left(f_i(x(\tau_i)) - f_{i+1}(x(\tau_i))\right) \tag{6.16}$$

Proof. See [37]. □

In our case, dynamics of the system is given by (6.11) and cost function is defined in (6.9) where $W(x) = \Gamma_1(X(4) - X(5)) + \Gamma_2(X(1) + X(3))$. There exist two types of switching instants in the system, i.e. $\{T_0\}_1^H$ and $\{\tau_1, \tau_2\}_1^H$, where $\{\tau_1, \tau_2\}_1^H$ are dependent on $\{T_0\}_1^H$. Hence, the derivative would be adjusted as:

$$\frac{dJ}{dT_0^h} = \frac{\partial J}{\partial T_0^h} + \frac{\partial J}{\partial \tau_1^h} \cdot \frac{d\tau_1^h}{dT_0^h} + \frac{\partial J}{\partial \tau_2^h} \cdot \frac{d\tau_2^h}{dT_0^h} \tag{6.17}$$

and based on Eq.(6.16), the ∇J is derived as:

$$\begin{aligned} \frac{dJ}{dT_0^h} =& p(T_0^h)^T \left(f_1(X) - f_2(X)\right) + \\ & p(\tau_1^h)^T \left(f_i(X) - f_2(X)\right) \frac{dT_0^h}{d\tau_1^h} + p(\tau_2^h)^T \left(f_5(X) - f_i(X)\right) \frac{dT_0^h}{d\tau_2^h} \end{aligned} \tag{6.18}$$

where $i = 3, 4$ (Eq. (6.11)). The gradient of J is calculated from (6.18) and is replaced in Algorithm 8 to find the optimal switching instants at each control horizon. For this

purpose the system dynamics (6.11) and the costate equation (6.14) are solved forward and backward, respectively.

6.3.3 Problem Extension

In PWM-controlled converter problems, duty cycle of PWM is usually the only parameter of concern and frequency would be considered constant. This is so since changing of the frequency of the PWM signal would pose implementation challenges and might not be economically feasible. Nevertheless, frequency of PWM signal is potentially a manipulating variable that can play a role in optimal control problem. The manipulation of duty cycle was addressed above in a switching time optimization framework. If one wants to extend the problem such that both D and f_s are considered as control variables, the problem would be solvable in the same manner as follows.

The new problem is defined as:

$$\begin{aligned} &\min_{D,f_s} J(X,D,f_s) = \min_{D,f_s} \int_{t_0}^{t_0+T} \left[\Gamma_1(X(4)-X(5)) + \Gamma_2(X(1)+X(3))\right] dt \\ &\text{subject to} \begin{cases} \dot{X} = F(X,D,f_s),\ t \in [t_0, t_0+T] \\ D \in (0,1) \\ f_{s,min} < f_s < f_{s,max} \end{cases} \end{aligned} \tag{6.19}$$

As discussed, D is translated into switching time to be incorporated into the problem. In the new problem, however, f_s would also change. From the switched hybrid system perspective, it means that not only the switching times are changing but also the number of switchings would be subject to change. In the previous problem, in a fixed HT_s interval, the number of switchings from system 1 to 2 would exactly be equal to H. In the newly defined problem, in a fixed T interval, T_s is also variable and thus the number of switchings can vary. It should be noted that the sequence of switched systems, i.e. $1 \to 2 \to 3/4 \to 5 \to 1$ would not be altered but only the number of such sequences might change. The new problem can conceptually be solved in a two-stage algorithm as shown in Algorithm 9 [133]:

Algorithm 9 Two stage algorithm to optimize both switching times and frequency of PWM signal

- Stage 1.
  a) Fix the number of switchings to be S.
  b) Minimize J with respect to switching times, i.e. $\{T_0\}_1^S$. (Algorithm 8)
- Stage 2. Vary the number of switchings S to find an optimal solution for problem (6.19).

The stage 2 of Algorithm 9 is a searching problem that can be implemented independently of stage 1. Although this solution exists for frequency optimization, the focus of simulation studies would be on optimal control based on D which is more relevant, in practice.

6.4 Simulation Studies

For the simulation studies, the battery model (Figure(6.1)) by the model elements given in (6.2) is employed. The following elements are considered for the balancing circuit: $L_1 = L_2 = 100\mu H$ and $C = 470\mu F$. The frequency of the PWM signal is considered as $f_s = 5KHz$. The control horizon for the controller is considered as $H = 3$. The simulations are conducted for multiple cases in terms of the initial state of the batteries as follows, i. There is a big SoC gap between cells (i.e. $\Delta SoC > 0.3$), ii. The SoC difference is in intermediate range (i.e. $\Delta SoC \simeq 0.2$), iii. The SoC values are close (i.e. $\Delta SoC \leq 0.1$). The results for the SoC trajectory and the Efficiency values is shown in Figure(6.3). All the results are shown for the first 500 seconds of the simulation which can demonstrate the effectiveness of the controller.

Figure (6.3) demonstrates that as the cells are very off the controller would push more aggressively towards balancing, and thus the efficiency would be sacrificed to some extent. In contrast, when the cells are within the similar range, the efficiency plays more important role in determining of the manipulation variable which is duty cycle. Please note that a resolution of 0.05 is considered for Duty cycle manipulation.

The impact of capacitance value C, and frequency of PWM signal f_s is also investigated in the simulation studies. The balancing circuit is simulated for different values of capacitance as shown in Figure(6.4). Normally, as C increases the balancing time would decrease, however the efficiency would be compromised. Please note that the large values of capacitance (e.g. $C = 4.7mF$) would not be very practical in real application. Therefore, the simulations were conducted with $C = 470\mu F$. Figure (6.5) demonstrates the results for different frequency values. The selection of frequency of PWM signal is in fact a compromise between the speed of balancing, efficiency, and the practicality. As frequency increases, the balancing time would decrease but the practicality would be affected, and efficiency is also slightly reduced. As discussed and formulated in Section (6.3.3), frequency can also be considered as one of the manipulating variables in the controller which however it is not practically favorable.

The applied method obtains the optimal solutions in terms of switching instants. However, the problem is that it imposes a high computational load which would not be very feasible for online implementation. The remedy to this problem would be two fold. First, we can extract the rules using this method to adjust a fuzzy controller that fulfills the sub-optimal controller for the system. The next solution is to solve the optimal control within

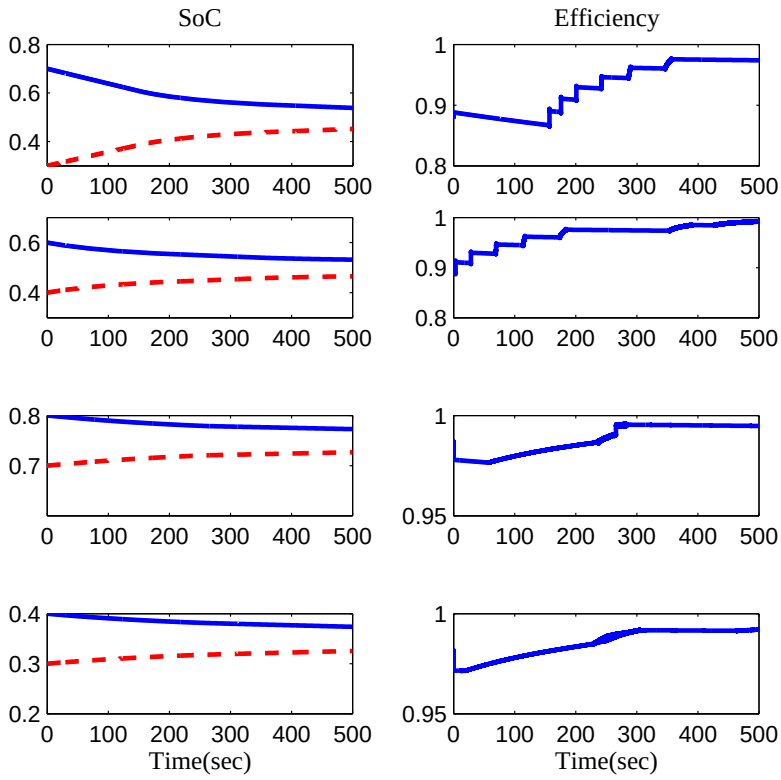

Figure 6.3: Simulation results of the trajectory of SoC values and efficiency value for $500sec$. The simulation is conducted for multiple cases with different initial ΔSoC

larger time-steps. In other words, a sub-optimal controller can be developed that does not update D at each sample time. Due to the slow dynamics of the battery, this would not alter the performance of the balancing circuit significantly.

6.5 Summary

Cell balancing is defined and practiced as a preventive measure to overcome the cell mismatches and ensure the safety of the battery operation in battery packs and cell stacks. It also leads to improved efficiency as well as increased overall capacity and lifetime of the battery cell stack. The technology of cell balancing circuits is shifting from passive methodologies to active ones in order to address the efficiency. The semiconductor and microcontroller companies has also shown interest to active methods recently [6]. This work is also moving towards this direction to propose an appropriate controller for implementing a fast and reliable cell balancing circuit on chip.

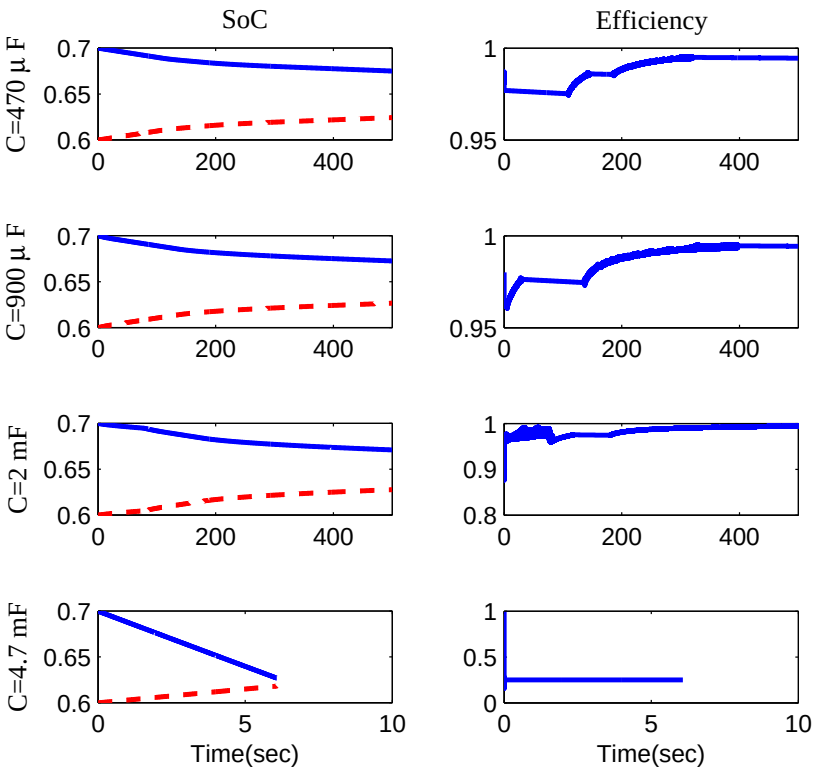

Figure 6.4: Simulation results for different capacitance values.

This Chapter developed an optimal control approach to cell balancing problem of Li-ion batteries. The proposed approach is novel in its structure and formulation. The previous works are also enhanced by taking a more comprehensive model of the battery. The optimal control of cell balancing circuit with Cuk converter is reformed into a switching time optimization problem of switched hybrid systems. The proposed methodology provides a framework to address the balancing problem by optimally setting the duty cycle of PWM signals. It was also discussed that how this method can be extended to incorporate the frequency of PWM signals as a manipulating control variable. A drawback of this method is high computational load for which the potential remedies are proposed. Moreover, digital implementation of the proposed methodology with appropriate hardware design is also another solution that can address the real-time implementation of the proposed algorithm.

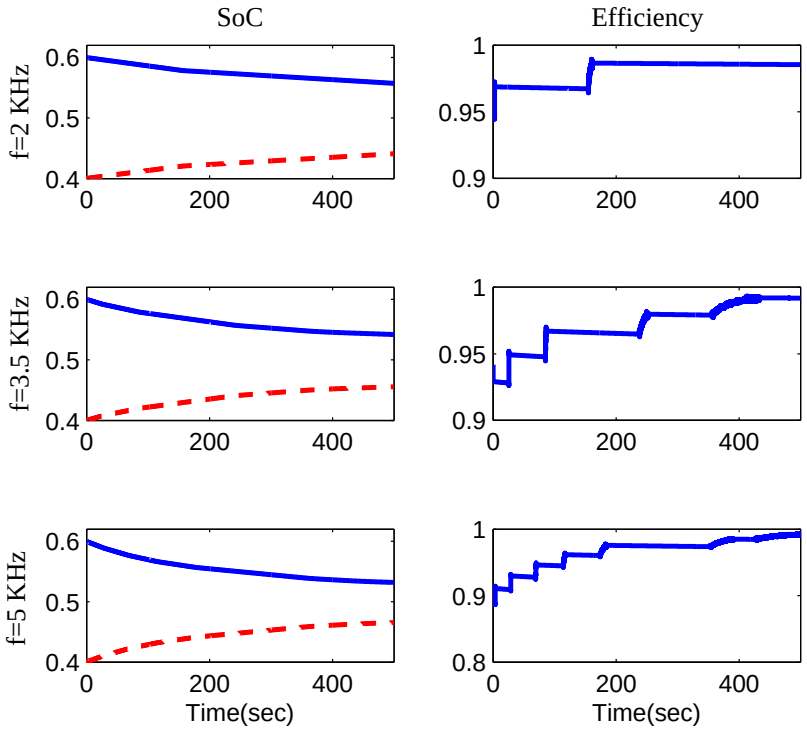

Figure 6.5: Simulation results for different frequency values.

Chapter 7

Conclusions and Future Work

We believe that Lithium ion batteries are an important field of study for future of electrified transportation industry. They present an opportunity to move from the current internal combustion engine vehicles to all-electric fleet where many current challenges with regards to emission, and fuel economy can be addressed. To reach this goal, however, the existing challenges regarding their manufacturing, control, and safety should be effectively address. Thus, they provide an interesting field of research with enticing challenges and numerous opportunity. Our hope is that this Thesis may shed some light on the control and monitoring challenges of Li-ion batteries, and planted some ideas that might grow to become mainstream in the future. In this Chapter we summarize and point out the main results that have been achieved in this thesis. In addition several directions and ideas for future research are presented.

7.1 Conclusions and Contributions

In this thesis, the problem of control and monitoring of Li-ion batteries was investigated from multiple angles. The problem of state of charge estimation, state of health estimation, and parameter estimation of Li-ion batteries was explored. In this regard, new approaches to battery modeling was also examined. Moreover, the diagnostics and health monitoring of the battery was also studied using a control oriented approach. Another area of focus was cell-balancing of the battery which is essentially a protection measure to prevent overcharge/overdischarge of the battery cells. The concluding remarks of each developed methodology would be briefly explained in the following.

7.1.1 SoC and Parameter Estimation

Two algorithms for state and state and parameter estimation of Li-ion batteries were presented in Chapter 3. The proposed algorithms employ a particle filter engine for estimation and are developed based on the fundamental electrochemical model. The appealing feature

of this algorithm is that it provides the opportunity to consider the very basic electrochemical model of the battery. In comparison with Kalman filter-based algorithms, there is no need to average the field variables in order to eliminate the position dimension (x-dimension) of equations. Therefore, the spatial distribution of field variables in a battery can be obtained using this algorithm. This feature is in fact exploited later in Chapter 5 for battery diagnostics.

The goal of the first algorithm is to estimate the state of charge of the battery where the results confirm the effectiveness of the proposed algorithm. A multi-rate particle filter was developed in the second algorithm for simultaneous parameter and state estimation of a lithium-ion cell. In this algorithm, parameter and states of the battery are estimated at different time rates in order to efficiently use the computational capacity. Merging of the parameter estimation in the state estimation scheme, opens a window to study of the degradation of the battery and taking the parameter changes into account.

7.1.2 T-S Fuzzy Approach to Battery Modeling

A T-S fuzzy model was employed to model the dynamics of a Li-ion battery. The proposed model can be fitted to data produced by simulation of electrochemical model or experimental data and thus reduce the computational load for real-time monitoring tasks. The inherent multiple-model structure of T-S model help to capture the non-linearities of the model and also cope with the parameter dynamics in different operation regions of the battery which is usually disregarded in practice.

The importance of obtaining a state-space model is that a broad spectrum of control theories would be available where in the case of electrochemical model, we would be limited to a narrow band of options for control/estimation tools. In this regard, a robust observer design using the developed model was conducted to estimate the SoC value which is the unmeasured state in the system. Robustness of the observer (filter) means that it can cope with a certain level of noise/disturbance/uncertainty in the system and the observer performance is guaranteed. The observer gains were obtained analytically by solving a number of linear matrix inequalities. The effectiveness of the method was verified through extensive simulation and was demonstrated for some typical cases.

7.1.3 Battery Monitoring Based on Dynamic Resistance

"Dynamic resistance" was introduced as a novel methodology to model the behaviour of the Li-ion battery versus state of charge and cycle number of the battery. A mathematical description of this resistance was obtained using a GMDH neural network using experimental data gathered from extensive cycling of the battery. Simulation studies show a good level of precision for the acquired model. The practical aspect of this method for monitoring of battery is that a battery management system can be easily equipped with the ability

to measure the dynamic resistance of the battery at some particular SoC of the battery without need of excessive extra circuitry or some external signals that affect the normal operation of the battery. This information can be applied to either estimate the SoC or predict the state of health of the battery.

7.1.4 Battery Diagnostics

A control-oriented look towards the diagnostics challenges of Li-ion batteries was presented in chapter 5. The main problem was defined by a rather comprehensive survey of the different chemical and mechanical mechanisms that degrade the operation of a Li-ion battery. Also, some physics-based models that have been presented for modeling of some degradation mechanisms of the battery were briefly reviewed. However, not all the degradation processes are yet modeled in the literature. This is, in fact, an area that needs much more research investigations to address all the problems in modeling of the degradation mechanisms within the battery. Understanding the physics of the degradation processes is a major challenge towards the modeling of them. In fact, the problem of fault diagnostics of the battery deserves a number of Ph.D. theses to be addressed.

However, Bayesian-based fault detection algorithms were developed for "plating mechanism" and "positive electrode dissolution" as two of common battery degradation mechanisms. It was shown that by proper estimation of the states of the battery, the conditions that lead to plating process can be prevented. Also, it was studied and discussed that how the estimation of electrochemical model can be employed to measure and quantify the degree of "positive electrode dissolution" fault.

7.1.5 Cell Balancing

Cell balancing plays an important role in safety of Li-ion battery packs operation. However, the optimality of cell balancing is not usually considered in the proposed control methodologies. The control scheme should be designed such that different, sometimes conflicting, objectives such as fast balancing, energy efficiency in the circuit, optimization of SoH of batteries are all considered. An analytical approach towards the control problem of cell balancing was considered in this thesis. A nonlinear model predictive control is proposed for this purpose. The proposed approach is novel in its structure and formulation. The previous works are also enhanced by taking a more comprehensive model of the battery. The proposed methodology provides a framework to address the balancing problem by optimally setting the duty cycle of PWM signals. It can also be extended to include the frequency of PWM signals as a manipulating control variable.

7.1.6 Contributions

The most important contributions of this Thesis are summarized in the following list.

- To the best of our knowledge, the algorithms developed in this Thesis were the first attempt to employ full electrochemical model in the battery monitoring. The nature of the algorithms that are based on particle filtering makes it possible to cope with complicated dynamics of the battery described by nonlinear partial differential algebraic equations.

- In addition to SoC which is the common parameter of concern in battery monitoring algorithms, estimation of other battery quantities such as potential of solid and electrolyte state material, and concentration of Lithium, as well as battery parameters are also incorporated in the proposed estimation algorithms. This feature not only improves the accuracy of SoC estimation but also facilitates the use of these algorithms in battery diagnostics due to the fact that the electrochemical model of the battery is not a mere mathematical model but actually describes the real physics of the system.

- Development of a multiple-model structure in a fuzzy sense to deal with nonlinearities of battery dynamics is another contribution of this Thesis. Although it is a data-based model but due to its nature it can provide a reliable model on an extended range of operation. Moreover, the developed robust observers are able to deal with uncertainties inherent in the model.

- Dynamic Resistance is a new parameter introduced in this Thesis to bring a new idea in battery monitoring. This easy-to-monitor parameter provides a new framework to consider aging effect on SoC monitoring. It was also investigated that dynamic resistance shows a strong correlation with SoH of the battery. Hence, it can also provide a potential solution to a major challenge of incorporation of SoH in SoC monitoring.

- The work presented on fault monitoring is the first of its kind to analyze the diagnostics of the battery from a control theoretic point of view. It was shown that how particle filtering methods can be employed to develop a fault diagnostics framework. The results of this work can also be extended to SoL estimation by further studies.

- Considering the desired objectives explicitly in the control design of cell balancing circuits is another contribution of this Thesis. Logic-based or heuristic-based algorithms were often considered for control of these circuits. In this work, the control design was conducted analytically in an optimal control structure where efficiency of balancing strategy as well as the speed of balancing are optimized adaptively.

7.2 Future Work

We believe that monitoring, control and diagnostics of Li-ion battery would be an important active field of research in the years to come and have the potential to provide an appropriate

framework for safe and optimal utilization of the battery. Our hope is that this Thesis will help instigate more research efforts in this area. In the following, we review some directions that seem promising for future research efforts in this field.

1. *Cell estimation versus pack estimation:*
   Most of the work in the area of battery modeling and estimation is conducted for a battery electrode and cell. In reality, however, for most of the applications we have to deal with battery modules or packs. Battery module is a set of battery cells connected in series or parallel and battery pack is then assembled by connecting modules together, again either in series or parallel or a mix of both to deliver the desired voltage, capacity, or power density.

   Large number of cells, spatial distribution of cells and its implication on the modeling, temperature distribution in a battery module/pack, present new challenges and adds another dimension to battery modeling and estimation problem that calls for further investigation. Reference [113] for instance studies the temperature distribution in a battery pack and derives a PDE model for thermal dynamics in a large Li-ion battery pack. However, more studies are needed to address the challenges in both modeling and estimation of battery modules/packs.

2. *T-S fuzzy modeling:*
   The T-S fuzzy structure provide an appropriate framework for battery modeling where nonlinearity of the model and parameters is accounted for in a multiple-model structure. The proposed model however only considers the state of charge and models the time evolutions of this state. The information about spatial distribution of other quantities such as solid and electrolyte potential as well as the spatial distribution of concentration in solid material is also particularly important in health monitoring of the battery. Thus, development of 2D T-S fuzzy models that incorporates time evolution and spatial distribution of the battery quantities can introduce a future field of study with potential results for health monitoring of the battery.

3. *Dynamic resistance and frequency analysis:*
   A major problem with battery equations monitoring is that so many parameters and states are involved in the equations but only current, voltage and temperature are measurable in a real-time application. This is actually the main reason that causes difficulty with the observability issue of the equations as well. There does not appear to be any solution for this because most of the battery states can only be measured if we stop the normal operation of the battery, and in most cases, it needs destructive methods to measure the states such as concentration or battery parameters.

   Introduction of "dynamic resistance" in this Thesis was indeed an effort to import new information in the battery monitoring. It was actually quite successful and have

the capacity to be expanded more with more experiments particularly to find the correlation of dynamic resistance to state of health of the battery under different conditions. Incorporation of temperature in the experiments can also define another important extension to the current work. Development of similar ideas to correlate possible real-time observation to main electrochemical battery quantities would open new windows to battery monitoring.

Moreover, many processes occurring in the battery are frequency sensitive and can be distinguished in frequency domain. Hence, development of the real-time methods that can incorporate the frequency analysis to the current model-based time analysis would enhance the battery monitoring schemes considerably. In particular, it would have a promising potential in battery diagnostics.

4. *Incorporation of SoH in battery control:*
   A parameter that is missing from most of the current control strategies of the battery is state of health of the battery. This is mainly due to lack of appropriate models or estimation methods for this parameter. However, incorporation of SoH in energy management strategies in HEV and cell-balancing methods would help to optimize the utilization schemes in terms of the battery life span.

5. *Development of PDE-system observers and observers for uncertain nonlinear systems :*

   The literature in the control community dealing with partial differential equations is rather limited and narrow. Most of the observer or filter design methods are appropriate for systems described by ordinary set of differential equations (ODE). The battery dynamics are however described by partial differential algebraic equations (PDAE), and for this class of systems, there are not many results available for design of proper observers or filters. Many theories and methods developed for ODEs are not applicable or at least not directly applicable to PDAE equations. The particle filter method proposed in this thesis is quite powerful in dealing with such dynamics but suffers from high computational load. Hence, development of appropriate observers for the high fidelity physics-based model of the battery would be promising for battery monitoring. There has been some efforts such as [76], however they have reduced the battery equations quite considerably and maybe unjustified in some operational conditions.

   In order to counteract the problem of observer design for battery systems, there has also been many efforts to reduce the order of the equations, simplify the equations, reformulate them into fast and slow modes, and etc [121, 111, 101, 33]. However, all those models would inherently possess uncertainties in both process and observation equations. Therefore, development of appropriate nonlinear observers that can

effectively cope with uncertainties can provide a promising solution to state of charge estimation of the battery.

Bibliography

[1] János Abonyi, Johannes A Roubos, Marcel Oosterom, and Ferenc Szeifert. Compact ts-fuzzy models through clustering and ols plus fis model reduction. In *Fuzzy Systems, 2001. The 10th IEEE International Conference on*, volume 3, pages 1420–1423. IEEE, 2001.

[2] Mohamed Alamgir and Ann Marie Sastry. Efficient batteries for transportation applications. Technical report, SAE Technical Paper, 2008.

[3] SM Alavi and Mehrdad Saif. Fault detection in nonlinear stable systems over lossy networks. *Control Systems Technology, IEEE Transactions on*, 21(6):2129–2142, 2013.

[4] Pankaj Arora, Ralph E White, and Marc Doyle. Capacity fade mechanisms and side reactions in lithium-ion batteries. *Journal of the Electrochemical Society*, 145(10):3647–3667, 1998.

[5] M Sanjeev Arulampalam, Simon Maskell, Neil Gordon, and Tim Clapp. A tutorial on particle filters for online nonlinear/non-gaussian bayesian tracking. *Signal Processing, IEEE Transactions on*, 50(2):174–188, 2002.

[6] Atmel. *Active Cell Balancing Methods for Li-Ion Battery Management ICs using the ATA6870*, 2015. Rev. 9184CâĂŞAUTOâĂŞ07/15.

[7] Doron Aurbach. Review of selected electrode–solution interactions which determine the performance of li and li ion batteries. *Journal of Power Sources*, 89(2):206–218, 2000.

[8] Doron Aurbach, Ella Zinigrad, Yaron Cohen, and Hanan Teller. A short review of failure mechanisms of lithium metal and lithiated graphite anodes in liquid electrolyte solutions. *Solid State Ionics*, 148(3):405–416, 2002.

[9] PG Balakrishnan, R Ramesh, and T Prem Kumar. Safety mechanisms in lithium-ion batteries. *Journal of Power Sources*, 155(2):401–414, 2006.

[10] IN Li-ION BATTERIES, E Skou, R Koksbang, S Yde-Andersen, and J Thomas. Anode current collector corrosion. In *Proceedings of the Symposium on Batteries for Portable Applications and Electrical Vehicles*, volume 18, pages 19–25. The Electrochemical Society, 1997.

[11] Bikramjit S Bhangu, Paul Bentley, David A Stone, and Christopher M Bingham. Nonlinear observers for predicting state-of-charge and state-of-health of lead-acid batteries for hybrid-electric vehicles. *Vehicular Technology, IEEE Transactions on*, 54(3):783–794, 2005.

[12] I Bloom, BW Cole, JJ Sohn, SA Jones, EG Polzin, VS Battaglia, GL Henriksen, C Motloch, R Richardson, T Unkelhaeuser, et al. An accelerated calendar and cycle life study of Li-ion cells. *Journal of Power Sources*, 101(2):238–247, 2001.

[13] Ira Bloom, Scott A Jones, Vincent S Battaglia, Gary L Henriksen, Jon P Christophersen, Randy B Wright, Chinh D Ho, Jeffrey R Belt, and Chester G Motloch. Effect of cathode composition on capacity fade, impedance rise and power fade in high-power, lithium-ion cells. *Journal of power sources*, 124(2):538–550, 2003.

[14] A Blyr, C Sigala, G Amatucci, D Guyomard, Y Chabre, and J-M Tarascon. Self-discharge of $LiMn_2O_4$/CLi-ion cells in their discharged state understanding by means of three-electrode measurements. *Journal of The Electrochemical Society*, 145(1):194–209, 1998.

[15] Jeffrey W Braithwaite, Angelo Gonzales, Ganesan Nagasubramanian, Samuel J Lucero, Diane E Peebles, James A Ohlhausen, and Wendy R Cieslak. Corrosion of lithium-ion battery current collectors. *Journal of The Electrochemical Society*, 146(2):448–456, 1999.

[16] Aviva Brecher. Assessment of needs and research roadmaps for rechargeable energy storage system (ress) onboard electric drive buses. Technical report, US DOT Federal Transit Administration, 2010.

[17] M Broussely, Ph Biensan, F Bonhomme, Ph Blanchard, S Herreyre, K Nechev, and RJ Staniewicz. Main aging mechanisms in li ion batteries. *Journal of power sources*, 146(1):90–96, 2005.

[18] M Broussely, S Herreyre, Ph Biensan, P Kasztejna, K Nechev, and RJ Staniewicz. Aging mechanism in li ion cells and calendar life predictions. *Journal of Power Sources*, 97:13–21, 2001.

[19] Stephan Buller, Marc Thele, Rik WAA De Doncker, and Eckhard Karden. Impedance-based simulation models of supercapacitors and Li-ion batteries for power electronic applications. In *Industry Applications Conference, 2003. 38th IAS Annual Meeting. Conference Record of the*, volume 3, pages 1596–1600. IEEE, 2003.

[20] Jian Cao, Nigel Schofield, and Ali Emadi. Battery balancing methods: A comprehensive review. In *Vehicle Power and Propulsion Conference, 2008. VPPC'08. IEEE*, pages 1–6. IEEE, 2008.

[21] CC Chan, EWC Lo, and Shen Weixiang. The available capacity computation model based on artificial neural network for lead–acid batteries in electric vehicles. *Journal of Power Sources*, 87(1):201–204, 2000.

[22] Mohammad Charkhgard and Mohammad Farrokhi. State-of-charge estimation for lithium-ion batteries using neural networks and ekf. *Industrial Electronics, IEEE Transactions on*, 57(12):4178–4187, 2010.

[23] N A Chaturvedi, R Klein, J Christensen, J Ahmed, and A Kojic. Algorithms for advanced battery-management systems. *IEEE Control Systems Magazine*, 30(3):49–68, 2010.

[24] Tao Chen, Julian Morris, and Elaine Martin. Particle filters for state and parameter estimation in batch processes. *Journal of Process Control*, 15(6):665–673, 2005.

[25] Young-Min Choi and Su-Il Pyun. Effects of intercalation-induced stress on lithium transport through porous licoo< sub> 2</sub> electrode. *Solid State Ionics*, 99(3):173–183, 1997.

[26] John Christensen and John Newman. Cyclable lithium and capacity loss in li-ion cells. *Journal of the Electrochemical Society*, 152(4):A818–A829, 2005.

[27] Claus Danielson, Francesco Borrelli, Douglas Oliver, Dyche Anderson, Ming Kuang, and Tony Phillips. Balancing of battery networks via constrained optimal control. In *American Control Conference (ACC), 2012*, pages 4293–4298. IEEE, 2012.

[28] Mohamed Daowd, Noshin Omar, Peter Van Den Bossche, and Joeri Van Mierlo. Passive and active battery balancing comparison based on matlab simulation. In *Vehicle Power and Propulsion Conference (VPPC), 2011 IEEE*, pages 1–7. IEEE, 2011.

[29] Robert Darling and John Newman. Modeling side reactions in composite $Li_yMn_2O_4$ electrodes. *Journal of The Electrochemical Society*, 145(3):990–998, 1998.

[30] C Delmas, M Menetrier, L Croguennec, I Saadoune, A Rougier, C Pouillerie, G Prado, M Grüne, and L Fournes. An overview of the Li(Ni, M)O_2 systems: syntheses, structures and properties. *Electrochimica Acta*, 45(1):243–253, 1999.

[31] C Delmas, JP Peres, A Rougier, A Demourgues, F Weill, A Chadwick, M Broussely, F Perton, Ph Biensan, and P Willmann. On the behavior of the Li_xNiO_2 system: an electrochemical and structural overview. *Journal of Power Sources*, 68(1):120–125, 1997.

[32] Shuvashis Dey, Beshah Ayalew, and Pierluigi Pisu. Nonlinear robust observers for state-of-charge estimation of lithium-ion cells based on a reduced electrochemical model. *Control Systems Technology, IEEE Transactions on*, 2015.

[33] Domenico Di Domenico, Anna Stefanopoulou, and Giovanni Fiengo. Lithium-Ion Battery State of Charge and Critical Surface Charge Estimation Using an Electrochemical Model-Based Extended Kalman Filter. *Journal of Dynamic Systems, Measurement, and Control*, 132(6):061302 (1–11), 2010.

[34] Arnaud Doucet. *Sequential monte carlo methods*. Wiley Online Library, 2001.

[35] Marc Doyle, Thomas F Fuller, and John Newman. Modeling of Galvanostatic Charge and Discharge of the Lithium / Polymer / Insertion Cell. *Journal of The Electrochemical Society*, 140(6):1526–1533, 1993.

[36] Akram Eddahech, Olivier Briat, Nicolas Bertrand, Jean-Yves Delétage, and Jean-Michel Vinassa. Behavior and state-of-health monitoring of Li-ion batteries using impedance spectroscopy and recurrent neural networks. *International Journal of Electrical Power & Energy Systems*, 42(1):487–494, 2012.

[37] Magnus Egerstedt, Yorai Wardi, and Henrik Axelsson. Transition-time optimization for switched-mode dynamical systems. *Automatic Control, IEEE Transactions on*, 51(1):110–115, 2006.

[38] Christopher R Fell, Miaofang Chi, Ying Shirley Meng, and Jacob L Jones. In situ x-ray diffraction study of the lithium excess layered oxide compound Li $[Li_{0.2}Ni_{0.2}Mn_{0.6}]$ O_2 during electrochemical cycling. *Solid State Ionics*, 207(Complete):44–49, 2012.

[39] Gang Feng. *Analysis and Synthesis of Fuzzy Control Systems: a model-based approach*. CRC Press, 2010.

[40] Carsten Fritsche, TB Schon, and Anja Klein. The marginalized auxiliary particle filter. In *Computational Advances in Multi-Sensor Adaptive Processing (CAMSAP), 2009 3rd IEEE International Workshop on*, pages 289–292. IEEE, 2009.

[41] Thomas F Fuller, Marc Doyle, and John Newman. Simulation and Optimization of the Dual Lithium Ion Insertion Cell. *Journal of The Electrochemical Society*, 141(1):1–10, 1994.

[42] Parthasarathy M Gomadam and John W Weidner. Modeling volume changes in porous electrodes. *Journal of The Electrochemical Society*, 153(1):A179–A186, 2006.

[43] Neil J Gordon, David J Salmond, and Adrian FM Smith. Novel approach to nonlinear/non-gaussian bayesian state estimation. *IEE Proceedings F (Radar and Signal Processing)*, 140(2):107–113, 1993.

[44] Michael Grant, Stephen Boyd, and Yinyu Ye Cvx. Matlab software for disciplined convex programming. *Online accessiable: http://stanford. edu/boyd/cvx*, 2008.

[45] Christoph Hametner and Stefan Jakubek. State of charge estimation for lithium ion cells: Design of experiments, nonlinear identification and fuzzy observer design. *Journal of Power Sources*, 238(15):413–421, 2013.

[46] BC Han, A Van der Ven, D Morgan, and G Ceder. Electrochemical modeling of intercalation processes with phase field models. *Electrochimica Acta*, 49(26):4691–4699, 2004.

[47] Bala S Haran, Branko N Popov, and Ralph E White. Determination of the hydrogen diffusion coefficient in metal hydrides by impedance spectroscopy. *Journal of Power Sources*, 75(1):56–63, 1998.

[48] Stephen J Harris, Adam Timmons, Daniel R Baker, and Charles Monroe. Direct *in situ* measurements of li transport in li-ion battery negative electrodes. *Chemical Physics Letters*, 485(4):265–274, 2010.

[49] Hongwen He, Rui Xiong, and Jinxin Fan. Evaluation of lithium-ion battery equivalent circuit models for state of charge estimation by an experimental approach. *Energies*, 4(4):582–598, 2011.

[50] Xiaosong Hu, Shengbo Li, and Huei Peng. A comparative study of equivalent circuit models for Li-ion batteries. *Journal of Power Sources*, 198:359–367, 2012.

[51] O Iliev, A Latz, J Zausch, and S Zhang. *An overview on the usage of some model reduction approaches for simulations of Li-ion transport in batteries*. Fraunhofer Inst. für Techno-und Wirtschaftsmathematik, ITWM, 2012.

[52] Simon J Julier and Jeffrey K Uhlmann. A new extension of the kalman filter to nonlinear systems. In *Int. symp. aerospace/defense sensing, simul. and controls*, pages 182–193. Orlando, FL, 1997.

[53] Rudolph Emil Kalman. A new approach to linear filtering and prediction problems. *Journal of Fluids Engineering*, 82(1):35–45, 1960.

[54] Keiji Kanazawa, Daphne Koller, and Stuart Russell. Stochastic simulation algorithms for dynamic probabilistic networks. In *Proceedings of the Eleventh conference on Uncertainty in artificial intelligence*, pages 346–351. Morgan Kaufmann Publishers Inc., 1995.

[55] Marie Kerlau, Jeffrey A Reimer, and Elton J Cairns. Investigation of particle isolation in li-ion battery electrodes using Li NMR spectroscopy. *Electrochemistry communications*, 7(12):1249–1251, 2005.

[56] Il-song Kim. The novel state of charge estimation method for lithium battery using sliding mode observer. *Journal of Power Sources*, 163:584–590, 2006.

[57] IL-Song Kim. A technique for estimating the state of health of lithium batteries through a dual-sliding-mode observer. *Power Electronics, IEEE Transactions on*, 25(4):1013–1022, 2010.

[58] Jonghoon Kim, Seongjun Lee, and Bohyung Cho. The state of charge estimation employing empirical parameters measurements for various temperatures. In *Power Electronics and Motion Control Conference, 2009. IPEMC'09. IEEE 6th International*, pages 939–944. IEEE, 2009.

[59] Costas Kiparissides, Panagiotis Seferlis, George Mourikas, and A Julian Morris. Online optimizing control of molecular weight properties in batch free-radical polymerization reactors. *Industrial & engineering chemistry research*, 41(24):6120–6131, 2002.

[60] Reinhardt Klein, Nalin a. Chaturvedi, Jake Christensen, Jasim Ahmed, Rolf Findeisen, and Aleksandar Kojic. Electrochemical Model Based Observer Design for a Lithium-Ion Battery. *IEEE Transactions on Control Systems Technology*, 21(2):289–301, March 2013.

[61] Tadashi Kondo. Gmdh neural network algorithm using the heuristic self-organization method and its application to the pattern identification problem. In *SICE'98. Proceedings of the 37th SICE Annual Conference. International Session Papers*, pages 1143–1148. IEEE, 1998.

[62] James D Kozlowski, Carl S Byington, Amulya K Garga, Matthew J Watson, and Todd A Hay. Model-based predictive diagnostics for electrochemical energy sources. In *Aerospace Conference, 2001, IEEE Proceedings.*, volume 6, pages 3149–3164. IEEE, 2001.

[63] Manish Kulkarni and Vishwani D Agrawal. A tutorial on battery simulation-matching power source to electronic system. In *Proc. 14th IEEE VLSI Design and Test Symp*, 2010.

[64] Jaemoon Lee, Oanyong Nam, and BH Cho. Li-ion battery soc estimation method based on the reduced order extended kalman filtering. *Journal of Power Sources*, 174(1):9–15, 2007.

[65] Seongjun Lee, Jonghoon Kim, Jaemoon Lee, and BH Cho. State-of-charge and capacity estimation of lithium-ion battery using a new open-circuit voltage versus state-of-charge. *Journal of Power Sources*, 185(2):1367–1373, 2008.

[66] Yuang-Shung Lee and Ming-Wang Cheng. Intelligent control battery equalization for series connected lithium-ion battery strings. *Industrial Electronics, IEEE Transactions on*, 52(5):1297–1307, 2005.

[67] Yuang-Shung Lee, Chun-Yi Duh, Guo-Tian Chen, and Shen-Ching Yang. Battery equalization using bi-directional cuk converter in dcvm operation. In *Power Electronics Specialists Conference, 2005. PESC'05. IEEE 36th*, pages 765–771. IEEE, 2005.

[68] Yuang-Shung Lee, Wei-Yen Wang, and Tsung-Yuan Kuo. Soft computing for battery state-of-charge (bsoc) estimation in battery string systems. *Industrial Electronics, IEEE Transactions on*, 55(1):229–239, 2008.

[69] Jane Liu and Mike West. Combined parameter and state estimation in simulation-based filtering. In *Sequential Monte Carlo methods in practice*, pages 197–223. Springer, 2001.

[70] Languang Lu, Xuebing Han, Jianqiu Li, Jianfeng Hua, and Minggao Ouyang. A review on the key issues for lithium-ion battery management in electric vehicles. *Journal of power sources*, 226:272–288, 2013.

[71] John MacCormick and Andrew Blake. A probabilistic exclusion principle for tracking multiple objects. *International Journal of Computer Vision*, 39(1):57–71, 2000.

[72] Hema Rao Madala and Alexy G Ivakhnenko. *Inductive learning algorithms for complex systems modeling*. CRC press Boca Raton, 1994.

[73] J Mahdavi, A Emadi, and HA Toliyat. Application of state space averaging method to sliding mode control of pwm dc/dc converters. In *Industry Applications Conference, 1997. Thirty-Second IAS Annual Meeting, IAS'97., Conference Record of the 1997 IEEE*, volume 2, pages 820–827. IEEE, 1997.

[74] E Markevich, MD Levi, and D Aurbach. Comparison between potentiostatic and galvanostatic intermittent titration techniques for determination of chemical diffusion coefficients in ion-insertion electrodes. *Journal of Electroanalytical Chemistry*, 580(2):231–237, 2005.

[75] Jorge J Moré. The levenberg-marquardt algorithm: implementation and theory. In *Numerical analysis*, pages 105–116. Springer, 1978.

[76] SJ Moura, NA Chaturvedi, and M Krstic. PDE estimation techniques for advanced battery management systemsâĂŤpart i: Soc estimation. In *American Control Conference (ACC), 2012*, pages 559–565. IEEE, 2012.

[77] SJ Moura, NA Chaturvedi, and M Krstic. PDE estimation techniques for advanced battery management systemsâĂŤpart ii: Soh identification. In *American Control Conference (ACC), 2012*, pages 566–571. IEEE, 2012.

[78] Seung-Taek Myung, Yashiro Hitoshi, and Yang-Kook Sun. Electrochemical behavior and passivation of current collectors in lithium-ion batteries. *Journal of Materials Chemistry*, 21(27):9891–9911, 2011.

[79] Seung-Taek Myung, Shinichi Komaba, and Naoaki Kumagai. Enhanced structural stability and cyclability of Al-doped $LiMn_2O_4$ spinel synthesized by the emulsion drying method. *Journal of The Electrochemical Society*, 148(5):A482–A489, 2001.

[80] Johanna Nelson, Sumohan Misra, Yuan Yang, Ariel Jackson, Yijin Liu, Hailiang Wang, Hongjie Dai, Joy C Andrews, Yi Cui, and Michael F Toney. In operando x-ray diffraction and transmission x-ray microscopy of lithium sulfur batteries. *Journal of the American Chemical Society*, 134(14):6337–6343, 2012.

[81] Kenneth C Nisbet, Bernard Mulgrew, and Stephen McLaughlin. Reduced state methods in nonlinear prediction. *Signal processing*, 48(1):37–49, 1996.

[82] Sung-Kwun Oh, Witold Pedrycz, and Byoung-Jun Park. Polynomial neural networks architecture: analysis and design. *Computers & Electrical Engineering*, 29(6):703–725, 2003.

[83] Hong-Sun Park, Chong-Eun Kim, Gun-Woo Moon, Joong-Hui Lee, and Jeon Keun Oh. Two-stage cell balancing scheme for hybrid electric vehicle lithium-ion battery strings. In *Power Electronics Specialists Conference, 2007. PESC 2007. IEEE*, pages 273–279. IEEE, 2007.

[84] Jonghyun Park, Jeong Hun Seo, Gregory Plett, Wei Lu, and Ann Marie Sastry. Numerical simulation of the effect of the dissolution of limn2o4 particles on li-ion battery performance. *Electrochemical and Solid-State Letters*, 14(2):A14–A18, 2011.

[85] Kristin Persson, Vijay A Sethuraman, Laurence J Hardwick, Yoyo Hinuma, Ying Shirley Meng, Anton van der Ven, Venkat Srinivasan, Robert Kostecki, and Gerbrand Ceder. Lithium diffusion in graphitic carbon. *The Journal of Physical Chemistry Letters*, 1(8):1176–1180, 2010.

[86] Michael K Pitt and Neil Shephard. Filtering via simulation: Auxiliary particle filters. *Journal of the American statistical association*, 94(446):590–599, 1999.

[87] Gregory L. Plett. Extended Kalman filtering for battery management systems of LiPB-based HEV battery packs. *Journal of Power Sources*, 134(2):262–276, August 2004.

[88] Gregory L Plett. Extended kalman filtering for battery management systems of LiPB-based HEV battery packs: Part 3. state and parameter estimation. *Journal of Power sources*, 134(2):277–292, 2004.

[89] Gregory L Plett. Sigma-point kalman filtering for battery management systems of LiPB-based HEV battery packs: part 2: simultaneous state and parameter estimation. *Journal of power sources*, 161(2):1369–1384, 2006.

[90] Harry J Ploehn, Premanand Ramadass, and Ralph E White. Solvent diffusion model for aging of lithium-ion battery cells. *Journal of The Electrochemical Society*, 151(3):A456–A462, 2004.

[91] Valer Pop, Henk Jan Bergveld, JHG Op het Veld, PPL Regtien, D Danilov, and PHL Notten. Modeling battery behavior for accurate state-of-charge indication. *Journal of the Electrochemical Society*, 153(11):A2013–A2022, 2006.

[92] Ramadass Premanand, Anand Durairajan, Bala Haran, Ralph White, and Branko Popov. Studies on capacity fade of spinel-based li-ion batteries. *Journal of the Electrochemical Society*, 149(1):A54–A60, 2002.

[93] P Ramadass, Bala Haran, Parthasarathy M Gomadam, Ralph White, and Branko N Popov. Development of first principles capacity fade model for Li-ion cells. *Journal of the Electrochemical Society*, 151(2):A196–A203, 2004.

[94] A Ravindran, Gintaras Victor Reklaitis, and Kenneth Martin Ragsdell. *Engineering optimization: methods and applications*. John Wiley & Sons, 2006.

[95] James B Rawlings and Bhavik R Bakshi. Particle filtering and moving horizon estimation. *Computers & chemical engineering*, 30(10):1529–1541, 2006.

[96] Jürgen Remmlinger, Michael Buchholz, Markus Meiler, Peter Bernreuter, and Klaus Dietmayer. State-of-health monitoring of lithium-ion batteries in electric vehicles by on-board internal resistance estimation. *Journal of Power Sources*, 196(12):5357–5363, 2011.

[97] Sindhuja Renganathan, Godfrey Sikha, Shriram Santhanagopalan, and Ralph E White. Theoretical analysis of stresses in a lithium ion cell. *Journal of the Electrochemical Society*, 157(2):A155–A163, 2010.

[98] Shalini Rodrigues, N Munichandraiah, and AK Shukla. A review of state-of-charge indication of batteries by means of ac impedance measurements. *Journal of Power Sources*, 87(1):12–20, 2000.

[99] Leon Christopher Rosario. *Power and energy management of multiple energy storage systems in electric vehicles*. PhD thesis, Dept. Aerosp. Power Sens., Cranfield Univ.,Bedfordshire, U.K., 2007.

[100] M F Samadi, S M Alavi, and M Saif. An electrochemical model-based particle filter approach for Lithium-ion battery estimation. In *Decision and Control (CDC), 2012 IEEE 51st Annual Conference on*, pages 3074–3079. IEEE, 2012.

[101] Shriram Santhanagopalan and Ralph E White. Online estimation of the state of charge of a lithium ion cell. *Journal of Power Sources*, 161:1346–1355, 2006.

[102] Shriram Santhanagopalan and Ralph E White. State of charge estimation using an unscented filter for high power lithium ion cells. *International Journal of Energy Research*, 34(2):152–163, 2010.

[103] Shriram Santhanagopalan, Qi Zhang, Karthikeyan Kumaresan, and Ralph E White. Parameter estimation and life modeling of lithium-ion cells. *Journal of The Electrochemical Society*, 155(4):A345–A353, 2008.

[104] Ronald W Schafer. What is a savitzky-golay filter?[lecture notes]. *Signal Processing Magazine, IEEE*, 28(4):111–117, 2011.

[105] Thomas B Schön. *Estimation of nonlinear dynamic systems: Theory and applications*. PhD thesis, Department of Electrical Engineering, Automatic Control, Linköping University, 2006.

[106] Jeong Hun Seo, Jonghyun Park, Gregory Plett, and Ann Marie Sastry. Gas-evolution induced volume fraction changes and their effect on the performance degradation of Li-ion batteries. *Electrochemical and Solid-State Letters*, 13(9):A135–A137, 2010.

[107] H Shibata, S Taniguchi, K Adachi, K Yamasaki, G Ariyoshi, K Kawata, K Nishijima, and K Harada. Management of serially-connected battery system using multiple switches. In *Power Electronics and Drive Systems, 2001. Proceedings., 2001 4th IEEE International Conference on*, volume 2, pages 508–511. IEEE, 2001.

[108] Godfrey Sikha, Branko N Popov, and Ralph E White. Effect of porosity on the capacity fade of a lithium-ion battery theory. *Journal of The Electrochemical Society*, 151(7):A1104–A1114, 2004.

[109] Dan Simon. *Optimal state estimation: Kalman, H infinity, and nonlinear approaches*. John Wiley & Sons, 2006.

[110] Pritpal Singh, Ramana Vinjamuri, Xiquan Wang, and David Reisner. Design and implementation of a fuzzy logic-based state-of-charge meter for Li-ion batteries used in portable defibrillators. *Journal of Power Sources*, 162(2):829–836, 2006.

[111] Kandler A Smith, Christopher D Rahn, and Chao-Yang Wang. Control oriented 1d electrochemical model of lithium ion battery. *Energy Conversion and Management*, 48(9):2565–2578, 2007.

[112] Kandler A Smith, Christopher D Rahn, and Chao-Yang Wang. Model-based electrochemical estimation and constraint management for pulse operation of lithium ion batteries. *Control Systems Technology, IEEE Transactions on*, 18(3):654–663, 2010.

[113] Andrey Smyshlyaev, Miroslav Krstic, Nalin Chaturvedi, Jasim Ahmed, and Aleksandar Kojic. PDE model for thermal dynamics of a large li-ion battery pack. In *American Control Conference (ACC), 2011*, pages 959–964. IEEE, 2011.

[114] Iryna Snihir, William Rey, Evgeny Verbitskiy, Afifa Belfadhel-Ayeb, and Peter HL Notten. Battery open-circuit voltage estimation by a method of statistical analysis. *Journal of Power Sources*, 159(2):1484–1487, 2006.

[115] Harold W Sorenson. *Kalman filtering: theory and application*, volume 38. IEEE press New York, 1985.

[116] Carmelo Speltino, Anna Stefanopoulou, and Giovanni Fiengo. Cell equalization in battery stacks through state of charge estimation polling. In *American Control Conference (ACC), 2010*, pages 5050–5055. IEEE, 2010.

[117] R Spotnitz and J Franklin. Abuse behavior of high-power, lithium-ion cells. *Journal of Power Sources*, 113(1):81–100, 2003.

[118] Robert Spotnitz. Simulation of capacity fade in lithium-ion batteries. *Journal of Power Sources*, 113(1):72–80, 2003.

[119] Sarah G Stewart and John Newman. The use of UV/vis absorption to measure diffusion coefficients in $LiPF_6$ electrolytic solutions. *Journal of the Electrochemical Society*, 155(1):F13–F16, 2008.

[120] Venkat R Subramanian, Vijayasekaran Boovaragavan, Venkatasailanathan Ramadesigan, and Mounika Arabandi. Mathematical model reformulation for lithium-ion battery simulations: Galvanostatic boundary conditions. *Journal of The Electrochemical Society*, 156(4):A260–A271, 2009.

[121] Venkat R Subramanian, Vinten D Diwakar, and Deepak Tapriyal. Efficient macro-micro scale coupled modeling of batteries. *Journal of The Electrochemical Society*, 152(10):A2002–A2008, 2005.

[122] Fengchun Sun, Xiaosong Hu, Yuan Zou, and Siguang Li. Adaptive unscented kalman filtering for state of charge estimation of a lithium-ion battery for electric vehicles. *Energy*, 36(5):3531–3540, 2011.

[123] Kazuo Tanaka, Takayuki Ikeda, and Hua O Wang. Fuzzy regulators and fuzzy observers: relaxed stability conditions and lmi-based designs. *Fuzzy Systems, IEEE Transactions on*, 6(2):250–265, 1998.

[124] Freedom CAR Program Electrochemical Energy Storage Team. Freedomcar battery test for power-assist hybrid electric vehicles. Technical report, U.S. Department of Energy, 2003.

[125] William Tiedemann and John Newman. Growing porous layers. *Journal of The Electrochemical Society*, 119(2):186–188, 1972.

[126] Uwe Tröltzsch, Olfa Kanoun, and Hans-Rolf Tränkler. Characterizing aging effects of lithium ion batteries by impedance spectroscopy. *Electrochimica Acta*, 51(8):1664–1672, 2006.

[127] Peter Van den Bossche, Frédéric Vergels, Joeri Van Mierlo, Julien Matheys, and Wout Van Autenboer. Subat: An assessment of sustainable battery technology. *Journal of power sources*, 162(2):913–919, 2006.

[128] A Van der Ven and G Ceder. Lithium diffusion mechanisms in layered intercalation compounds. *Journal of power sources*, 97:529–531, 2001.

[129] Mark W Verbrugge and Brian J Koch. The effect of large negative potentials and overcharge on the electrochemical performance of lithiated carbon. *Journal of Electroanalytical Chemistry*, 436(1):1–7, 1997.

[130] J Vetter, P Novak, MR Wagner, C Veit, K-C Möller, JO Besenhard, M Winter, M Wohlfahrt-Mehrens, C Vogler, and A Hammouche. Ageing mechanisms in lithium-ion batteries. *Journal of power sources*, 147(1):269–281, 2005.

[131] CY Wang, WB Gu, and BY Liaw. Micro-macroscopic coupled modeling of batteries and fuel cells i. model development. *Journal of The Electrochemical Society*, 145(10):3407–3417, 1998.

[132] Yebin Wang, Huazhen Fang, Zafer Sahinoglu, Toshihiro Wada, and Satoshi Hara. Adaptive estimation of the state of charge for lithium-ion batteries: Nonlinear geometric observer approach. *Control Systems Technology, IEEE Transactions on*, 23(3):948–962, 2015.

[133] Xuping Xu and Panos J Antsaklis. Optimal control of switched systems based on parameterization of the switching instants. *Automatic Control, IEEE Transactions on*, 49(1):2–16, 2004.

[134] Jingyu Yan, Zhu Cheng, Guoqing Xu, Huihuan Qian, and Yangsheng Xu. Fuzzy control for battery equalization based on state of charge. In *Vehicular Technology Conference Fall (VTC 2010-Fall), 2010 IEEE 72nd*, pages 1–7. IEEE, 2010.

[135] John Yen and Liang Wang. Simplifying fuzzy rule-based models using orthogonal transformation methods. *Systems, Man, and Cybernetics, Part B: Cybernetics, IEEE Transactions on*, 29(1):13–24, 1999.

[136] Baoyong Zhang, James Lam, Shengyuan Xu, and Zhan Shu. Robust stabilization of uncertain T-S fuzzy time-delay systems with exponential estimates. *Fuzzy sets and systems*, 160(12):1720–1737, 2009.

[137] D Zhang, BS Haran, A Durairajan, RE White, Y Podrazhansky, and BN Popov. Studies on capacity fade of lithium-ion batteries. *Journal of Power Sources*, 91(2):122–129, 2000.

[138] Sheng Shui Zhang. The effect of the charging protocol on the cycle life of a li-ion battery. *Journal of Power Sources*, 161(2):1385–1391, 2006.

[139] Shengshui Zhang, Michael S Ding, and T Richard Jow. Self-discharge of $Li/Li_xMn_2O_4$ batteries in relation to corrosion of aluminum cathode substrates. *Journal of power sources*, 102(1):16–20, 2001.

[140] Feng Zhu and Panos J Antsaklis. Optimal control of switched hybrid systems: a brief survey. Technical report, University of Notre Dame, Department of Electrical Engineering, July 2011.

Appendix A

Nomenclature

The nomenclature of the models and algorithms presented in this thesis are summarized in this appendix.

A.1 Battery

$a_{s,j}$	active surface area of an electrode $[cm^{-1}]$
$c_{s,j}$	solid concentration $[mol\ cm^{-3}]$
$\bar{c}_{s,j}$	volume averaged concentration $[mol\ cm^{-3}]$
$c_{s,surf,j}$	solid concentration at the surface of sphere $[mol\ cm^{-3}]$
c_e	electrolyte concentration $[mol\ cm^{-3}]$
$D_{s,j}$	diffusion coefficient in solid phase $[cm^2 s^{-1}]$
$D_{e,j}$	diffusion coefficient in electrolyte phase $[cm^2 s^{-1}]$
F	Faraday's constant $[C\ mol^{-1}]$
$i_{0,j}$	exchange current density $[A\ cm^{-2}]$
$i_{0,sd}$	side reaction current density $[A\ cm^{-2}]$
I	applied current density to the cell $[A\ cm^{-2}]$
$J_{Li,j}$	volumetric rate of electrochemical reaction $[A\ cm^{-3}]$
J_{sd}	local volumetric rate for side reactions $[A\ cm^{-3}]$
k_j	rate constant of reaction
L_j	length of each domain $[cm]$
M_j	molecular weight $[kg\ mol^{-1}]$
M_p	molecular weight of side reactions $[kg\ mol^{-1}]$
N_i	molar flux of species i, $[mol\ cm^{-2}\ s^{-1}]$
p	Bruggeman coefficient
$\bar{q}_{s,j}$	volume averaged concentration flux $[mol\ cm^{-4}]$
R	gas constant $[JK^{-1}mol^{-1}]$
R_f	current collector contact resistance $[\Omega\ cm^2]$
R_{film}	film resistance at anode/solution interface $[\Omega\ cm^2]$
R_{SEI}	film resistance due to solid electrolyte interface $[\Omega\ cm^2]$

$R_{s,j}$	radius of particle spheres at each electrode $[cm]$
t_+^0	Li^+ transference number
T	temperature $[K]$
$\mathbf{u}$	local velocity vector in the electrode velocity $[cm\ s^{-1}]$
U_j	open circuit voltage at the electrode $[V]$
V	cell voltage $[V]$
V_p	volume of electrode particle $[cm^3]$
$\hat{V}$	molar volume of reaction product $[cm^3\ mol^{-1}]$
$\bar{V}_{s,j}$	partial molar volume of lithium in the intercalation material $[cm^3\ mol^{-1}]$
w_j	displacement vector $[cm]$

Greek

α_a	anodic transfer coefficient of electrochemical reaction
α_c	cathodic transfer coefficient of electrochemical reaction
δ	thickness $[cm]$
ϵ	volume fraction-porosity
$\epsilon_{s,j}$	volume fraction of active material
$\epsilon_{e,j}$	volume fraction of electrolyte phase
η_j	overpotential $[V]$
η_{sd}	local overpotential for side reaction $[V]$
$\kappa_{eff,j}$	electrolyte phase effective conductivity $[\Omega^{-1}\ cm^{-1}]$
$\kappa_{eff,j}^D$	effective diffusional conductivity $[\Omega^{-1}\ cm^{-1}]$
ν	Poisson's ration
ρ_p	density of active material $[kg\ cm^{-3}]$
$\sigma_{eff,j}$	conductivity of electrode $[\Omega^{-1}\ cm^{-1}]$
$\sigma_{h,j}$	hydrostatic stress $[N\ cm^{-2}]$
σ_r	radial component of stress $[N\ cm^{-2}]$
σ_t	tangential component of stress $[N\ cm^{-2}]$
$\phi_{s,j}$	solid potential $[V]$
$\phi_{e,j}$	electrolyte potential $[V]$

Subscript

e	electrolyte phase
eff	effective
i	species index
j	battery domains: negative electrode (n), positive electrode (p), separator (s)
k	reaction number
n	negative electrode
p	positive electrode
s	solid phase (if comes first)
sd	due to side reaction
$surf$	surface

Superscript

$-$	negative electrode boundaries
$+$	positive electrode boundaries
b	bulk
s	surface
sep	separator boundaries
i	particle/electrolyte interface
α	lithium rich phase
β	lithium deficient phase

A.2 Fuzzy Model and Observer

c	number of initiated fuzzy rules
D	distance measure between local models and data points
e	modeling error
F	fuzzy set
I_{ED}	measure index for ED algorithm
m	weighting exponent
M	rule set
N	size of data
r	number of reduced fuzzy rules
u	input
U	partition matrix
v	center of cluster
V	Objective function for clustering
W	weighting matrix for LM algorithm
x	state
$\hat{x}$	estimated state by observer
$\tilde{x}$	state estimation error using observer
y	output
$\hat{y}$	estimated output by observer
z	premise variables of fuzzy rules

Greek

β	degree of fulfilment
γ	damping factor for LM algorithm
ϵ	threshold for stopping conditions of algorithms
ζ	diagonal matrix of membership degrees
η	cluster prototypes
θ	parameter of the local models
λ	eigen values of correlation matrix
μ	normalized membership function
σ_i^2	standard deviation of the modeling error

$\sigma_{i,j}^2$	standard deviation of cluster
Φ_{uu}	correlation matrix
χ	chi-square criterion
ψ	eigen vector of correlation matrix
ω	impact of rules

Superscript

l	iteration index of T-S identification algorithm
m	iteration index of LM algorithm

Subscript

i	cluster index
j	premise variable index
k	time index
l	rule index
q	number of premise variables in each rule

A.3 Dynamic Resistance

A	vector of coefficients of each PD
C	useable capacity of battery
E	prediction error of each PD
I	battery current
L	No. of neurons in each layer
M	No. of data points
N	No. of input variables
p	No. of input variables of each PD
P	power
P_{tot}	total power throughput of battery
r	order of PD
R_e	Dynamic resistance (electronic resistance)
R_d	diffusion related resistance
V	battery voltage
x	input of the model
y	output of the model

Subscript

m	neuron index

A.4 Cell Balancing

D	duty cycle of PWM signal
f_s	frequency of PWM signal
F	hybrid dynamics of the whole circuit
$h(.)$	feasible direction in optimization algorithm

H	control and prediction horizon
i_{Li}	current of inductor i
J	cost function
$p(t)$	costate
Q	nominal capacity of battery
T_0	Mosfet switching time (on to off)
T_s	period of PWM signal
V_C	voltage of capacitor
X	system states

Greek

α	constant parameter in optimization algorithm
β	constant parameter in optimization algorithm
Γ	weight of objectives in cost function
ζ	step-size in gradient descent algorithm
θ	optimization parameters (i.e. switching times)
Λ	feasible set of switching times
τ	switching time

Superscript

h	control horizon index
k	iteration index in gradient descent algorithm